June
2012

AN INTELLIGENT APPROACH FOR MULTI-RESPONSE OPTIMIZATION: A CASE STUDY OF NON-TRADITIONAL MACHINING PROCESS

Jambeswar Sahu
Department of Mechanical Engineering
National Institute of Technology
Rourkela

AN INTELLIGENT APPROACH FOR MULTI-RESPONSE OPTIMIZATION: A CASE STUDY OF NON-TRADITIONAL MACHINING PROCESS

A THESIS SUBMITTED IN PARTIAL FULFILLMENT OF THE REQUIREMENTS FOR THE DEGREE OF

MASTER OF TECHNOLOGY
IN

PRODUCTION ENGINEERING

[MECHANICAL ENGINEERING]

By

JAMBESWAR SAHU

210ME2245

Under the supervision of

Prof. S.S.MAHAPATRA

DEPARTMENT OF MECHANICAL ENGINEERING
NATIONAL INSTITUTE OF TECHNOLOGY, ROURKELA
ODISHA, INDIA-769008

Dedicated to my parents & Guide

*

NATIONAL INSTITUTE OF TECHNOLOGY
ROURKELA-769008

CERTIFICATE

This is to certify that the thesis entitled "AN INTELLIGENT APPROACH FOR MULTI-RESPONSE OPTIMIZATION: A CASE STUDY OF NON-ITRADITIONAL MACHINING PROCESS" which is being submitted by JAMBESWAR SAHU as partial fullfilment of Master of Technology degree in Production Engineering (Mechanical Engineering) during the academic year 2010-2012 in the Department of Mechanical Engineering, National Institute of Technology, Rourkela.

Date:

Prof. Siba Sankar Mahapatra
Department of Mechanical Engineering
National Institute of Technology
Rourkela-769008

ACKNOWLEDGEMENT

Successful completion of work will never be one man's task. It requires hard work in right direction. There are many who have helped to make my experience as a student a rewarding one. In particular, I express my gratitude and deep regards to my thesis supervisor **Dr. S.S. Mahapatra, Department of Mechanical Engineering, NIT Rourkela** for kindly providing me to work under his supervision and guidance. I extend my deep sense of indebtedness and gratitude to him first for his valuable guidance, inspiring discussions, constant encouragement & kind co-operation throughout period of work which has been instrumental in the success of thesis.

I extend my thanks to **Dr. K.P. Maity, and Head, Dept. of Mechanical Engineering** for extending all possible help in carrying out the dissertation work directly or indirectly.

I express my sincere gratitude to **Dr. Saurav Datta, Kunal Nayak, Department of Mechanical Engineering, NIT, Rourkela** and other staff members for their indebted help in carrying out experimental work and valuable suggestions. I am also thankful to all the staff members of the department of Mechanical Engineering, NIT Rourkela and to all my well-wishers for their inspiration and help.

I greatly appreciate & convey my heartfelt thanks to Shailesh Dewangan, Chinmaya Mohanty, Debaprasanna Puhan, Layatit Dev Das, dear ones & all those who helped me in completion of this work.

I feel pleased and privileged to fulfill my parent's ambition and I am greatly indebted to them for bearing the inconvenience during my M Tech. course.

JAMBESWAR SAHU

DECLARATION

We hereby declare that the thesis entitled “AN INTELLIGENT APPROACH FOR MULTI-RESPONSE OPTIMIZATION: A CASE STUDY OF NONITRADITIONAL MACHINING PROCESS” is a bonafied record of work done by me, as a functional part towards the fulfillment of Master of Technology degree in Production Engineering specialization (Mechanical) from National Institute of Technology, Rourkela during the academic year 2010-2112.

This is purely academic in nature and it has not formed the basis, for the award of any Degree/ Diploma/Ascertain ship/ fellowship or similar title to any candidate.

JAMBESWAR SAHU

ROLL NO. 210ME2245

ABSTRACT

The present work proposes an intelligent approach to solve multi-response optimization problem in electrical discharge machining of AISI D2 using response surface methodology (RSM) combined with optimization techniques. Four process parameters (factors) such as discharge current (Ip), pulse-on-time (Ton), duty factor (τ) and flushing pressure (Fp) and four important responses like material removal rate (MRR), tool wear rate (TWR), surface roughness (Ra) and circularity (r_1/r_2) of machined component are considered in this study. A Box-Behnken RSM design is used to collect experimental data and develop empirical models relating input parameters and responses. Genetic algorithm (GA), an efficient search technique, is used to obtain the optimal setting for desired responses. It is to be noted that there is no single optimal setting which will produce best performance satisfying all the responses. In industries, to solve such problems, managers frequently depend on their past experience and judgement. Human intervention causes uncertainties present in the decision making process gleaned into solution methodology resulting in inferior solutions. Fuzzy inference system has been a viable option to address multiple response problems considering uncertainties and impreciseness caused during judgement process and experimental data collection. However, choosing right kind of membership functions and development of fuzzy rule base happen to be cumbersome job for the managers. To address this issue, a methodology based on combined neuro-fuzzy system and particle swarm optimization (PSO) is adopted to optimize multiple responses simultaneously. To avoid the conflicting nature of responses, they are first converted to signal-to-noise (S/N) ratio and then normalized. The proposed neuro-fuzzy approach is used to convert the responses into a single equivalent response known as Multi-response Performance Characteristic Index (MPCI). The effect of parameters on MPCI values has been studied in detail and a process model has been developed. Finally, optimal parameter setting is obtained by particle swarm optimization technique. The optimal setting so generated that satisfy all the responses may not be the best one due to aggregation of responses into a single response during neuro-fuzzy stage. In this direction, a multi-objective optimization based on non-dominated sorting genetic algorithm (NSGA) has been adopted to optimize the responses such that a set of mutually dominant solutions are found over a wide range of machining parameters. The proposed optimal settings are validated using thermal-modeling of finite element analysis.

Contents

LIST OF FIGURES

List of Tables

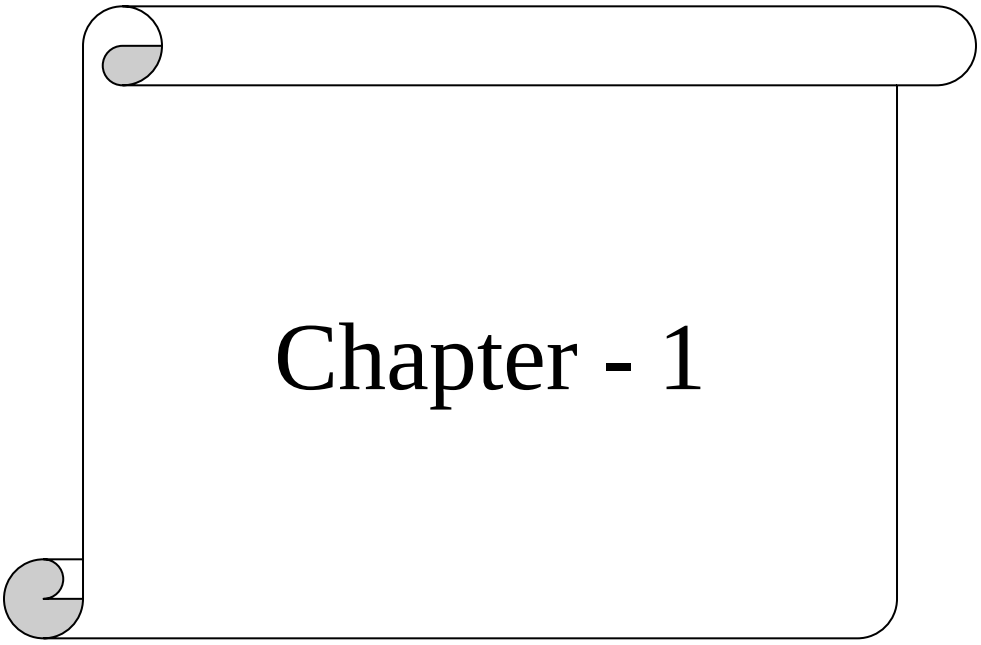
Chapter - 1

Chapter 1

BACKGROUND AND MOTIVATION

1.1. Introduction

The world is advancing technically in the field of space research, missile and nuclear industry. These industries demand very complicated and precise components having some special requirements. The challenges are taken by the new development taking place in manufacturing field. Now-a-days, many new materials and non-traditional machining and forming methods have been evolved to process difficult-to-machine materials, which are being put to commercial use with time. The non-traditional methods of machining have several advantages over traditional method of machining. Non-traditional methods are not limited by hardness, toughness, and brittleness of materials and can produce any intricate shape on any work piece material by suitable control over various process parameters. Non-traditional machining process can be classified into various groups depending on type of energy required, mechanism of material removal, source of energy required, and medium of energy transfer as described in Figure 1.1. [1].

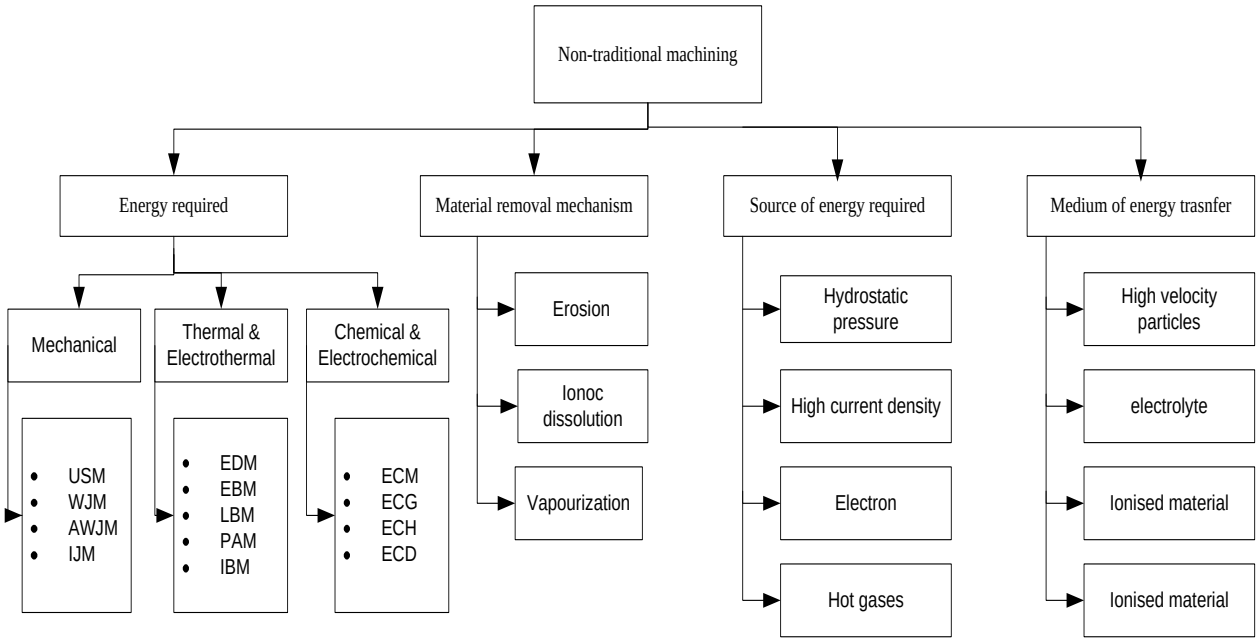

Figure 1.1. Classification of non-traditional machining processes

1.2. Electric discharge machining

Electrical Discharge Machining (EDM) is a non-traditional machining process used for machining any toughened and high strength to weight ratio conductive materials which are hard enough to cut by traditional processes (for example hardened steel, tungsten carbide, special alloys for aerospace applications). Furthermore, any complex cutting geometry, sharp angles and internal corners having surface state roughness less than 100 μm and precise machining (<1μm) can be produced. Therefore, EDM process and AISI D2 steel have extensively used in manufacturing industries, especially aerospace, ordnance, automobile, electronics, domestic appliances, packaging, telecommunication, surgical instruments and general engineering [2,3,4]. On the other hand, low material removal rate (order of 100 mm^3/min), surface modification of the machined work piece (white layer and heat affected zone) and limited size of work piece and tool have a disadvantage towards EDM process.

1.2.1. Principle

The material removal mechanism is owing to controlled erosion through a series of electric sparks between the tool and the work piece. The thermal energy of the sparks leads to intense heat conditions on the work piece causing melting and vaporizing of work piece material. The sparks are created in a dielectric liquid may be water or oil. There is no mechanical contact between tool and work piece during the whole process but in machining process small volumes of work piece material successively removed by melting or vaporized during a discharge. A simple explanation of erosion process as a result of single discharge is shown in Figure 1.2.

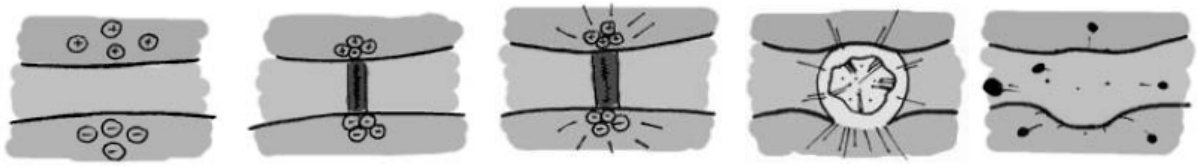

(a) Pre-breakdown: voltage applied between the Electrode and the workpiece

(b) Breakdown : dielectric breakdown, creation of the plasma channel

(c) Discharge : heating, melting and vaporizing of the workpiece material

(d) End of the discharge : plasma implosion, removing of the molten metal pool

(e) Post-discharge : solidifying and flushing of the eroded particles by the dielectric

Figure 1.2. Principle of EDM process

Initially, voltage is applied between tool and work piece. The dielectric break down is initiated, while tool moves towards work piece and gap voltage increases till sufficient breakdown occurs. The break down location is the closest point between the electrodes [5]. As

breakdown occurs voltage falls and a current rises sharply. The dielectric has been ionised and plasma channel has been created between electrodes. The current is then maintained for continuous bombardment of ions and electrons on the electrodes, which leads to a huge amount heat generation and creates a molten metal pool (of both work piece and tool) at the surface. There may be possibility that, a small amount of metal can be directly vaporised due to huge amount heat generation. As the plasma channel expands with time, the radius of molten metal pool is also increases. During the discharge, maintaining inter electrode gap (IEG) is a difficult task as IEG increases with discharge current. Therefore an automatic positioning system (APOS) and sensitivity (SEN) is employed for maintaining the IEG. After the discharge current and voltage are shut down during Toff time and the molten pool is carried out by flushing leaving a tiny crater in the work piece.

1.2.2. History

The history of electric discharge machining describes from the discovery of electric discharge. In the first half of the 18th century investigation of electrostatic phenomena were performed with frictional machines. Then the around 1745, first sparks and pulsed arcs were produced with "Leyden jars", an early form of capacitor invented in Germany and in the Netherlands [6] (Figure 1.3). Powerful discharges were created by putting several Leyden jars in parallel, creating thus a "battery".

Joseph Priestley (1733-1804), an English theologian and chemist, was the first to discover erosion craters left by electric discharges on the cathode surface in 1766:

> *"June the 13th, 1766. After discharging a battery, of about forty square feet, with a smooth brass knob, I accidentally observed upon it a pretty large circular spot, the center of which seemed to be superficially melted. (...) After an interruption of melted places, there was an intrie and exact circle of shining dots, consisting of places superficially melted, like those at the center." (Figure 1.4)*
>
> *"June the 14th, 1766. (...) Examining the spots with a microscope, both the shining dots that formed the central spot, and those which formed the external circle, appeared evidently to consist of cavities, resembling those on the moon, as they appear through a telescope, the edges projecting shadows into them, when they were held in the sun" [7].*

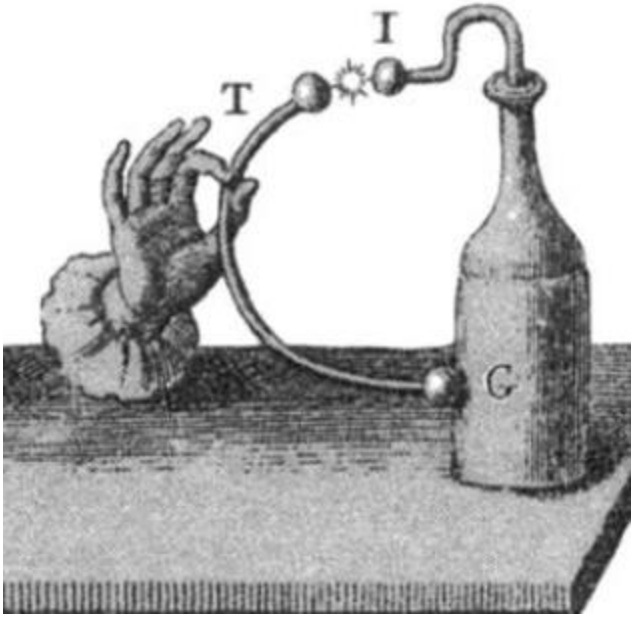

Figure 1.3. Engraved plate sent by Alessandro Volta to Joseph Priestley, showing the spark produced by short-circuit of a Leyden jar (1775) [8];

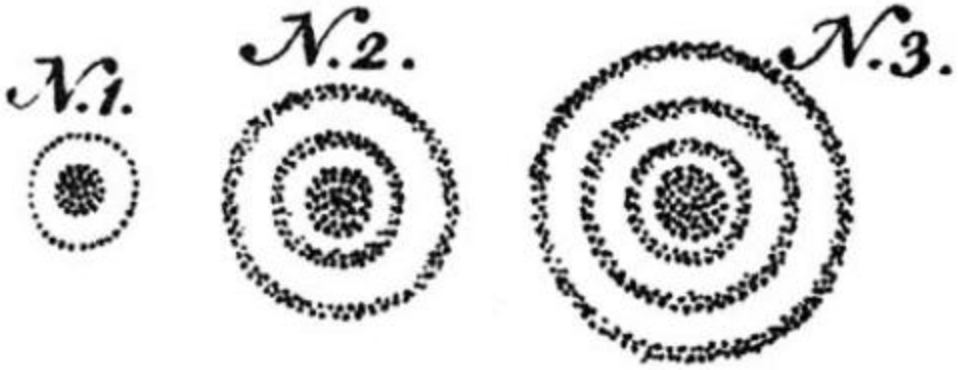

Figure 1.4. Sketches of erosion craters on cathode surface, observed by Joseph Priestley in 1766 [7].

Priestley used pulsed and oscillating discharge to investigate the influence of electrode material on the crater size. In 1799 Alessandro Volta (1745-1827) was invented that continuous discharges can be produced with battery of electrochemical cells. In 1802, Vasilii Petrov at St-Petersburg first to produce continuous carbon arc by developing very large voltaic batteries [9]. Humphry Davy (1778-1829) was discovered arcs, but his discovery remained ignored and forgotten for over a century. Petrov's in the Royal Institution of London around 1808, re-discovered independently carbon arcs using the huge voltaic battery.

The principle of EDM was invented by Russian scientists Boris and Natalya Lazarenko in Moscow in 1943, while they are assigned to Soviet government to investigate the wear caused by sparking between tungsten electrical contacts that was a problem for maintenance of automotive engines. Putting the electrodes in oil, they found that the sparks were more uniform than in air. Then they reverse the phenomenon, and to use controlled sparking as an erosion method [10]. Lazarenkos developed the first EDM machines during world war, which were very useful to erode hard metals like tungsten or tungsten carbide. The 'Lazarenko circuit' remained the standard EDM generator for years. In the 1950's, by understanding the erosion phenomenon, Swiss industries produced the first EDM machines [11-13].

1.2.3. State-of-the-art

Sixty-two year after the first industrial machine, EDM has made significant progress. Recently improvements in accuracy of machined parts, speed of machining and surface roughness is achieved by adopting automation, process control, changing dielectric, flushing and generator design [14-17]. Though EDM have the ability such as machining hard material and complex geometry, this process has to improve constantly in order to stay competitive and economically interesting in the modern tooling market against other traditional or new machining technique [16-18].

These limitations offer new opportunities for EDM development and growth as follows:

- There is a need to develop screening methodologies for EDM process for a high strength to weight ratio material (AISI D2 steel) machined by copper and brass tool.
- A much better understanding is needed for the basic physics and chemistry of EDM processes that capture the complexity part production.
- Technical and operation related advances are needed to ensure that EDM processes are more reliable and predictable than other non-traditional manufacturing processes.
- Control algorithms based on predictive models of system response to process changes are needed to maximize the performance of EDM machines.
- Developments of formalized standards for the EDM industry will help to achieve continued growth and further advancements of EDM technologies.

1.3. Research objectives

To sustain in this competitive market, product has to be modified and new product has to be developed. There are many external things which impose for development or modification. Among these materials, technologies, services and the attention paid to the end user requirements are significant. Though technological barriers exist, as in most technology areas, it is important to overcome them by developing proper understanding of process with related attributes. In this direction, next chapter (Chapter 2) explains the various efforts directed for improving the industrial feasibility of EDM process. Exhaustive literature review reveals that, there are many work carried out in EDM, but less work carried out using brass as tool material. The work represents choosing the best tool among two and a suitable condition for improving EDM performance. In this direction, present work emphasise on the EDM process functionality to understand the multiple interacting phenomena involved with this process and make it more reliable and predictable than other non-traditional manufacturing processes.

Based on these guiding principles, the objective of present research are as follows:

- Study on effect of process parameters on EDM performance. EDM performance is measured in terms of material removal rate, tool wear rate, surface roughness and circularity.
- Analysis of experimental results using statistical methods.
- Determination of relationship between process parameters and properties studied.
- Neuro-fuzzy approach for solving multi-response problem.
- Optimum parameters selection for overall improvement in EDM performance using genetic algorithm and particle swarm optimization.
- Non-dominated sorting genetic algorithm (NSGA) to obtain pareto optimal setting.
- Theoretical validation of material removal rate and tool wear rate model by thermal modeling using finite element analysis.

Methodology adopted for achieving these objectives are quite general and can provide common methods for measuring the benefits and limitations of various RP processes.

1.4. Thesis outline

The remainder of this thesis is organized as follows:

- Chapter 2: Literature review

Includes a literature review to provide a summary of the base of knowledge already available involving the issues of interest.

- Chapter 3: Experimental details

Include a description of the setup, material, sample preparation, measurement, design of experiments methodology and observation.

- Chapter 4: Optimization stratergy

Describes the methodology and algorithm for multi-response optimization using neuro-fuzzy approach, optimization technique such as genetic algorithm, particle swarm optimization, and multi-objective optimization using non-dominated sorting genetic algorithm.

- Chapter 5: Results and discussions

The effects of process parameters on responses are discussed. The relation between process parameter with responses are established by regression equation and optimized by genetic algorithm. Neuro-fuzzy method is proposed to covert multi-responses into an equivalent single response and optimum process conditions are determined for overall improvement of EDM performance using particle swarm optimization technique. The single optimal solution may change according to the requirement and also setting may not be available in machine, therefore non-dominated sorting genetic algorithm (NSGA) is proposed to obtain a set of pareto optimal solution to improve decision makers space.

- Chapter 6: Theoretical validation of MRR and TWR

The optimal setting may not available in machine. Therefore to check validation of model, thermal modeling has been carried out using ANSYS software.

- Chapter 8: Executive summary and conclusions

The conclusion and scope for future work are given in this part of thesis

1.5. Conclusions

Present chapter highlights the importance of EDM in manufacturing industry, history of EDM and objective of work. The general attributes of EDM can be put together as:

- Any conductive material can be machined irrespective of hardness.
- Able to build complex 3D geometries including enclosed cavities.
- Process is automatic and based tool design.
- Require minimal or no human intervention to operate.

These characteristics open new opportunities for faster product development in a simplified, minimal time, better performance and cost effective way. To improve the EDM performance in particular, research objective together with work outline is presented in this chapter.

In next chapter, the literature review is presented through exhaustive study.

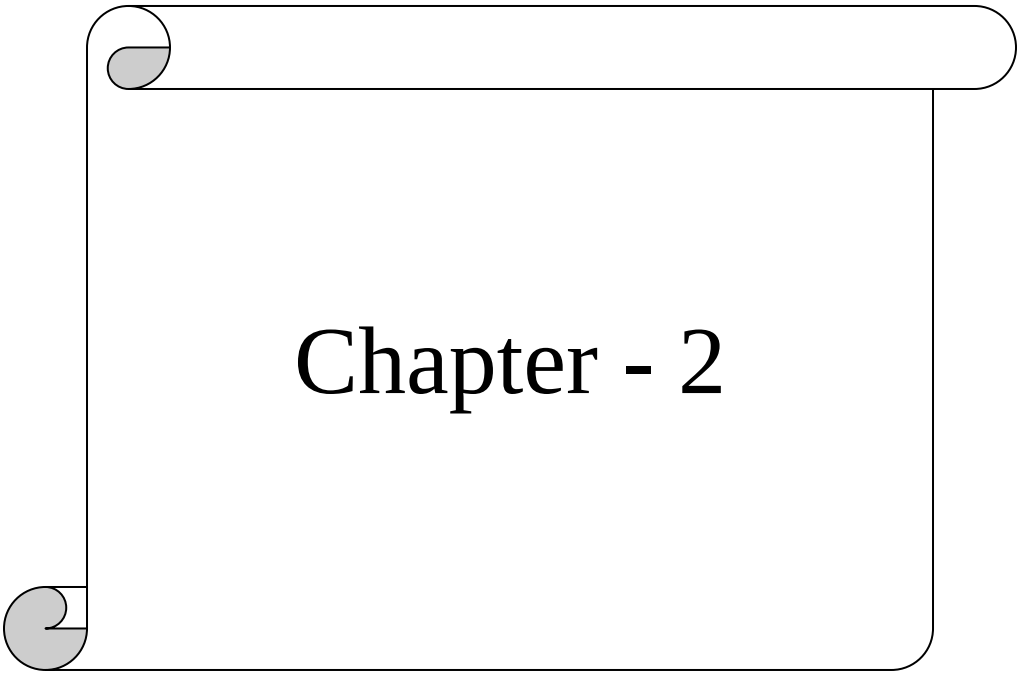
Chapter - 2

Chapter 2

LITERATURE SURVEY

2.1. Introduction

One of the current challenges faced by manufacturing industries is the reduction of process time and improvement of performance through optimization of controllable process parameter using different optimization technique. This can be obtained by experimentation or using any model developed from experiment. Although performance improvement in EDM has been studied extensively, proper selection of machining parameters for the best process performance is still a challenging job. In this direction, the current chapter highlights some research paper on EDM describing the effect of process parameters on EDM performance like material removal rate (MRR), tool wear rate (TWR), surface roughness (Ra), white layer thickness, surface cracks, etc. Literature survey begins with papers published after 1995 with maximum attention paid to last ten years. The search was restricted on those articles for which full text was available. Table 2.1 provides the source and number of citations from each source.

Table 2.1. Summary of publications referred

Source	**Citation**
Applied Mathematical Modelling	1
Applied Soft Computing	1
Computational Material Science	1
European Journal of Operational Research	1
IEEE Transaction on Evolutionary Computation	2
IEEE Transaction on Plasma Science	2
International Journal of Advanced Manufacturing Technology	8
International Journal of Engineering and Technology	1
International Journal of Integrated Engineering.	1
International Journal of Machine Tools and Manufacture	13
Journal of Applied Physics	3
Journal of Decision and Mathematical Sciences	1
Journal of Materials Processing Technology	18
Journal of Engineering for Industry	2
Journal of Manufacturing Processes	1
Journal of Engineering Research and Studies	1
Journal of Manufacturing Technology Management	1

Journal of Reinforced Plastics and Composites	1
Mathematical and Computer Modelling	1
Materials and Manufacturing Processes	3
Material Science and Applications	1
Proceedings of Institution of Mechanical Engineering Journal of Engineering Manufacture	1
Proceedings of the 11th International Symposium for Electro Machining	1
Proceedings of the 12th International Symposium for Electro Machining	2
Quality and Reliability Engineering	2
Soviet Physics-Technical Physics	1
The Arabian Journal for Science and Engineering Science	1
Total Quality Management	1
World Academy of Science, Engineering and Technology	1
World Congress on Computer Science and Information Engineering	1
http://www.lindquiststeels.com/documentation/d2.pdf	1
http://cadm.zut.edu.pl/pub/prawie%20wszystko%20o%20edm%20(ang).pdf	1
Books	10
Total	87

The papers are broadly classified into five categories, such as theoretical model of EDM, numerical model of EDM, statistical model of EDM, soft computing model of EDM and technological modification of basic EDM process.

2.2. Theoretical model of EDM

Singh and Ghosh considered that melting is the main process for metal removal. For short pulse (< 5μs), melting does not accounted as metal does not get enough time to get adequately heated and almost no melting takes place. The electrostatic force acting on the surface is a very important factor in the removal of metal for short pulses. For long pulses (discharge duration > 100μs), this electrostatic force becomes very small and does not play a significant role in the removal of metal. In the model proposed, the electro- static force acting on the metal surface and the stress distribution inside the metal due to this electrostatic force have been estimated. The variation of the yield strength with depth inside the metal has also been found out and finally the 'crater depth' due to this electrostatic force has been calculated. The model also predicts that for, short pulses the crater depth is proportional to square root of current. The same result is also found by the experiments of Williams [19, 20]. Marafona and Wykes investigated the optimisation of the process which uses the effect of carbon, which has migrated from the

dielectric to tungsten–copper electrodes. This work has led to the development of a two-stage EDM machining process where different EDM settings are used for the two stages of the process giving a significantly improved material removal rate for a given tool wear ratio. It is observed that, a black layer modified surface is produced on the tool in the first stage which inhibits tool wear, thus giving better tool wear for a given material removal rate in the second stage. The responses MRR, TWR, Ra are taken as EDM performance and conclude that the percentage of carbon in the 'black' layer is very important in the improvement of the EDM performance [21]. Chen and Mahdivian proposed a theoretical model to estimate the material removal rate and surface quality. The model provides equations to calculate work piece MRR and maximum peak-to-valley height is used for surface finish. Process parameters such as discharge current, pulse duration time and interval time at different level wear taken to conduct experiment and their effect on MRR and surface roughness were studied. It is observed that the theoretical model and experimental results are identical [22]. A finite element model has been developed to estimate the temperature field and thermal stresses in HSS due to Gaussian distributed heat flux of a spark during EDM. First, the developed code calculates the temperature in the work piece and then the thermal stress field is estimated using this temperature field. The effects of process variables (current and duty cycle) on temperature distribution and thermal stress distribution have been reported. The damaging nature of the thermal stresses as they develop during EDM is illuminated. It is observed that, after one spark, substantial compressive and tensile stresses develop in a thin layer around the spark location. It is also found that the thermal stresses exceed the yield strength of the work piece mostly in an extremely thin zone near the spark [23]. Thermo-physical model using finite element analysis and joule heating factor is developed by Marafona and Chousal to obtain the material removal from anode electrode, cathode electrode and maximum roughness at cathode surface. The theoretical results are compared with experimental results. It is observed that the anode material removal efficiency is smaller than that of cathode because there is a high amount of energy going to the anode and also a fast cooling of this material. A comparison is made 2D and 3D finite element analysis and observed that 2D axisymmetric finite element has an easier formulation than the 3D finite element and allows a reduction in the CPU time with very similar results. The difference between both axisymmetric and 3D was found around 100 times, i.e. 3D modelling has taking1180 s while the 2D only 14.5 s [24]. Recently, a new approach is proposed by Mahardika et al. to determine machining by

EDM processes using the product of the thermal conductivity (λ), melting point (θ) and electrical resistivity (ρ) of the work piece in relation to the machining time. Earlier developed theory was the function of thermal conductivity (λ) and melting point (θ). It is observed that the recent theory gives better result than previous one [25].

2.3. Numerical model of EDM

Das et al. developed an EDM simulation model using finite element for calculation of deformation, microstructure and residual stresses. The process parameters such as power input, pulse duration, etc. are used to predict the transient temperature distribution, liquid- and solid-state material transformation, and residual stresses that are induced in the work piece as a result of a single-pulse discharge. The model developed by DEFORM software has been validated using experimental data [26]. The measured and simulated crater morphology of EDM using ANSYS is compared for single discharge and a sequence of discharges. The thermal channel base parameters are computed along with measured current and voltage curves [27]. An axisymmetric two-dimensional model for powder mixed electric discharge machining (PMEDM) has been developed using the finite element method (FEM) in ANSYS (version 5.4) software. Some aspects such as temperature- sensitive material properties, shape and size of heat source, percentage distribution of heat among tool, work piece and dielectric fluid, pulse on/off time, material ejection efficiency and phase change (enthalpy) are used in the model to predict the thermal behaviour and material removal mechanism. The effect of various process parameters on temperature distributions along the radius and depth of the work piece are studied. Finally, the model has been validated by comparing the theoretical MRR with the experimental data [28]. Joshi and Pande developed an intelligent technique using ANSYS to study the effect of current, spark on time, discharge voltage, duty factor on MRR, TWR, crater-depth and crater,-height. A neural-network-based process model is proposed to establish the relation input process and process response and to optimize the process parameters for better performance [29]. In 2010 Joshi and Pande developed an axisymmetric two-dimensional model using ANSYS to study the effect of of process parameter such as discharge current, discharge duration, discharge voltage and duty cycle on the process performance. Experimental studies were carried out to study the MRR and crater shapes produced during actual machining. When compared with the reported analytical models, ANSYS model was found to predict results closer to the experimental results

[30]. Pradhan used ANSYS 12.0 to develop an axisymmetric two-dimensional model for electric discharge machining AISI d2 steel. It is observed that the compressive thermal stresses are developed beneath the crater and become tensile as we move away from the axis of symmetry. The radial component of the residual stresses reaches its maximum values close to the surface but diminishes very rapidly to comparatively low values of compressive residual stresses. It is found that the radial component of the residual stresses acquired from FEM are dominant than other components for all the machining parameter combinations [30].

2.4. Statistical model of EDM

Habib has analyzed the effect of machining parameters such as pulse current, gap voltage and pulse-on-time on MRR and TWR in EDM using response surface methodology. It is observed how MRR and TWR increase with increasing values of process parameters [32]. Chattopadhyay et al. have used Taguchi's design of experiment (DOE) approach to conduct experiment on rotary EDM using EN8 steel and copper as work piece-tool combination and developed empirical relations between performance characteristics (MRR and EWR) and process parameters such as peak current, pulse-on-time and rotational speed of tool electrode. It is found that peak current and rotational speed of tool electrode influence significantly on both the responses [33]. DOE approaches have been extensively used to determine best machining parameters in EDM. The DOE approaches are well suited to obtain optimal parametric combination for a single response problem. The method breaks down when multiple responses are simultaneously optimized due to some technical and practical reasons [34]. The influence of gap voltage, discharge current, pulse duration, pulse interval, flushing pressure on material removal rate, tool wear rate and surface roughness of EDM process using tungsten carbide (WC) as work piece and copper tungsten as electrode (CuW). It is observed that WC is suitable for EDM tool material and there exist an optimal condition for precision machining of WC although the condition may vary with composition of material [35]. Tebin et al. conducted the experiment on EDM to study the effect of discharge current, the pulse-on duration, the pulse-off duration, the tool electrode gap, and the tool material on MRR and TWR using steel 50CrV4 as work piece, copper and graphite as tool [36]. Pradhan and Biswas have adopted RSM design to conduct experiment on EDM and investigated the effect of four controllable input variables viz., discharge current, pulse duration, pulse-off-time and voltage on machining performance using

AISI D2 steel and copper as work piece-tool combination. It is observed that discharge current and pulse-on-time have significant effect on surface roughness [37]. Helmi et al. have investigated surface roughness and material removal rate in electro discharge grinding process employing Taguchi method when tool steel is machined with brass and copper electrodes. It is observed from analysis of variance that peak current and pulse-on-time are the significant factors influencing the performance characteristics [38]. Yunus analyzed the effect of factors such as pulse current, pulse-on-time, pulse-off-time, and voltage on surface roughness of machined component using factorial experiments and suggested optimal parameter setting to minimize surface roughness [39]. Prabhu and Vinayagam have experimentally demonstrated that surface roughness and micro-cracks on work piece (AISI D2 tool steel) can be substantially reduced if the tool (electrode) is coated with a carbon nono-tube layer [40]. Metal removal process in EDM is characterized by nonlinear, stochastic and time varying characteristics. In EDM, a quantitative relationship between the operating parameters and controllable input variables is often required. Many regression techniques have been used for modelling the EDM process [41].

Neural networks and fuzzy systems form an alternative approach to generalize the experimental results and develop the system model accurately. Unlike milling and drilling operations, operating speeds in EDM are very low. Large electric current discharge can enhance speeds but reduces the dimensional quality of machined surface. Similarly, the material removal rate is also affected by other process parameters. These parameters are selected from standard tables or by experience to improve the output performance of the process. Even in the computer controlled environments involving online process control, this selection is not an easy task. Presently many optimization techniques are being used in EDM practice to obtain the best process parameters. Kansal et al. adopted the response surface optimization scheme to select the parameters in powder mixed EDM process [42]. The next year Keskin et al. used design of experiments (DOE) for the determination of the best machining parameters in EDM [43].

The approaches based on DOE are well suited to obtain optimal parametric combination for a single response problem. The methods break down when multiple responses are simultaneously optimized due to some technical and practical reasons. In this direction, Su and Tong indicated that Taguchi method can satisfactorily address a single response problem. However, they proposed that principal component analysis can be combined with Taguchi method to optimize the multi-response production process [44]. Tong et al. proposed a methodology that combines

principal component analysis with TOPSIS method to convert multiple responses into a single equivalent response. The reason of applying PCA is to obtain uncorrelated principal components when PCA is applied to responses. Finally, closeness coefficient obtained through TOPSIS is treated as single response [45]. Tong and Su proposed a fuzzy TOPSIS method to convert multi-responses (deposition thickness and refractive index) in plasma enhanced chemical vapor deposition (PECVD) process into single response. The relative closeness coefficient is regarded as a performance measurement index to find the optimal combination of eight controllable factors [46]. Tarng et al. have used fuzzy logic in Taguchi method for simultaneous optimization of multiple responses in a submerged arc welding process. The process parameters viz., arc current, arc voltage, welding speed, electrode protrusion, and preheat temperature are optimized with considerations of the responses such as deposition rate and dilution. The optimal setting suggested by Taguchi method is tested through few confirmatory tests [47]. To solve this type of multi-optimization problem in EDM, Lin et al. used grey relation analysis based on an orthogonal array and fuzzy based Taguchi method [48, 49, 50].

2.5. Soft computing model of EDM

Researchers, of late, are focusing upon employment of artificial intelligence (AI) techniques viz. ANN, GA, fuzzy logic, etc. for the process modelling and optimization of manufacturing processes which are expected to overcome some of the limitations of conventional process modelling techniques. Genetic algorithm (GA) with artificial neural network (ANN) is used to find out optimal process parameters for improving performances in EDM process using graphite as tool and nickel based alloy as work piece [51]. A similar approach has been considered by Su et al. from the rough cutting to the finish cutting stage. In most of the studies, multiple objectives are transformed into a single objective and attempts to find optimal parameters [52]. However, non-dominated sorting genetic algorithm (NSGA) is used to optimize machining parameters in WEDM considering surface roughness and cutting speed as the output parameters. Multiple linear regression models have been developed to represent the relation between inputs and outputs [53]. Mandal et al. used neural networks to predict the MRR and Ra trained by experimental data from EDM of SiC and multiple response problem is solved using NSGA-II by getting pareto-optimal solution [54]. In order to overcome the single response optimization problem of Taguchi method, Liao proposed an effective procedure called PCR-TOPSIS that is

based on process capability ratio (PCR) theory and on the theory of order preference by similarity to the ideal solution (TOPSIS) to optimize multi-response problems [55]. Two case studies performed by Tarang et al. [56] and Reddy et al. [57] were resolved using the proposed method and the result shows that PCR-TOPSIS can yield a good solution for multi-response problems.

Antony et al. have used Taguchi design and proposed a neuro-fuzzy system for simultaneous optimization of multiple responses [58]. A back propagation neural network (BPNN) with Levenberg-Marquardt (LM) algorithm have proposed by Panda and Bhoi [59] for the prediction of MRR. Recently, simulated annealing (SA) technique with ANN approach has been used for optimization of MRR and surface roughness [60]. The material removal rate has been optimized in micro-EDM usingartificial neural network and genetic algorithms [61].

Particle swarm optimization (PSO) is a computational simulation technique based on the movement of organisms such as flocks of birds and schools of fish used to solve optimization problems. It has a population of search points to probe the search space where each individual is referred as a 'particle' and represents a potential solution. These are associated with the best solution (fitness) it has achieved so far known as personal best (pbest) and overall best value and its location obtained so far by any particle in the population. This location is global best (gbest). Each particle moves its position in search domain and updates its velocity according to its own flying experience toward its pbest and gbest locations [62]. Neural network and non-dominating sorting genetic algorithm (NSGA II) is used to optimize the surface roughness and material removal rate of electro discharge machining of SiC parameters simultaneously. The effect of discharge current (Ip), pulse on time (Ton), pulse off time (Toff) on MRR and surface roughness were studied [63]. A multiple regression model is used to represent relationship between input and output variables of Wire-EDM process and a multi-objective optimization method based on a non-dominated sorting genetic algorithm (NSGA) is used to optimize machining performance such as cutting velocity and surface finish [64].

2.6. Technological modification of basic EDM

Many researchers have been carried out by modifying EDM process, changing dielectric or modifying dielectric medium. A silicon powder mixed electrical discharge machining experiment has been carried out and response surface methodology is used to plan the

experiment. The effect of process parameters such as pulse-on-time, discharge current, duty cycle and concentration of the silicon powder on material removal rate and surface roughness are analyzed. It is observed that MRR is increasing with concentration of silicon powder and discernible improvement in surface roughness is observed with suspended silicon powder [65]. An ultrasonic assisted dry machining experiment has been conducted with powder additives. It is observed that EDM with powder additives is concerning more on increasing surface quality and material removal rate [66]. Aluminium powder mixed electric discharge machining of hastelloy material is conducted to analyze the effect of machining parameter such as discharge current, gap voltage, pulse-on-time and duty cycle on material removal rate, tool wear rate and surface roughness. It is observed that all process parameter have strong influence on MRR, TWR, wear ratio and surface roughness [67].

2.7. Conclusions

This chapter provide the insight into basic EDM process, technologically modified EDM process, different modelling technique, some optimization technique to optimize EDM performance and some soft computing techniques. The next chapter describes the experimental details in this study.

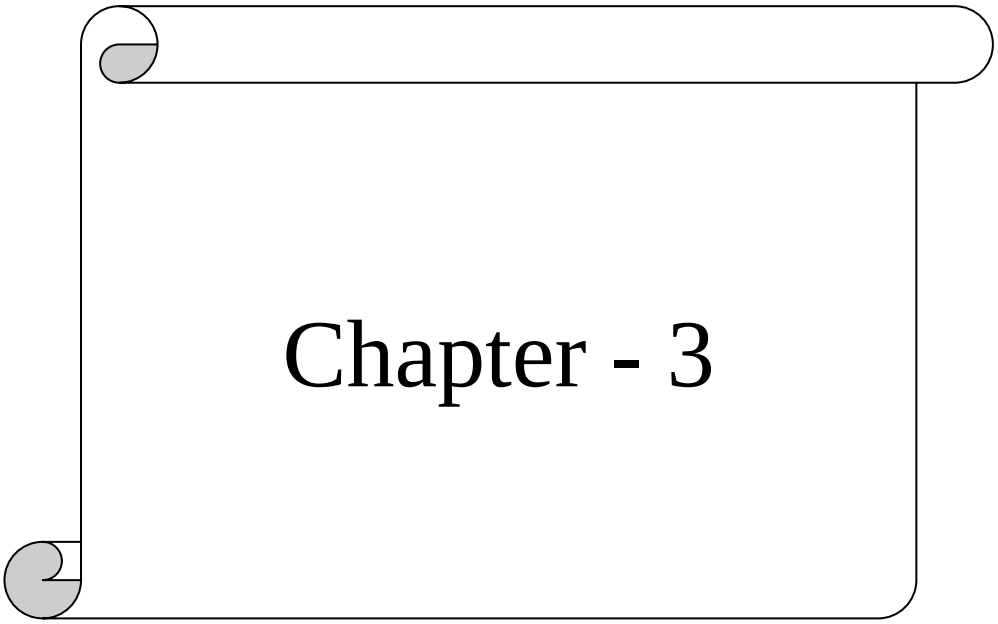
Chapter - 3

Chapter 3

EXPERIMENTAL DETAILS

3.1. Introduction

EDM has significant advantages in terms of machining high strength to weight ratio material, high strength to volume ratio material, the flexibility and the possibility of producing very complex parts and shapes. One of the current challenges faced by EDM users is the improvement of quality and productivity of parts produced, which is allied with the accurate application of the specified performance. This makes it essential to understand the performance of EDM process with the variation of process parameters so make them reliable for industrial applications. To achieve this, the present chapter describes the materials and methods used for the testing of EDM process under investigation. It presents the details of material property, sample preparation, measurements. Material removal rate (MRR), tool wear rate (TWR), surface roughness (Ra) and circularity characteristics are considered as measure of process quality and productivity in accordance to industrial requirements. The methodology related to the design of experiment technique based on response surface method (RSM) is presented in this part of the thesis.

3.2. Set up

Experiments are carried out in a die sinking EDM machine (ELECTRONICA-ELECTRAPULS PS 50ZNC) shown in Figure 3.1 with servo-head (constant gap). The specification of machine is given in Table 3.1. Commercial grade EDM oil (specific gravity= 0.763, freezing point= 94°C) was used as dielectric fluid. Positive polarity for electrode and side flushing was used to conduct the experiments.

Figure 3.1. Die Sinker EDM Model: PS 50ZNC

Table 3.1. Specification of PS 50ZNC

Mechanism of process	Controlled erosion (melting and evaporation) through a series of electric spark
Spark gap	0.010- 0.500 mm
Spark frequency	200 – 500 kHz
Peak voltage across the gap	30- 250 V
Metal removal rate (max.)	5000 mm^3/min
Specific power consumption	2-10 W/mm^3/min
Dielectric fluid	EDM oil, Kerosene, liquid paraffin, silicon oil, deionized water etc.
Tool material	Copper, Brass, graphite, Ag-W alloys, Cu-W alloys .
Materials that can be machined	All conducting metals and alloys.
Shapes	Microholes, narrow slots, blind cavities
Limitations	High specific energy consumption, non-conducting materials can't be machined.

3.3. Work piece material

Steel is the common name for a large family of iron alloys. Steels can either be cast directly to shape, or into ingots which are reheated and hot worked into a wrought shape by forging, extrusion, rolling, or other processes. Wrought steels are the most common engineering material used, and come in a variety of forms with different finishes and properties. Tool steels typically have excess carbides (carbon alloys) which make them hard and wear-resistant. Most tool steels are used in a heat-treated state, generally hardened and tempered. The material used as work piece for electrical discharge machining is AISI D2 steel, which is basically an air-hardened high carbon, high chromium tool steel alloyed with molybdenum and vanadium characterized by:

- High wear resistance
- High compressive strength
- Good through-hardening properties
- High stability in hardening
- Good resistance to tempering-back
- Moderate toughness (shock-resistance)

Composition

It is composed of (in weight percentage) 1.55% Carbon (C), 0.60% Manganese (Mn), 0.60% Silicon (Si), 11.8% Chromium (Cr), 0.30% Nickel (Ni), 0.8% Molybdenum (Mo), 0.8% Vanadium (V), 1.00% Cobalt (Co), 0.25% Copper (Cu), 0.03% Phosphorus (P), 0.03% Sulphur (S), and the base metal Iron (Fe). Other designations of AISI D2 tool steel include UNS T30402. Table 3.2 list the properties of commercially available AISI D2 steel.

Table 3.2. Properties of AISI D2 steel

Property	**Value**	**Unit**
Density	7700	kg/m^3
Mechanical property		
Hardness Rockwell R	57	HRC
Tensile Strength	1736	MPa
Modulus of elasticity	200	GPa
Poissions ratio	0.29	
Thermal properties		
Thermal Conductivity	20	W/m-K
Thermal expansion,	10.4×10^{-6}	Per °C

Machinability

AISI D2 steel has a machinability rating 65, as compared with a rating of 100 for a 1% carbon tool steel [68]. Since AISI D2 steel has conductive in nature it is also suitable for electrical discharge machining process.

Application

Manufacturing sectors especially industries

- Aerospace
- Ordnance
- Automobile
- General engineering
- Die making
- Tool material

3.4. Sample preparation

The material, AISI D2 steel has brought in the form of bar of 85 mm diameter and 300 mm length. This is cut into round plates of size 85 mm diameter and 6 mm thickness, that suitable for machining. Then the sample is grind and properly cleaned to get flat surface.

3.5. Tool preparation

Since a large amount of heat is dealt in EDM owing to spark, the tool should be of a good conductive material with high melting point. Therefore, pure brass and pure copper are taken as the tool material having density 8400 kg/m^3 and 8940 kg/m^3 respectively. Two stepped tool of 25 mm machining diameter and 10 mm shank is made from a 25 mm diameter bar.

Figure 3.2. Brass Tool

Figure 3.3. Copper Tool

3.6. Measurements

3.6.1.Weighing machine

The weight of work piece and tool has taken by high precision balance Figure 3.4. This machine capacity is 300 gram and accuracy is 0.001 gram and Brand: SHINKO DENSHI Co. LTD, JAPAN, and Model: DJ 300S.

Figure 3.4. Electronic Balance weight machine

3.6.2.Talysurf

Surface roughness measurement was carried out using a portable stylus type profilometer, Talysurf (Taylor Hobson, Surtronic 3+) as shown in Figure 3.5. The roughness measuring

conditions are shown in Table 3.3. Roughness measurements were carried out in the transverse direction. The measured profile was digitized and processed through the dedicated advanced surface finish analysis software Talyprofile for evaluation of the roughness parameters. Roughness is defined as the arithmetic value of the profile from the centreline along the length and can be express as

$$Ra = \frac{1}{L} \int \left| y(x) \right| d(x) \right\| \tag{3.1}$$

where L is the sampling length, y is the profile curve and x is the profile direction. The average 'Ra' is measured within L = 0.8 mm.

Figure 3.5. Talysurf

Table 3.3. Roughness measuring conditions

Condition	Value
Probe tip radius	0.005 mm
Measuring range	0.800 mm
Traverse length	4.000 mm
Speed	1.000 mm/s
Filter	2 CR

3.6.3.Microscope

The photo graphs of the machined parts were taken by microscope (RADIAL INS-TRUMENT) with Samsung camera setup (45X magnification) Figure 3.6.

Figure 3.6. Microscope with camera attachment

3.6.4.Scanning electron microscope

The surfaces of the specimens are examined directly by scanning electron microscope (SEM) JEOL JSM-6480LV as shown in Figure 3.7. The JEOL JSM-6480LV is a high-performance, scanning electron microscope with 1000 magnification. The low vacuum (LV) mode (which can be accessed by the click of a mouse), allows for observation of specimens which cannot be viewed at high vacuum due to excessive water content or due to a non-conductive surface. Its asynchronous five-axis stage can accommodate a specimen of up to 8-inches in diameter.

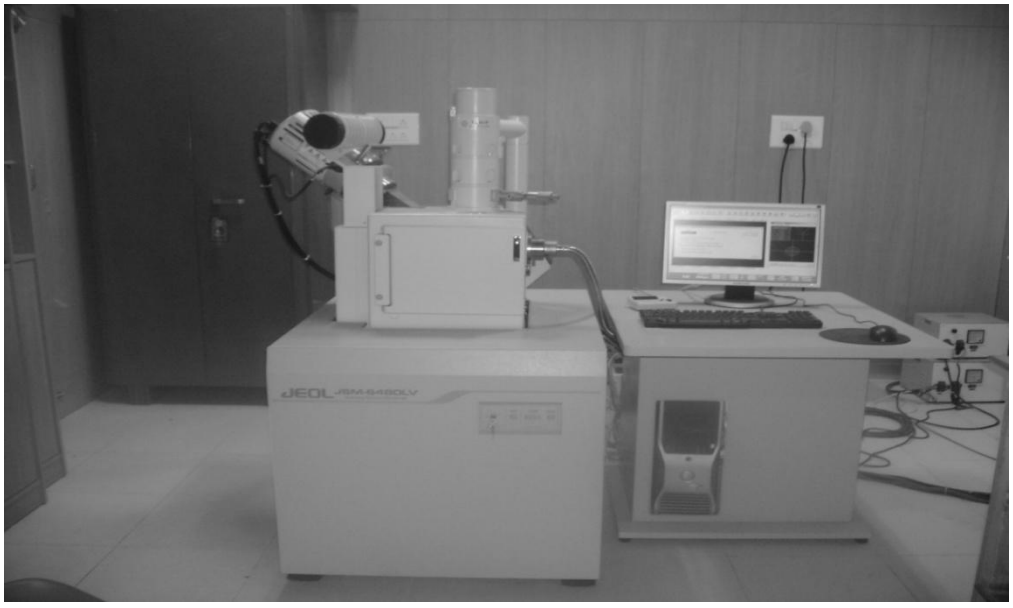

Figure 3.7. Scanning Electron Microscope (SEM).

3.7. Experimental design

A commonly use approach in scientific and engineering investigation is to study one factor at a time or study several factors one at a time. This approach has inherent disadvantages like, more experimental runs are require for the precision in effect estimation, factor interaction effects cannot be studied, conclusions are not general and may miss the optimal settings of factor. To overcome this problem design of experiment (DOE) is a scientific approach to effectively plan and perform experiments, using statistics and are commonly used to improve the quality of a products or processes. Such methods enable the user to define and study the effect of every single condition possible in an experiment where numerous factors are involved [69, 70]. EDM is such a process in which a number of control factors collectively determine the performance output in other words the part quality and productivity. Hence, in the present work a statistical technique called response surface methodology is used to optimize the process parameters leading to the improvement in performance output of the part under study. The most important stage in the DOE lies in the selection of the control factors and their levels. EDM process has large number of process related parameters which are defined in Table 3.4.

Based on initial trials and exhaustive literature review [71] four parameters namely, discharge current (Ip), pulse-on-time (Ton), duty factor (τ) and flushing pressure (Fp) are identified as significant factors and hence are selected to study their influence on output responses as material removal rate (MRR), tool wear rate (TWR), surface roughness (Ra) and circularity (r_1/r_2). The levels of factors are selected in accordance with the permissible minimum and maximum settings recommended by the equipment manufacturer, experience, and real industrial applications. The operating conditions under which tests are carried out are given in Table 3.5.

Table 3.4. Process parameters in EDM

Process parameter	Definition
Spark On-time (pulse time or Ton)	The duration of time (μs) the current is allowed to flow per cycle. Material removal is directly proportional to the amount of energy applied during this pulse-on-time. This energy is really controlled by the peak current and the length of the pulse-on-time.
Spark Off-time (pause time or Toff)	The duration of time (μs) between the sparks (that is to say, pulse-on-time). This time allows the molten material to solidify and to be wash out of the arc gap. This

	parameter is to affect the speed and the stability of the cut. Thus, if the off-time is too short, it will cause sparks to be unstable.
Arc gap (or gap)	The Arc gap is distance between the electrode and work piece during the process of EDM. It may be called as spark gap. Spark gap can be maintained by servo system.
Discharge current (Ip)	Current is measured in amp Allowed to per cycle. Spark energy is directly controlled by discharge current which leads to the Material removal rate.
Duty factor (τ)	Duty factor is the pulse-on-time relative to the total cycle time (Ton+Toff) and expressed in percentage. It refers to the stability of spark.
The open circuit voltage - V_o	V_o is the potential that can be measure by volt meter when there is no spark between electrodes.
The working voltage - V_w	V_w is the potential exerted during machining.
Polarity	There are two type of polarity according to the connectivity of work piece. If work piece is connected to anode then it is positive (+ve) polarity and if connected to cathode, it is negative (-ve) polarity. Positive polarity is significant to MRR and negative polarity is significant to surface roughness.
Flushing	Flushing is necessary to carry out the eroded material from work piece to avoid deposition.
Dielectric medium	Since EDM is spark erosion process a medium is necessary. Initially the medium is ionised and plasma channel is created which leads to spark.

Table 3.5. Factors and their levels

Parameters	Symbols	Level Codes		
		-1	0	1
Discharge current (Ip) in A	A	3	5	7
Pulse on time (Ton) in µs	B	100	200	300
Duty Factor (τ) in %	C	80	85	90
Flushing Pressure in bar	D	0.2	0.3	0.4

3.7.1.Response surface experimental design

Response surface methodology (RSM) is a collection of statistical and mathematical technique useful for developing, improving and optimizing process. It deals with the situation where several input variable potentially influence the performance measure or quality of the product or process. The performance measure or quality is known as response. Response surface methodology (RSM) quantifies the relationship between the controllable input parameters and the obtained response. The goal is to find a suitable approximation for the true functional relationship between independent variables and the response. Usually a second-order model as given in Eq. 3.2 is utilized in response surface methodology.

$$Y = \beta_0 + \sum_{i=1}^{k} \beta_i x_i + \sum_{i=1}^{k} \beta_{ii} x_i^2 + \sum_{i<j} \sum \beta_{ij} x_i x_j + \varepsilon \qquad (3.2)$$

where Y is the corresponding response of input variables X_i, X_i^2 and X_iX_j are the square and interaction terms of parameters respectively. β_0, β_i, β_{ii} and β_{ij} are the unknown regression coefficients and ε is the error.

A full factorial design would provide estimation of all the required regression parameters (β). However, full factorial designs are expensive to use as the number of runs increases rapidly with the number of factors. Therefore, for the purpose of analysis Box-Behnken design is useful as it help to fit the second order model to the response with the use of a minimum number of runs [69, 70]. Box-Behnken design performs non-sequential experiments. That is, only planning to perform the experiment once. These designs allow efficient estimation of the first- and second-order coefficients. Because Box-Behnken designs have fewer design points, they are less expensive to run than central composite designs with the same number of factors.

Box-Behnken designs can also prove useful in the safe operating zone for the process. Central composite designs usually have axial points outside the "cube" (unless it is specified less than or equal to one). These points may not be in the region of interest, or may be impossible to run because they are beyond safe operating limits. Box-Behnken designs do not have axial points, thus, it can be sure that all design points fall within the safe operating zone. Box-Behnken designs also ensure that all factors are never set at their high levels simultaneously. In practice, two or three centre runs are sufficient. In order to get a reasonable estimate of experimental error, three centre runs are chosen in the present work. Twenty seven base runs including three centre points are generated in MINITAB 15 as shown in Table 3.6.

Table 3.6. Experimental plan for Box-Behnken design

Run Order	Ip(A)	Ton(B)	τ(C)	Fp(D)
1	0	-1	0	1
2	0	0	1	-1
3	-1	0	1	0
4	1	0	0	-1
5	0	0	0	0
6	0	0	0	0
7	0	0	-1	1
8	-1	0	0	1
9	-1	-1	0	0
10	0	-1	1	0
11	1	1	0	0
12	1	-1	0	0
13	0	1	0	1
14	0	0	-1	-1
15	0	1	1	0
16	0	1	0	-1
17	0	0	1	1
18	1	0	-1	0
19	0	-1	0	-1
20	0	-1	-1	0
21	0	1	-1	0
22	1	0	0	1
23	-1	1	0	0
24	-1	0	-1	0
25	-1	0	0	-1
26	0	0	0	0
27	1	0	1	0

3.8. Data collection

Four controllable parameters such as discharge current (Ip), pulse-on-time (Ton), duty factor (τ) and flushing pressure (Fp) are considered in this study. The experimental design is made as per Box-Behnken design of response surface methodology because it is capable of generating a satisfactory prediction model with few experimental runs [72, 73]. In three level four factor experimental design, the total number of experimental runs is twenty seven having three center points. To run the experiment smoothly the parametric levels are decoded using the Eq. 3.3.

$$\text{Coded Value } (Z) = \frac{X - \frac{X_{max} + X_{min}}{2}}{\frac{X_{max} - X_{min}}{2}} \quad (3.3)$$

where Z is coded value (-1, 0, 1), X_{max} and X_{min} is maximum and minimum value of actual variable and X is the actual value of corresponding variable.

The weight of tool and work piece is taken and positioned at two electrodes. Each experiment is carried out for one hour and final weight of tool and work piece is measured. The initial weight and final weight for different experiment along with surface roughness are listed in Table 3.7 and Table 3.8. Table 3.7 and Table 3.8 shows experimental table for brass and copper tool, AISI D2 steel tool work piece combination respectively.

Table 3.7. Experiment table for brass AISI D 2 steel combination

Expt. No.	Ip (A)	Ton (µs)	τ (%)	Fp (bar)	Initial Wt. (Job)	Final Wt. (Job)	Initial Wt. (Tool)	Final Wt. (Tool)	Ra
1	3	100	85	0.3	244.261	243.534	213.45	212.503	3.93
2	7	100	85	0.3	243.534	241.976	212.503	210.712	4.57
3	3	300	85	0.3	241.976	241.229	210.597	209.955	4.65
4	7	300	85	0.3	239.166	235.915	208.967	207.289	7.59
5	5	200	80	0.2	245.607	244.261	214.428	213.45	6.52
6	5	200	90	0.2	215.439	213.562	200.44	198.822	6.15
7	5	200	80	0.4	213.562	212.209	188.685	187.624	6.4
8	5	200	90	0.4	208.646	206.72	177.531	175.858	5.93
9	3	200	80	0.3	239.928	239.207	207.284	206.614	5.17
10	7	200	80	0.3	239.207	236.76	206.614	205.166	6.47
11	3	200	90	0.3	236.76	235.801	205.166	204.188	4.55
12	7	200	90	0.3	235.801	232.924	204.188	201.853	5.48
13	5	100	85	0.2	232.924	231.734	201.853	200.44	5.49
14	5	300	85	0.2	231.732	230.023	195.305	194.178	7.35
15	5	100	85	0.4	230.02	228.851	194.178	192.749	5.07
16	5	300	85	0.4	228.851	227.145	192.749	191.599	7.46
17	3	200	85	0.2	249.21	248.337	217.197	216.378	5.27
18	7	200	85	0.2	248.337	245.607	216.378	214.428	7.73
19	3	200	85	0.4	227.145	226.278	191.599	190.736	4.69
20	7	200	85	0.4	226.278	223.508	190.736	188.683	6.83
21	5	100	80	0.3	212.209	211.276	187.624	186.586	4.28
22	5	300	80	0.3	211.276	209.86	180.026	179.152	8.51
23	5	100	90	0.3	209.86	208.648	179.152	177.532	4.47
24	5	300	90	0.3	206.72	204.757	175.858	174.475	7.79
25	5	200	85	0.3	204.757	203.072	174.475	173.083	6.21
26	5	200	85	0.3	203.072	201.417	173.083	171.636	5.77
27	5	200	85	0.3	201.417	199.777	171.636	170.219	5.8

Table 3.8. Experiment table for copper AISI D 2 steel combination

Expt. No.	Ip (A)	Ton (µs)	τ (%)	Fp (bar)	Initial Wt. (Job)	Final Wt. (Job)	Initial Wt. (Tool)	Final Wt. (Tool)	Ra
1	3	100	85	0.3	193.862	192.495	162.795	162.788	3.61
2	7	100	85	0.3	192.495	186.496	162.788	162.765	6.38
3	3	300	85	0.3	186.496	185.889	162.765	162.762	2.6
4	7	300	85	0.3	185.889	181.45	162.762	162.749	4.3
5	5	200	80	0.2	181.447	179.097	162.727	162.724	4.33
6	5	200	90	0.2	179.097	175.815	162.724	162.719	4.6
7	5	200	80	0.4	175.815	173.403	162.719	162.715	5.1
8	5	200	90	0.4	173.403	169.997	162.684	162.679	4.52
9	3	200	80	0.3	170.001	168.988	162.673	162.67	3.42
10	7	200	80	0.3	168.988	164.93	162.67	162.656	6.11
11	3	200	90	0.3	232.859	231.558	162.65	162.646	2.83
12	7	200	90	0.3	231.558	224.684	162.646	162.639	5.38
13	5	100	85	0.2	224.684	221.74	162.639	162.621	4.78
14	5	300	85	0.2	221.74	220.057	162.62	162.611	3.92
15	5	100	85	0.4	220.053	217.02	152.271	152.265	5.54
16	5	300	85	0.4	217.02	215.216	152.265	152.259	3.22
17	3	200	85	0.2	234.119	232.857	162.86	162.856	3.11
18	7	200	85	0.2	214.07	208.685	152.254	152.245	5.45
19	3	200	85	0.4	215.216	214.07	152.259	152.254	3.21
20	7	200	85	0.4	208.685	203.15	152.245	152.225	6.33
21	5	100	80	0.3	179.9	177.241	152.22	152.207	5.42
22	5	300	80	0.3	177.241	175.699	149.535	149.53	4.27
23	5	100	90	0.3	175.699	172.057	149.53	149.52	4.67
24	5	300	90	0.3	172.057	170.034	149.52	149.514	3.64
25	5	200	85	0.3	170.034	167.37	149.514	149.507	3.8
26	5	200	85	0.3	167.37	164.691	149.507	149.503	4.24
27	5	200	85	0.3	164.691	162.077	149.503	149.497	4.52

3.9. Calculation of response

3.9.1 Material removal rate (MRR): The weight of work piece before machining and after machining is found form experiment is shown in Table 3.7 and Table 3.8 is utilised to calculate material removal rate (MRR) using Eq. 3.4.

$$MRR = \frac{1000 \times \Delta Ww}{\rho_W \times T} \tag{3.4}$$

Where ΔWw is weight of material removed from work piece during machining, ρ_W is the density of work piece, T is the machining time.

3.9.2 Tool wear rate (TWR): The weight of tool before machining and after machining is found form experiment is shown in Table 3.7 and Table 3.8 is utilised to calculate tool wear rate (TWR) using Eq. 3.5.

$$TWR = \frac{1000 \times \Delta Wt}{\rho_t \times T} \tag{3.5}$$

ΔWt is the weight of material removed from tool during machining, ρt is the density of the tool, T is the machining time.

3.9.3 Roughness is measured by portable stylus type profilometertalysurf (Taylor Hobson, Surtronic 3+).

3.9.4 Circularity is measured as the ratio of minimum to maximum Feret's diameter. Feret's diameter is the distance between two parallel tangents on two opposite sides of the hole as shown in Figure 3.8 [74]. The diameters are measured using magnified photographs obtained through microscope (RADIAL INSTRUMENT with Samsung camera setup, 45-X magnification.

The responses MRR, TWR, Ra and Circularity are calculated and listed in Table 3.9 and Table 3.10.

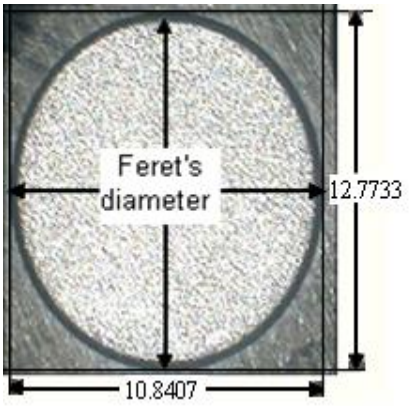

Figure 3.8. Feret's diameter

Table 3.9. Response table using brass tool

Expt. No.	Ip (A)	Ton (µs)	τ (%)	Fp (bar)	MRR (mm^3/min)	TWR (mm^3/min)	Ra (µm)	circularity
1	3	100	85	0.3	1.573593	1.842771	0.85	3.93
2	7	100	85	0.3	3.372294	3.485114	0.852	4.57
3	3	300	85	0.3	1.616883	1.24927	0.8842	4.65
4	7	300	85	0.3	7.036797	3.265227	0.8557	7.59
5	5	200	80	0.2	2.91342	1.903094	0.8488	6.52
6	5	200	90	0.2	4.062771	3.148472	0.852	6.15
7	5	200	80	0.4	2.928571	2.064604	0.8375	6.4
8	5	200	90	0.4	4.168831	3.255497	0.8598	5.93
9	3	200	80	0.3	1.560606	1.303756	0.8366	5.17
10	7	200	80	0.3	5.296537	2.817669	0.8888	6.47
11	3	200	90	0.3	2.075758	1.903094	0.8435	4.55
12	7	200	90	0.3	6.227273	4.543686	0.8028	5.48
13	5	100	85	0.2	2.575758	2.749562	0.8275	5.49
14	5	300	85	0.2	3.699134	2.193034	0.8461	7.35
15	5	100	85	0.4	2.530303	2.780697	0.8411	5.07
16	5	300	85	0.4	3.692641	2.237789	0.8439	7.46
17	3	200	85	0.2	1.88961	1.593695	0.8494	5.27
18	7	200	85	0.2	5.909091	3.794513	0.8424	7.73
19	3	200	85	0.4	1.876623	1.679315	0.8383	4.69
20	7	200	85	0.4	5.995671	3.994941	0.8397	6.83
21	5	100	80	0.3	2.019481	2.019848	0.8329	4.28
22	5	300	80	0.3	3.064935	1.70072	0.8479	8.51
23	5	100	90	0.3	2.623377	3.152364	0.8536	4.47
24	5	300	90	0.3	4.248918	2.691185	0.8369	7.79
25	5	200	85	0.3	3.647186	2.708698	0.8402	6.21
26	5	200	85	0.3	3.582251	2.815723	0.8366	5.77
27	5	200	85	0.3	3.549784	2.757346	0.846	5.8

Table 3.10. Response table using copper tool

Expt. No.	Ip (A)	Ton (µs)	τ (%)	Fp (bar)	MRR (mm^3/min)	TWR (mm^3/min)	Ra (µm)	circularity
1	3	100	85	0.3	2.9589	0.01305	3.61	0.8403
2	7	100	85	0.3	12.9848	0.042878	6.38	0.8437
3	3	300	85	0.3	1.3139	0.005593	2.6	0.818
4	7	300	85	0.3	9.6082	0.024236	4.3	0.8415
5	5	200	80	0.2	5.0866	0.005412	4.33	0.8437
6	5	200	90	0.2	7.1039	0.009321	4.6	0.8437
7	5	200	80	0.4	5.2208	0.009457	5.1	0.835
8	5	200	90	0.4	7.3723	0.009321	4.52	0.8412
9	3	200	80	0.3	3.189	0.005312	3.42	0.8211
10	7	200	80	0.3	10.32	0.0261	6.11	0.8442
11	3	200	90	0.3	2.816	0.007457	2.83	0.8402
12	7	200	90	0.3	14.587	0.016	5.38	0.8469
13	5	100	85	0.2	6.3723	0.027	4.78	0.8524
14	5	300	85	0.2	3.6429	0.012779	3.92	0.8355
15	5	100	85	0.4	6.5649	0.019	5.54	0.8351
16	5	300	85	0.4	3.9048	0.007	3.22	0.8453
17	3	200	85	0.2	2.7316	0.007457	3.11	0.8397
18	7	200	85	0.2	11.6558	0.018779	5.45	0.8446
19	3	200	85	0.4	2.4805	0.000321	3.21	0.84
20	7	200	85	0.4	11.9805	0.033286	6.33	0.8402
21	5	100	80	0.3	5.7554	0.024236	5.42	0.8392
22	5	300	80	0.3	3.3377	0.009321	4.27	0.8451
23	5	100	90	0.3	7.8831	0.018643	4.67	0.8443
24	5	300	90	0.3	4.817	0.011186	3.64	0.8344
25	5	200	85	0.3	5.7662	0.01305	3.8	0.84
26	5	200	85	0.3	5.7987	0.007457	4.24	0.8531
27	5	200	85	0.3	5.658	0.011186	4.52	0.8467

3.10. Conclusions

This chapter summarizes the experimental details that uses in present study and the responses are obtained. The next chapter is the optimization strategy used in present study.

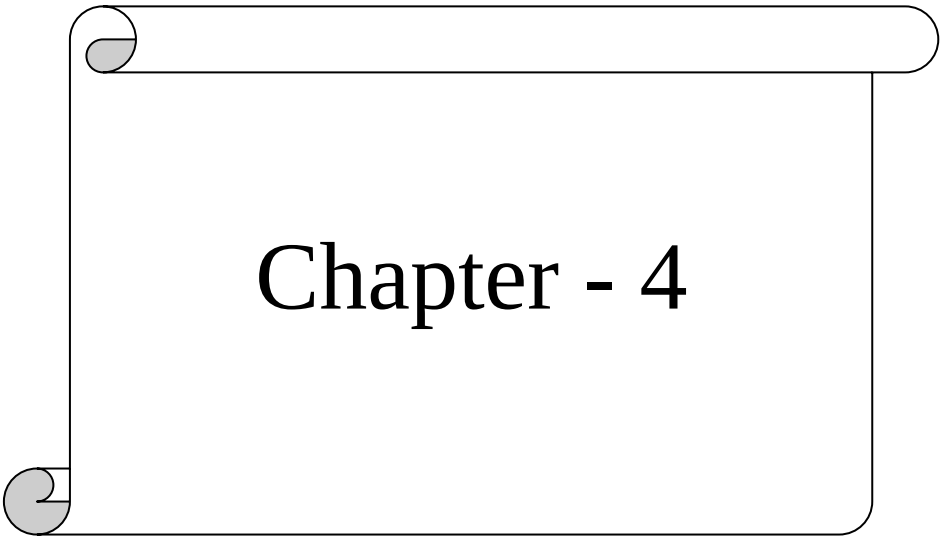
Chapter - 4

Chapter 4

OPTIMIZATION STRATEGY

4.1. Introduction

Optimization is a mathematical tool used to find the minima and maxima of functions subjected to constraints. In engineering and management, optimization or mathematical programming is generally used to select best element from some set of available alternatives. Optimization originated in the 1940s by George Dantzig to use mathematical techniques for generating programs (training timetables and schedules) for military application. Responses may not have same nature like productivity and quality are equally important for an production industry, but it is observed that better productivity is achieved with less quality. Optimization of both quality and productivity to find a setting of input factors from a number of alternatives is known as multiple response optimization. Therefore in case of multiple responses, it is need to convert them to equivalent single response. The present study represents a neuro-fuzzy method to convert the four responses to an equivalent single response. Optimization techniques like genetic algorithm, particle swarm optimization are proposed to optimize single response or equivalent single response. An intelligence technique, non-dominated shorting genetic algorithm (NSGA) is used to optimize multi-responses without converting them equivalent responses.

4.2. Multi-response optimization using NEURO-FUZZY system

This paper presents a structured and generic methodology that includes both RSM as well as AI tools to minimize the uncertainty in decision-making. The proposal is to map out multiple responses into a single performance characteristic index (MPCI) through neuro-fuzzy based model. Assume *n* experiments are conducted utilizing RSM and responses obtained as MRR, TWR, Ra, Circularity. Responses are divided into three main types: the smaller-the better (STB), the nominal-the-best (NTB), and the larger the-better (LTB) responses. In practice, all the responses are not of same category. Therefore, characteristic responses are converted to respective S/N ratios as follows [75]:

The larger-the-best performance characteristic can be expressed as:

$$\text{S/N ratio} = -10\,\text{Log}_{10}(1/n\ \Sigma\ 1/Y_i^2) \quad (4.1)$$

The smaller-the-best performance characteristic can be expressed as:

$$\text{S/N ratio} = -10\,\text{Log}_{10}(1/n\ \Sigma Y_i^2) \quad (4.2)$$

where Y_i is the i^{th} experimental data of response.

All the S/N ratio responses (X_{ij}) are normalized to obtain normalized response (Z_{ij}) so that they lie in the range, $0 \leq Z_{ij} \leq 1$. Normalization is carried out to avoid the scaling effect and minimize the variation of S/N ratio obtained at different scales. For responses of larger-the-better and smaller-the-better type, normalization is carried out using Eq. 4.3 [76].

$$Z_{ij} = \frac{X_{ij} - \min\{X_{ij}, j = 1,2,.....,n\}}{\max\{X_{ij}, j = 1,2,.....,n\} - \min\{X_{ij}, j = 1,2,.....,n\}} \quad (4.3)$$

Systems, where relationship between the input and output is highly nonlinear or not known at all, fuzzy logic can be effectively applied to classify the input and output data sets broadly into different fuzzy classes. There are many ways of assigning membership function to crisp data sets, for example by intuition, by inference, and by applying some AI tools. Data points are divided into different classes using conventional clustering technique. The two most popular methods of clustering the data are hard c mean clustering (HCM), and fuzzy c-mean clustering (FCM). HCM is used to classify data in a crisp sense. In this method, each data point is assigned a single membership in any one, and only one, data cluster. FCM extends the crisp classification idea into a fuzzy classification notion. Thus, the membership to the various data points can be assigned in each fuzzy set (fuzzy class, fuzzy cluster).With the restriction (analogous to the crisp classification) that the sum of all membership values for a single data point in all of the classes has to be unity. It is advantageous to use the FCM as it minimizes the uncertainty in assigning the membership function of a crisp data into various fuzzy classes. Basically, fuzzy c-means algorithm calculates fuzzy partition matrix to group some of data points into c clusters. Therefore, the aim is to cluster centers (centroids) that minimize dissimilarity function (J_m) [75].

$$J_m(U^*, v^*) = \min[J_m(U, v)] = \min\left[\sum_{k=1}^{n}\sum_{i=1}^{c}(\mu_{ik})^m (d_{ik})^2\right] \quad (4.4)$$

where, μ_{ik} is the membership value of the k^{th} data point in the i^{th} cluster, m' is weighting parameter varying in the range $[1, \infty]$, U is fuzzy partition matrix, viz cluster center matrix, and d

is similarity matrix given in Eq. 4.5. Utilizing the Euclidean distance measure to characterize the similarity, the elements of d are calculated by:

$$d_{ik} = d(x_k - v_i) = \|x_k - v_i\| = \sqrt{\sum_{j=1}^{m}(x_{jk} - v_{ij})^2} \quad \text{(for i = 1 to c and k = 1 to n)} \tag{4.5}$$

where m is the number of features, x_k is k^{th} data point and v_i is the centroid of i^{th} cluster that can be presented by:

$$v_i = \{v_{i1}, v_{i2}, \ldots\ldots v_{im}\} \text{ (for i = 1 to c)} \tag{4.6}$$

In addition, cluster centers are calculated using following formulation

$$v_{ij} = \frac{\sum_{k=1}^{n} \mu_{ik}^{m} x_{kj}}{\sum_{k=1}^{n} \mu_{ik}^{m}} \quad \text{(for i =1 to c and j = 1 to m)} \tag{4.7}$$

where, x is fuzzy variable describing data point. In essence, fuzzy partitioning is performed through an iterative optimization utilizing following formulation:

$$u_{ik}(s+1) = \frac{1}{\sum_{j=1}^{c}\left(\frac{d_{ik}(s)}{d_{jk}(s)}\right)^{\frac{2}{m-1}}} \tag{4.8}$$

It should be noted that, sum of membership values for a cluster must be equal to 1 i.e.

$$\sum_{i \in I_k} \mu_{ik} = 1 \tag{4.9}$$

Finally, the best available solution within a predefined accuracy criterion is determined by:

$$\left\|U^{(r+1)} - U^{(r)}\right\| \leq \in \tag{4.10}$$

where ε is error level for the termination of iteration which varies between 0 and 1. In detail, this iterative procedure converges to a local minimum of $\mathbf{J_m}$. Algorithmically; fuzzy c-means methodology can be explained as given below (Figure 4.1).

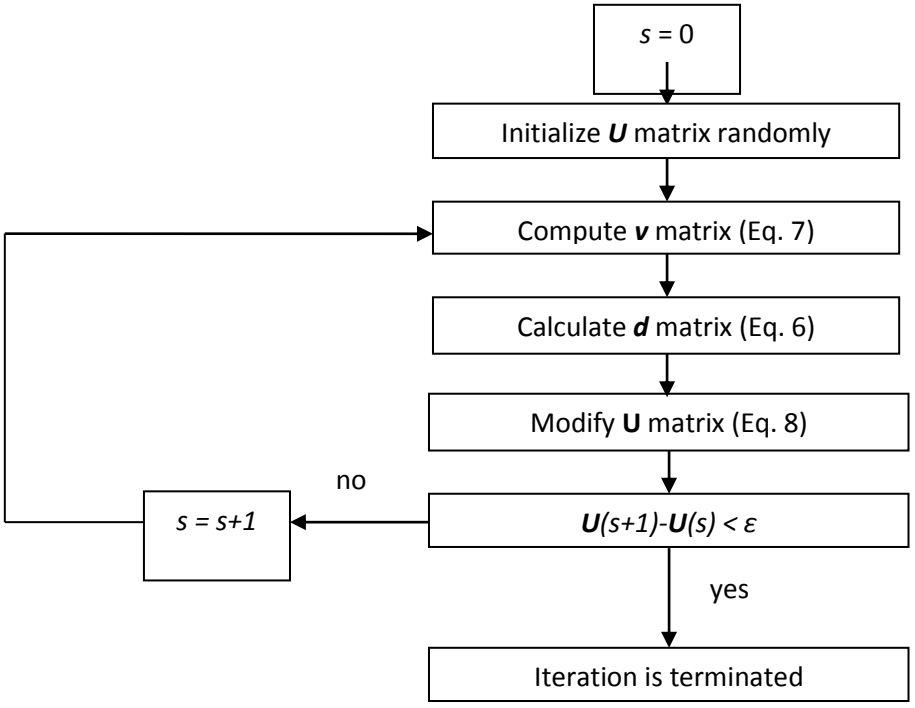

Figure 4.1. Flow Chart for fuzzy c-mean clustering

The membership function is repeatedly updated when the system parameters continuously changes in a non-deterministic fashion. Neural network is used for these types of systems, as it is capable of modifying itself by adapting the weights. Neural network do not learn by adding new rules to their knowledge base, they can learn by modifying their overall structure. In this paper, a back propagation neural network (BPN) is used to generate the fuzzy membership function for fuzzy classes of an output-data set. BPN is applied that uses each data in training-data set and corresponding membership values indifferent class, obtained by FCM, for training itself to simulate the relationship values between input data and membership values. Using BPN, each training-data set can be assigned a membership value in different fuzzy classes. Testing-data set is used to check the performance of neural network. Once the neural network is trained, its final version can be used to determine the membership values of any input data in the different fuzzy classes.

Neural network basically use models that simulate the working model of the neurons in the human brain. It consists of two fixed layers an input layer and an output layer and one or more hidden layers. In the input layer, number of neuron is equal to number of input data to the neural network and in output layer, the number on neuron is equal to the number of output, but in hidden layer the number of neurons are optimized to minimize the error between the input and

output predicted value. Among the neural network models, supervised learning neural networks are used to solve the parameter design problem with multiple responses and to establish a functional relationship between control factors and quality characteristic. In neural network, a set of training input data along with a corresponding set of output data is trained to adjust the weights in a network. Then, the well trained network is used to predict the membership functions to different fuzzy classes (clusters).The architecture of a typical m-h-n neural network indicates a basic three layered BPN represented by m-h-n neural model, where parameters m, h and n are the total number of neurons in input, hidden and output layers, respectively. For a multiple input and multiple output system, the data set for input and output comprising of vectors $\{(x_1; x_2; x_3. . .x_n); (y_1; y_2; y_3. . y_n)\}$ are used. A weight w_i as path joiner are randomly assigned in different layers. Then, an input x from the training-data set is passed through the neural network, corresponding to which an output y is computed and compared with desired output. The error (e) is computed as:

$$e=y_{actual}-y_{desired} \quad (4.11)$$

Error e is distributed to the neurons in hidden layer using a technique called back-propagation. The different weights w_i connecting different neurons in the network are updated as:

$$W_i(new)= W_i(old)+\alpha e x_i \quad (4.12)$$

where α is learning rate, e is associated error, x_i input to the i-th neuron.

Learning rate is defined as the rate by which a neural network updates its weight to minimize the error. It should be kept low to escape the local optima. The input value x_i is again passed through the neural network with updated weights, and the errors are computed. This iteration technique is continued until the error value of the final output is within the prescribed limit. This procedure is continued for all data in the training-data set. Then, a testing-data set is used to verify the efficiency of the neural network to simulate the nonlinear relationship. When network attains a satisfactory level of performance, a relationship between input and output data established and the weights are used to recognize the new input patterns.

It is advantageous to use the FCM as it minimizes the uncertainty in assigning the membership function of a crisp data into various fuzzy classes. Then, a BPN is applied that uses each data in training-data set and corresponding membership values in different class, obtained by FCM, for training itself to simulate the relationship values between input data and membership values. By the BPN method each training-data set can be assigned a membership value in different fuzzy

classes. Once the neural network is trained, its final version can be used to determine the membership values of any input data in the different fuzzy classes.

Defuzzification is the conversion of a fuzzy quantity to a precise quantity. Among the various methods, the COA method is used for defuzzifying fuzzy output function into a crisp data [77, 78]. In this method, the fuzzy output $\mu_A(y)$ transform into a crisp value y. It is given by the expression as in Eq.4.13.

$$y = \frac{\int \mu_A(y).ydy}{\int \mu_A(y)dy} \tag{4.13}$$

4.3. Optimization technique

4.3.1 Particle swarm optimization

In this study, the basic PSO algorithm is described, followed by a discussion on side and functional constraint handling, and finally, a discrete version of the algorithm is presented. Particle swarm optimization (PSO) is a stochastic optimization algorithm that was originally motivated by the thinking model of an individual of the social organism such as birds, fish, etc. by Kennedy and Eberhart [79]. The PSO has particles driven from natural group with communications based on evolutionary computation and it combines self-experiences with social experiences. Here a contestant is considered as a particle and the objective is to get a global optimum. This algorithm uses a collection of flying particles in a search area as well as the movement towards a promising area. The flying particle is compared with changing solutions and search area is compared with current and possible solutions [80, 81]. It should be noted that while the GA is inherently discrete, i.e. it encodes the design variables into bits of 0's and 1's, therefore it easily handles discrete design variables, PSO is inherently continuous and must be modified to handle discrete design variables.

The basic PSO algorithm consists of three steps, namely, generating particle's positions and velocities, velocity update and finally, position update. Here, a particle refers to a point in the design space that changes its position from one move (iteration) to another based on velocity updates. First, the positions, i^{th}, and velocities, i^{th}, of the initial swarm of particles are randomly generated using upper and lower bounds on the design variables values, x_{min} and x_{max}, as expressed in Eq. 4.14 and Eq. 4.15. The positions and velocities are given in a vector format with the superscript and subscript denoting the i^{th} particle at time t. In Eq. 4.14 and Eq. 4.15, rand is a

uniformly distributed random variable that can take any value between 0 and 1 [82]. This initialization process allows the swarm particles to be randomly distributed across the d dimensional design space.

$$x_{i0} = x_{min} + rand(x_{max} - x_{min}) \tag{4.14}$$

$$v_{i0} = \frac{x_{min} + rand(x_{max} - x_{min})}{\Delta t} = \frac{position}{time} \tag{4.15}$$

The second step is to update the velocities of all particles at time t+1 using the particles objective or fitness values which are functions of the particles current positions in the design space at time t. The fitness function value of a particle determines which particle has the best global value in the current swarm, $gbest_j(t)$, and also determines the best position of each particle over time, $pbest_i(t)$, i.e. in current and all previous moves. The velocity update formula uses these two pieces of information for each particle in the swarm along with the effect of current motion, $v_i(t)$, to provide a search direction, $v_i(t+1)$, for the next iteration. The velocity update formula includes some random parameters, represented by the uniformly distributed variables, rand, to ensure good coverage of the design space and avoid entrapment in local optima. The three values that effect the new search direction, namely, current motion, particle own memory, and swarm influence, are incorporated via a summation approach as shown in Eq. 4.16 with three weight factors, namely, inertia factor, w , self-confidence factor, c_1 , and swarm confidence factor, c_2 ,

$$\underbrace{v_i(t+1)}_{\substack{\text{Velocity of particle} \\ \text{i at time t+1}}} = \underbrace{w\, v_i(t)}_{\substack{\text{Current} \\ \text{motion}}} + c_1 \underbrace{rand \frac{pbest_i(t) - x_i(t)}{\Delta t}}_{\substack{\text{Particle memory} \\ \text{influence}}} + c_2 \underbrace{rand \frac{gbest_i(t) - x_i(t)}{\Delta t}}_{\text{Swarm influence}} \tag{4.16}$$

Position update is the last step in each iteration. The Position of each particle is updated using its velocity vector as shown in Eq. 4.17 and depicted in Figure 4.2.

$$x_i(t+1) = x_i(t) + v_i(t+1) \tag{4.17}$$

i=1, 2, ….., N

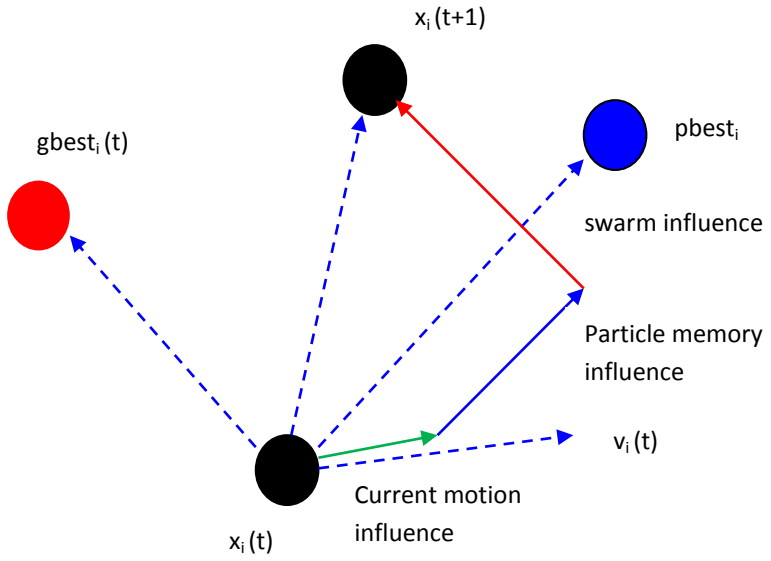

Figure 4.2. Depiction of the velocity and position updates in Particle Swarm Optimization

The three steps of velocity update, position update, and fitness calculations are repeated until a desired convergence criterion is met. In the PSO algorithm implemented in this study, the stopping criteria is that the maximum change in best fitness should be smaller than specified tolerance (ε) for a specified number of moves, S , as shown in Eq. 4.18.

$$\left|f(gbest_i(t)) - f(gbest_i(t-q))\right| \le \varepsilon \qquad q = 1,2,.....S \tag{4.18}$$

The procedure for implementing the PSO is given by the following steps.

Step 1: Initialization of swarm positions and velocities: Initialize a population (array) of particles with random positions and velocities in the D dimensional problem space using uniform probability distribution function.

Step 2: Evaluation of particle's fitness: Evaluate each particle's fitness value. Fitness function is maximized rather than minimize in this study.

Step 3: Comparison to pbest (personal best): Compare each particle's fitness with the particle's pbest. If the current value is better than pbest, then set the pbest value equal to the current value and the pbest location equal to the current location in a D-dimensional space.

Step 4: Comparison to gbest (global best): Compare the fitness with the population's overall previous best. If the current value is better than gbest, then reset gbest to the current particle's array index and value.

Step 5: Updating of each particle's velocity and position: Change the velocity, v_i, and position of the particle, x_i, according to Eq. 4.16 and Eq. 4.17 respectively.

4.3.2 Genetic algorithm

Genetic algorithm (GA) is the adaptive heuristic search algorithm based on mechanics of genetics and natural selection. GA is a family of computational models inspired by Darwin's theory of evolution i.e. survival-of-the-fittest. In nature, competition among individuals for resource results in the fittest individuals dominating over the weaker one. Genetic algorithms are noticed as function optimizer, which algorithms have been applied are quite broad area. Implementation of GA begins with a random population of chromosomes. Then these structures are evaluated and allocated in reproductive opportunities, so that the chromosomes representing better solution to the target are given more chances to reproduce than the chromosomes which are poorer solutions. Therefore goodness of a solution is typically defined with respect to the current population. Flow chart of genetic algorithm process is shown in Figure 4.3.

4.3.2.1. Basic Principle

The working principle of a GA is illustrated below, in which the major steps involved are generation of a population of solutions, finding the objective function and fitness function and the application of genetic operators. They are described in detail in the following subsection.

```
                    //* Algorithm GA*//
randomly initialize population
repeat
        evaluate objective function
        find fitness function
        apply genetic operators
                reproduction
                crossover
                mutation
until stopping criteria
```

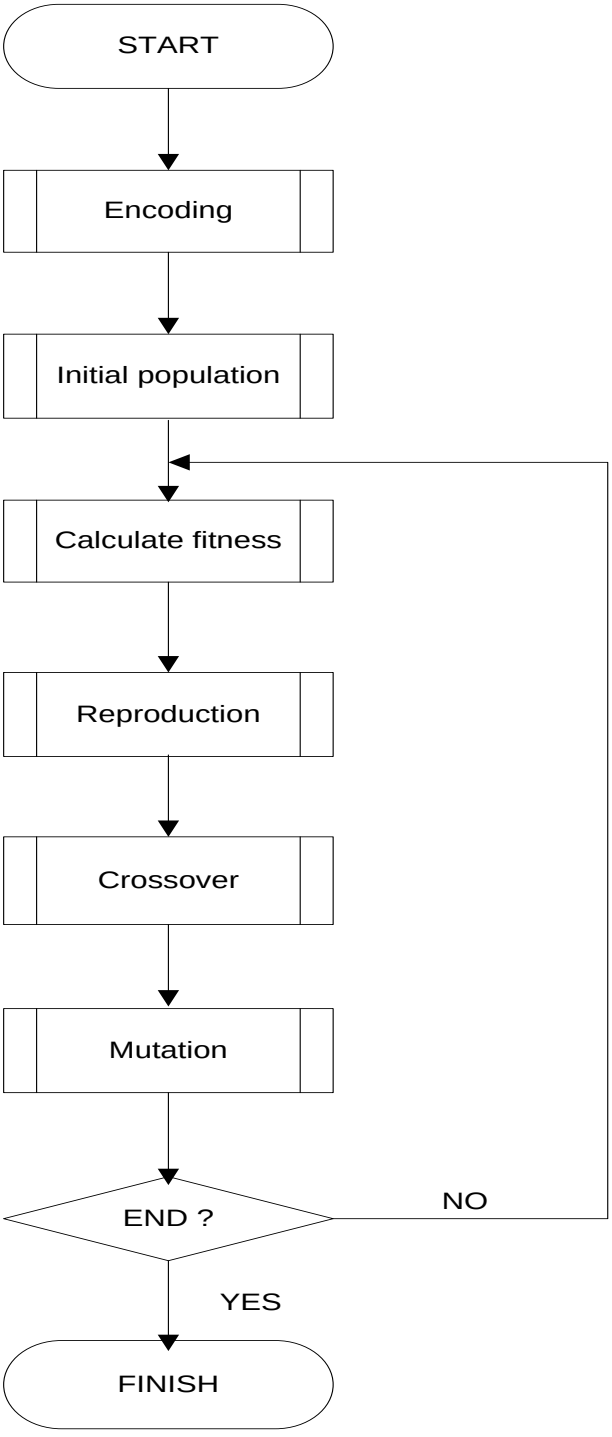

Figure 4.3. Flow chart of genetic algorithm

4.3.2.2. Working Principle

An unconstrained optimization problem is considered to illustrate the working principles of GA. Let us consider a maximization problem,

$$\text{Maximize } f(x),\ x_i^l \le x_i \le x_i^u \qquad i = 1,2,3,\ldots\ldots,N \tag{4.19}$$

where x_i^l and x_i^u are the lower and upper bound the variable x_i can take. Though a maximization problem is considered here, a maximization problem can also be handled using GA. The working of GA is done by performing the following tasks.

4.3.2.3. Encoding

To solve the above problem (Eq. 4.19) using GA, the variable x_i are first coded in some string structures. Binary-coded strings having 1's and 0's are used. The length of the string is usually determined according to the desired solution accuracy.

4.3.2.4. Fitness Function

GA mimics the survival-of-the-fittest principle of nature to make the search process. Therefore, GA is suitable for solving maximization problems. Minimization problems are usually transformed into maximization problem by suitable transformation. Initially the fitness function F(i) is derived from the objective function f(x) and used in successive genetic operations. Generally GA fitness is used to allocate reproductive character to the individuals in the population and thus act as a measure of goodness to be maximized. Therefore individual having higher fitness value have higher probability of being selected as candidates for further examination. The fitness function can be considered to be the same as the objective function or F(i) = f(x) for maximization problems. To generate non-negative values in all the cases, it is necessary to map the objective function to fitness function form. There are many type of such transformations possible, among them two usually approved fitness mappings are presented in Eq. 4.20 and Eq. 4.21.

$$F(x) = \frac{1}{1+f(x)} \tag{4.20}$$

This transformation does not alter the location of the minimum, but converts a minimization problem to an equivalent maximization problem. The other function to transform the objective function to get the fitness value F (i) is shown in Eq. 4.21.

$$F(i) = V - \frac{f(x)P}{\sum_{i=1}^{p} f(x)} \tag{4.21}$$

where, f(x) is the objective function value of individual, P is the population size and V is a large value to ensure non-negative fitness values. The value of V is the maximum value of the second term of Eq. 4.21 so that the fitness value corresponding to maximum value of the objective function is zero. This transformation also does not alter the location of the solution, but converts a minimization problem to an equivalent maximization problem. The fitness function value of a string is known as the string fitness.

4.3.2.5. GA operators

The operation of GA begins with a population of a random string representing design or decision variables. The population is then functioned by three main operators; reproduction, crossover and mutation to create a new population of points. GA can be viewed as trying to maximize the fitness function, by evaluating several solution vectors. These operators are to create new solution vectors by selection, combination or alteration of the current solution vectors that have shown to be good temporary solutions. The new population is further evaluated and tested till termination. If the termination criterion is not met, the population is iteratively operated by the above three operators and evaluated. This procedure is continued until the termination criterion is met. One cycle of these operations and the subsequent evaluation procedure is known as a generation in GA terminology.

4.3.2.6. Reproduction

Reproduction is the first operator applied on a population that makes more copies of better strings in a new population. Reproduction chooses good strings in a population and forms a mating pool. This is also known as the selection operator. The process of natural selection causes those individuals that encode successful structures to produce copies more frequently. Therefore, the reproduction of the individuals in the current population is necessary to sustain the generation of a new population. The essential idea of all reproduction operators in GA is that the above average strings are picked from the current population and their multiple copies are inserted in the mating pool in a probabilistic manner.

4.3.2.7. Crossover

The second operator, crossover is used to recombine two strings to get a better one. The successive generations carried out by combining material from two individuals of the previous generation rather than forming new string. Good strings in a population are probabilistically assigned a larger number of copies and a mating pool is formed. The new strings are created in

crossover by exchanging information among strings of the mating pool. The two strings participating in information changing are known as parent string and resulting string is known as children strings. Good strings created by crossover have more copies in the next mating pool generated by crossover. Therefore the effect of cross over may be detrimental or beneficial. Thus, in order to preserve some of the good strings that are already present in the mating pool, all strings in the mating pool are not used in crossover. When a crossover probability (p_c) is used, only $100p_c$ percent strings in the population are used in the crossover operation and 100 ($1-p_c$) percent of the population remains as they are in the current population. A crossover operator is mostly responsible for the search of new strings, however mutation operator is also used for this purpose sparingly. In the GA literature, there are many crossover operators exist. The most common adopted crossover operators are one site crossover and two site crossover. The one site crossover operator is achieved by randomly selecting a crossing site along the string of randomly selecting two strings from the mating pool and by exchanging all bits on the right side of the crossing site as shown in Figure 4.4. Thus the new string is a combination of the old strings.

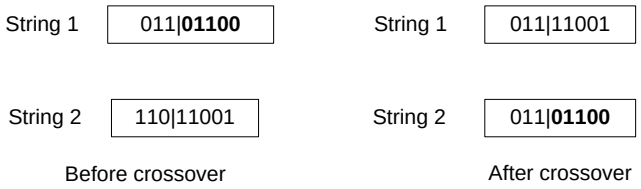

Figure 4.4. One site crossover operation

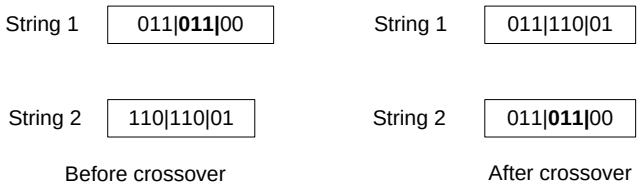

Figure 4.5. Two site crossover operation

In the two site crossovers, two crossover sites are chosen and the bits between the sites are exchanged as shown in Figure 4.5. For small string length one site crossover is mostly preferred wherever two site crossovers are suitable for large strings. The core objective of crossover is to get a new string by exchanging information between strings that is possibly better than the parents.

4.3.2.8. Mutation

Mutation is the process of adding new information to the genetic search in a random way and to avoid getting trapped at local optima. The population becomes homogeneous due to repeated use of reproduction and crossover operators and mutation operator introduces diversity in the population. Significant different between parent and children is possible only due to random distribution of genetic information by mutation.

Mutation operates at the bit level; there is a probability that each bit may become mutated, when the bits are being copied from the current string to the new string. This probability is usually a quite small value, known as mutation probability (p_m). If the random number between zero and one, is less than the mutation probability (P_m), then the bit is altered, so that zero becomes one and vice versa. Thus diversity introduces to the population by random scattering which result in better optima or even modify a part of genetic code. There may be possibility of weak individual formation, which never be selected for further operations. Therefore, mutation is necessary to create a point in the neighborhood of the current point and to maintain diversity in the population.

The function of these three operators are, reproduction operator selects good strings, the crossover operator recombines good sub-strings to create a better sub-string and the mutation operator alters a string locally expecting a better string. Even though none of these claims are guaranteed, the bad strings are eliminated by the reproduction operator and good strings are increasingly emphasized in the next generation, yielding solutions that are closer to the optimum solution. Finally the objective function value of the individuals of the new population is determined by decoding the strings, which is express the fitness of the solutions of the new generations. This is one generation, i.e. completes one cycle of genetic algorithm. The improved solution is stored as the best solution and this process is repeated till convergence.

4.4. Multi-objective optimization using non dominated sorting genetic algorithm NSGA

A single objective optimization algorithm provides a single optimal solution whereas most of the multi-objective problems, give rise to a set of optimal solutions instead of a single optimal solution. The set of solution is known as pareto-optimal solution, in which one of these pareto-optimal solutions cannot be said to be better than the other. Suitability of one solution depends on a number of factors including user's choice and problem environment. Hence, this demands

finding the entire set of optimal solutions. Optimization of conflicting nature response requires multi-objective optimization.

Genetic algorithm (GA) is a subclass of population based stochastic search procedure which is closely modelled on the natural process of evolution with emphasis on breeding and the survival of the fittest. Instead of starting with a single point, the algorithm starts with a set of initial solutions. Also, instead of a deterministic result at each iteration, GA operators produce probabilistic results leading to stochasticity. Proper search direction can be provided to the GA by simulating the natural process of evolution. In the process of evolution, the organisms which are better able to adapt to the environment have a higher chance of survival. This leads to a higher chance of breeding for such organisms and an increased probability of their traits being carried over to the next generation through their offspring. Thus, a trait which leads to a better organism has higher chances of making it to the next generation. Moreover, due to mating of two different organisms with better fitness leads to intermixing of favourable traits which hopefully would lead to better offspring. In case the new members are poorer, they would be lost in the next generation. At the same time, it is important to maintain diversity in the population so that potentially important regions of the search space are not eliminated during the initial stages.

To keep a track of which traits are favourable and which are not, traits are coded in the form of genetic material which is stored in a chromosome. Due to selection of better traits and intermixing, eventually the entire population has the same chromosome set which is also the best possible trait combination.

To incorporate the idea of natural evolution GA must have the following essential features:

- Encoding of solution: To keep track of favourable solutions
- Assigning fitness to a solution: To determine the chances of survival of the solution.
- Selection operator: To select the fit solutions for mating.
- Crossover or Recombination operator: For mixing of traits through mating of two different solutions.
- Mutation operator: Random variations in encoded solutions to obtain new solutions.
- Survivor operator: To determine the members which die off and those which go to the next generation

These operators are responsible for providing the search direction to a GA. Selection operator selects good solutions and crossover operator recombines good genetic material from two good

solutions to (hopefully) form a better solution. Mutation operator alters a string locally to (hopefully) create a better string. If bad strings are created they are be eliminated by the reproduction operator in the next generation and if good strings are created, they are emphasized. In a single objective optimization, there exists only one solution. But in the case of multiple objectives, there is a set of mutually dominant solution, which is exclusive and unique with respect to all objectives. Classical methods for solving multi-objective problem suffer from drawback of trading off among objectives when a weighted function is used. These methods transform the multi-objective problem into single objective by assigning some weights based on their relative importance (Yu e*t al* 2004). However, most of the multi-objective problems, in principle, give rise to a set of optimal solutions instead of a single optimal solution. The set of solution is known as pareto-optimal solution.

Real-world problems require simultaneous optimization of several incommensurable and often conflicting objectives. Often, there is no single optimal solution; rather there is a set of alternative solutions. These solutions are optimal in the wider sense that no other solutions in the search space are superior to another when all objectives are considered. They are known as pareto-optimal solutions. The image of the efficient set in the objective space is called non-dominated set. For example, consider a minimization problem and two decision vectors a, b ε X, the concept of pareto optimality can be defined as follows: a is said to dominate b if:

$i = \{1, 2, \ldots, n\} : fi(a) \leq fi(b)$ and

$j = \{1, 2, \ldots, n\} : fj(a) < fj(b)$

Conditions which a solution should satisfy to become dominant are (i) Any two solutions of X must be non-dominated with respect to each other (ii) Any solution not belonging to X is dominated by at least one member of X. All the objective function vectors, which are not dominated by any other objective function vector of a set of Pareto-optimal solutions, are called non-dominated set with respect to that set of Pareto-optimal solutions. There are two goals in a multi-objective optimization:

(i) Convergence to the Pareto-optimal set; and

(ii) maintenance of diversity and distribution in solutions

Non-dominated Sorting Genetic Algorithm II (NSGA II) is a multi-objective evolutionary algorithm based on non-dominated sorting [83]. The algorithm uses elitist non-dominated sorting along with crowding distance sorting to obtain the non-dominated set. The algorithm is capable

of handling constrained multi-objective optimization problems with binary coding and real parameters. The appropriate objective function in terms of the variables is coded in the algorithm. The algorithm produces the non-dominated set out of the entire population after a specific number of generations. Members of Pareto-front belong to the non-dominated set which is obtained on convergence of the algorithm. Selection is done with the help of crowded-comparison operator based on ranking (according to non-domination level) and crowding distance.

Randomly an initially parent population (solution) P of size N is generated. In order to identify the non-domination level, each solution is compared with every other solution and checked whether the solution under consideration satisfies the rules given below

$$\text{Obj.1}[i] > \text{Obj.1}[j] \text{ and } \text{Obj.2}[i] \geq \text{Obj.2}[j],$$

$$\text{or } \text{Obj.1}[i] \geq \text{Obj.1}[j] \text{ and } \text{Obj.2}[i] > \text{Obj.2}[j]$$

where, i and j are chromosome numbers.

Now if the rules are satisfied, then the selected solution is marked as dominated. Otherwise, the selected solution is marked as non-dominated. In the first sorting, all the non-dominated solution (N1) is assigned rank 1. From the remaining N−N1 dominated solution from the first sorting, again solution are sorted and the non-dominated solutions in second sorting are assigned rank 2. This process continues until all the solutions are ranked. Each solution is assigned fitness equal to its non-domination level (rank 1 is the best level, rank 2 is the next-best level, and so on). Solutions belong to a particular rank or non-domination level, none of the solution is better with respect to other solutions present in that non-domination level. After identifying the rank of each solution, crowding distance of each solution belongs to a particular non-nomination set or level is calculated. The crowding distance is the average distance of two points on either side of this selected solution point along each of the objectives function. For calculation of crowded distance, all the populations of particular non-dominated set are sorted in ascending order of magnitude according to each objective function value. Then, the boundary solution of each objective function, i.e., solution with largest and smallest values is assigned an infinity value. Rest of the intermediate solution are assigned a distance value equal to the absolute normalized difference in the function value at two adjacent solutions. For solving optimization problem using GA, it needs fitness value. The fitness values are nothing but the objective function values.

Therefore, there is a need of function or equation, which relates the decision variable with the objective. The flow chart of the above algorithm is shown in Figure 4.6.

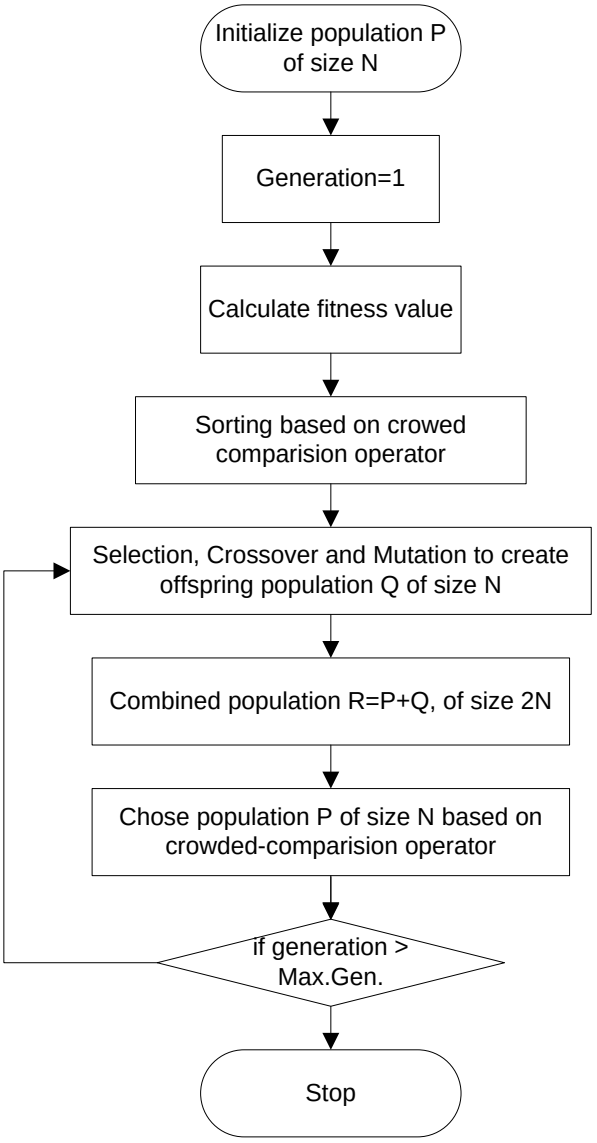

Figure 4.6. Flow chart for NSGA algorithm

4.5. Conclusions

The chapter summarizes different optimization technique proposed in this present study. Experimental results and optimal setting for the responses individually and simultaneously are discussed in the next chapter.

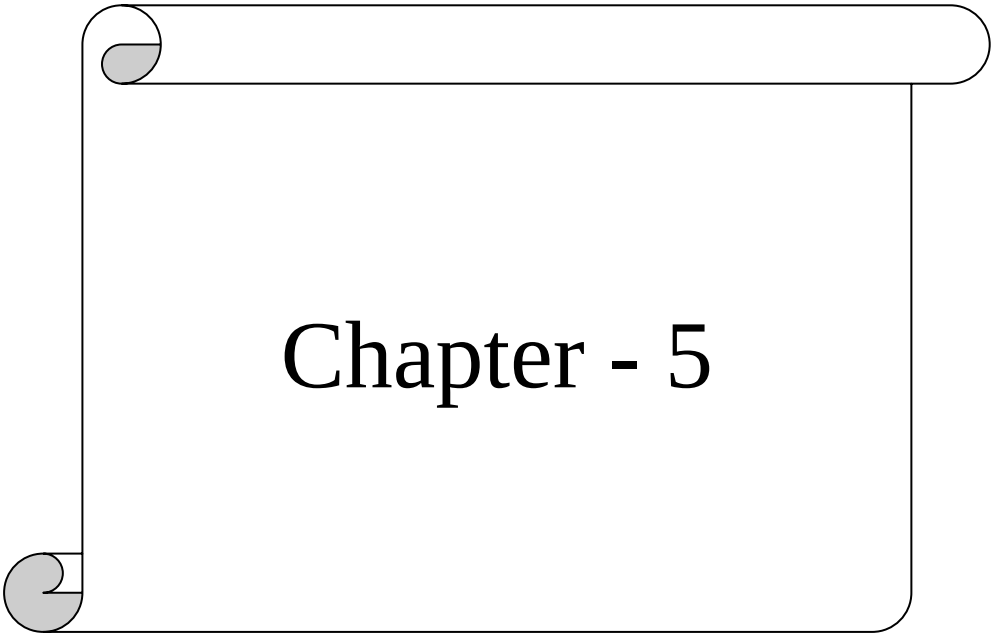
Chapter - 5

Chapter 5

RESULTS AND DISCUSSION

5.1. Introduction

This chapter presents experimental investigations on the influence of important process parameters such as discharge current (Ip), pulse-on-time (Ton), duty factor (τ) and flushing pressure (Fp) along with their interactions on responses like material removal rate (MRR), tool wear rate (TWR), surface roughness (Ra) and circularity (r_1/r_2). Response surface methodology (RSM) parameter design, being a simple and inexpensive method is adopted to understand effect of process parameters and their interaction on responses. Conventional RSM can effectively establish the relationship between parameters and a single response by developing regression equation. Genetic algorithm holds good to optimize the equation and finding optimal combination. When multiple performance characteristics with conflicting goals are considered, the approach becomes unsuitable. The multiple performance measures considered in this work are material removal rate (MRR), tool wear rate (TWR), surface roughness (Ra) and circularity (r_1/r_2). All these responses can be combined together into an equivalent response that, MRR, circularity should be maximized and TWR, Ra should be minimized. Neuro-fuzzy has the ability to combine all the objectives simultaneously, utilized in RSM to analyse and develop regression equation. Particle swarm optimization technique can optimize the regression equation to obtained optimal setting of process parameters (variables). Multi-response optimization by non-dominated sorting genetic algorithm has the capability to handle any number of equations of responses and to provide pareto solution satisfying all the responses.

5.2. Optimization of single response

5.2.1 Material Removal Rate

Material removal is the main objective of machining process. So it is need to calculate the material removal rate (MRR) and analyze the effect of controllable factors on material removal rate. The Table 5.1 shows the experimental results for material removal rate using brass and copper as electrode.

Table 5.1. MRR using Brass and Copper tool

Expt. No	Ip (A)	Ton (μs)	T (%)	Fp (bar)	MRR using brass tool (mm^3/min)	MRR using copper tool (mm^3/min)
1	3	100	85	0.3	1.5736	2.9589
2	7	100	85	0.3	3.3723	12.9848
3	3	300	85	0.3	1.6169	1.3139
4	7	300	85	0.3	7.0368	9.6082
5	5	200	80	0.2	2.9134	5.0866
6	5	200	90	0.2	4.0628	7.1039
7	5	200	80	0.4	2.9286	5.2208
8	5	200	90	0.4	4.1688	7.3723
9	3	200	80	0.3	1.5606	3.189
10	7	200	80	0.3	5.2965	10.32
11	3	200	90	0.3	2.0758	2.816
12	7	200	90	0.3	6.2273	14.587
13	5	100	85	0.2	2.5758	6.3723
14	5	300	85	0.2	3.6991	3.6429
15	5	100	85	0.4	2.5303	6.5649
16	5	300	85	0.4	3.6926	3.9048
17	3	200	85	0.2	1.8896	2.7316
18	7	200	85	0.2	5.9091	11.6558
19	3	200	85	0.4	1.8766	2.4805
20	7	200	85	0.4	5.9957	11.9805
21	5	100	80	0.3	2.0195	5.7554
22	5	300	80	0.3	3.0649	3.3377
23	5	100	90	0.3	2.6234	7.8831
24	5	300	90	0.3	4.2489	4.817
25	5	200	85	0.3	3.6472	5.7662
26	5	200	85	0.3	3.5823	5.7987
27	5	200	85	0.3	3.5498	5.658

ANOVA of Response Surface Quadratic Model for MRR

The satisfactoriness of the model is checked by using the analysis of variance (ANOVA) technique. As per this technique, if the calculated value of the P value of the developed model does not exceed the standard tabulated value of P for a desired level of confidence (say 95%), then the model is considered to be satisfactory within the confidence limit. ANOVA test results are presented in the Table 5.2 and Table 5.3.

ANOVA for MRR using brass tool, Table 5.2 shows that the factor Ip, Ton, τ, Flushing Pressure, interaction of Ip and Ton, square term of Ip and Ton have significant effect on MRR. Among these terms Ip has the highest effect on MRR with contribution is about 77.15%, Ton has the second highest effect on MRR with a contribution 9.35%. Then the interaction effect of Ip and Ton with a contribution of 5.37% & and then flushing pressure and other main effect and their square terms have very less contribution towards MRR.

Table 5.2. ANOVA for MRR using Brass Tool

Source	Sum of Squares	df	Mean Square	F Value	p-value Prob > F	% Contribution
Model	61.41277	14	4.386627	136.5908	< .0001	99.37639
A-Ip	47.67734	1	47.67734	1484.577	<0.0001	77.15011
B-Ton	5.778105	1	5.778105	179.9186	< .0001	9.349964
C- τ	0.274579	1	0.274579	8.549849	<0.0127	0.444316
D-Fp	1.53246	1	1.53246	47.71773	<0.0001	2.479782
AB	3.320413	1	3.320413	103.391	< .0001	5.372997
AC	0.00248	1	0.00248	0.077223	0.7858	0.004013
AD	0.043181	1	0.043181	1.344565	0.2688	0.069874
BC	0.000299	1	0.000299	0.009319	0.9247	0.000484
BD	0.084129	1	0.084129	2.619609	0.1315	0.136135
CD	0.000557	1	0.000557	0.017343	0.8974	0.000901
A^2	0.470804	1	0.470804	14.65991	<0.0024	0.761842
B^2	1.336135	1	1.336135	41.60457	<0.0001	2.162095
C^2	0.005246	1	0.005246	0.163347	0.6932	0.008489
D^2	0.052881	1	0.052881	1.646607	0.2236	0.08557
Residual	0.385381	12	0.032115			0.623613
Lack of Fit	0.380463	10	0.038046	15.47119	0.0622	0.615654
Pure Error	0.004918	2	0.002459			0.007959
Cor Total	61.79815	26				100
< Significant						

ANOVA for MRR using copper tool, Table 5.3 shows that factor Ip, Ton, τ, Flushing Pressure, interaction factor of Ip and Fp, square term of Ip and Ton are significant terms. Among these terms Ip has the highest effect on MRR with contribution is about 80.99 %, Ton has 6.6 % effect on MRR. Then square of Ip have a contribution of 4.24% & and flushing pressure along with other main effect and their square terms have very less contribution towards MRR.

Table 5.3. ANOVA for MRR using copper Tool

Source	Sum of Squares	df	Mean Square	F Value	p-value Prob > F	% of Contribution
Model	313.9927	14	22.42805	58.5686	< 0.0001	98.55762
A-Ip	258.0435	1	258.0435	673.8545	< 0.0001	80.99599
B-Ton	21.05399	1	21.05399	54.98036	< 0.0001	6.608532
C- τ	1.838406	1	1.838406	4.800811	<0.0489	0.577048
D-Fp	5.205574	1	5.205574	13.59383	<0.0031	1.633952
AB	0.74961	1	0.74961	1.96E+00	0.1871	0.235291
AC	0.082886	1	0.082886	0.216449	0.6501	0.026017
AD	5.3824	1	5.3824	1.41E+01	<0.0028	1.689455
BC	0.001201	1	0.001201	0.003135	0.9563	0.000377
BD	0.105106	1	0.105106	0.274473	0.6099	0.032991
CD	0.004502	1	0.004502	0.011758	0.9154	0.001413
A^2	12.88169	1	12.88169	33.63924	< 0.0001	4.043371
B^2	2.124591	1	2.124591	5.548155	<0.0364	0.666877
C^2	0.000485	1	0.000485	0.001266	0.9722	0.000152
D^2	0.9051	1	0.9051	2.363577	0.1501	0.284097
Residual	4.595238	12	0.382936			1.442376
Lack of Fit	4.584385	10	0.458438	84.47888	0.0118	1.43897
Pure Error	0.010853	2	0.005427			0.003407
Cor Total	318.588	26				100
< Significant						

Normal plot

Normal plot is a graphical technique which shows whether the points are normally distributed or not. The data are plotted against Residuals in such a way that the points should lay in a straight line. If the points follow a straight line then the points are normally distributed. Figure 5.1 shows the normal probability plot for MRR using brass tool. The MRR values are looks fairly straight line except experiment no. 1 and 9 due to higher residual values. Therefore MRR using brass tool are normally distributed. Figure 5.2 shows the normal probability plot for MRR using copper tool. The MRR values are following the straight line. Therefore MRR using copper tool are normally distributed.

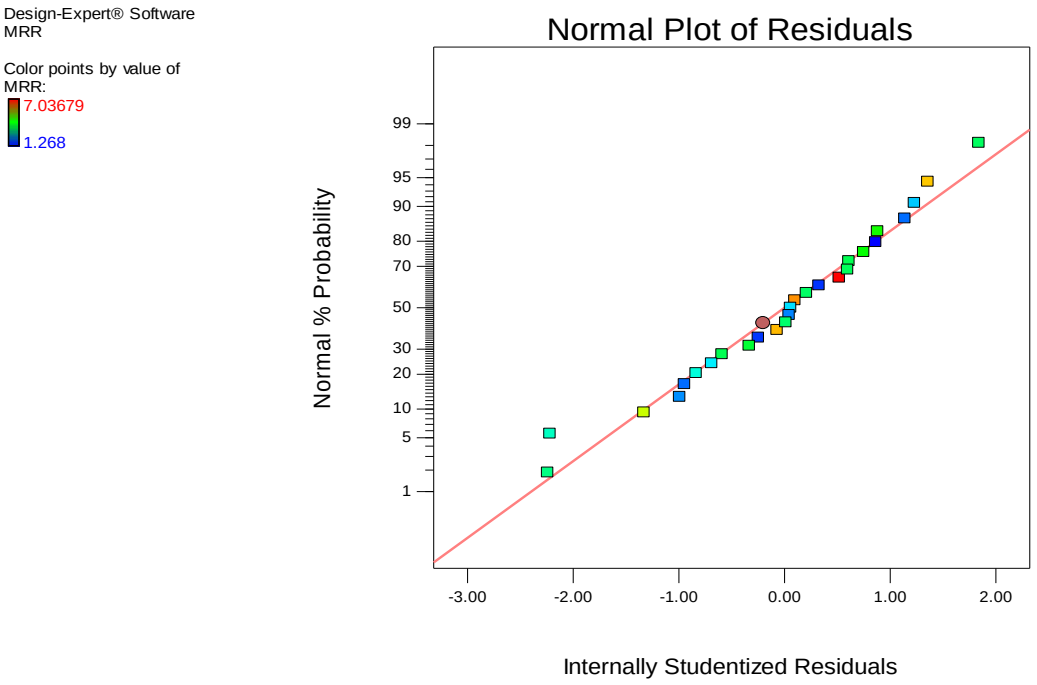

Figure 5.1. Normal plot of residuals for MRR using brass tool

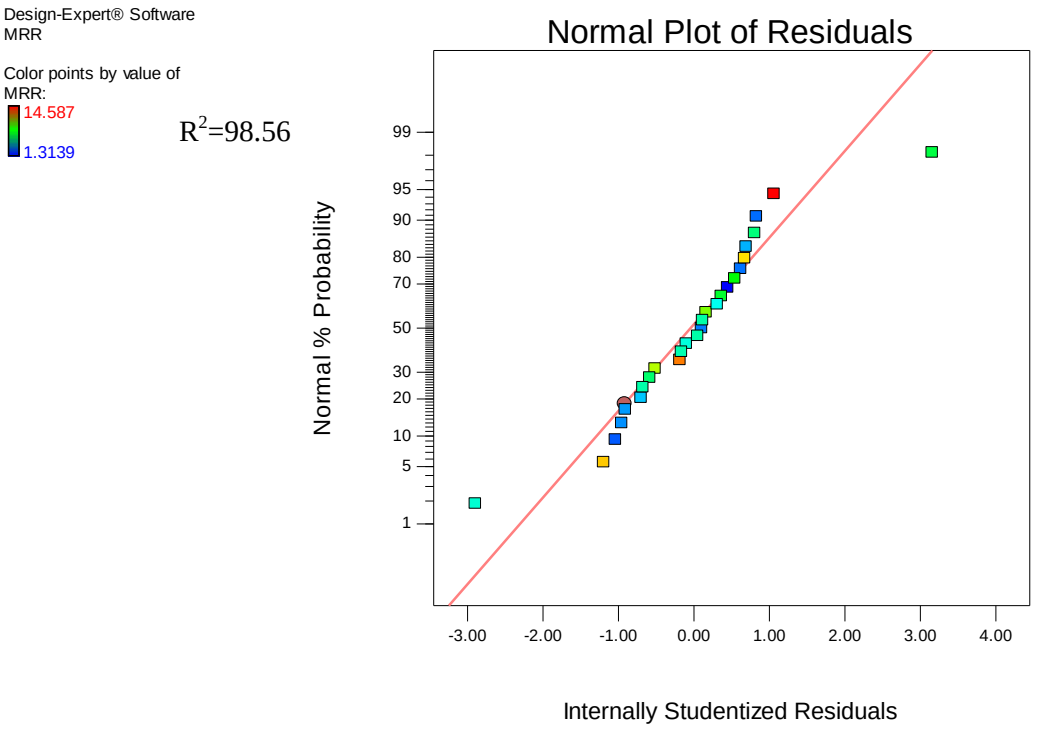

Figure 5.2. Normal plot of residuals for MRR using copper tool

Surface Plot

Figure 5.3 shows the surface plot for MRR using brass tool, in relation to the process parameters such as discharge current (Ip) and pulse-on-time (Ton). It can be observed that the MRR tends to increasing with discharge current from 3 A to 7A due to more heat generation as a result of strong spark for any value of Ton. MRR increases slowly with increasing Ton from 100 µs to 200 µs and then drop off up to 300 µs with increasing Ton for any value of Ip. This occurs due to increase of inter electrode gap (IEG). Also it can be observed that the MRR increases rapidly with the mutual effect of Ton and Ip. MRR attains maximum at 7A discharge current and 200 µs pulse-on-time.

Figure 5.4 shows the surface plot for MRR using brass tool, in relation to the process parameter such as duty factor and flushing pressure. It can be observed that MRR increases very slowly with increasing flushing pressure for any value of duty factor because this doesn't allow forming the carbon layer. Similarly MRR increases slowly with increasing τ value because work piece gets less time to cool between two spark. The figure shows that MRR increases at faster rate due to their mutual effect. MRR attains maximum at 0.4 bar flushing pressure and 90 % duty factor.

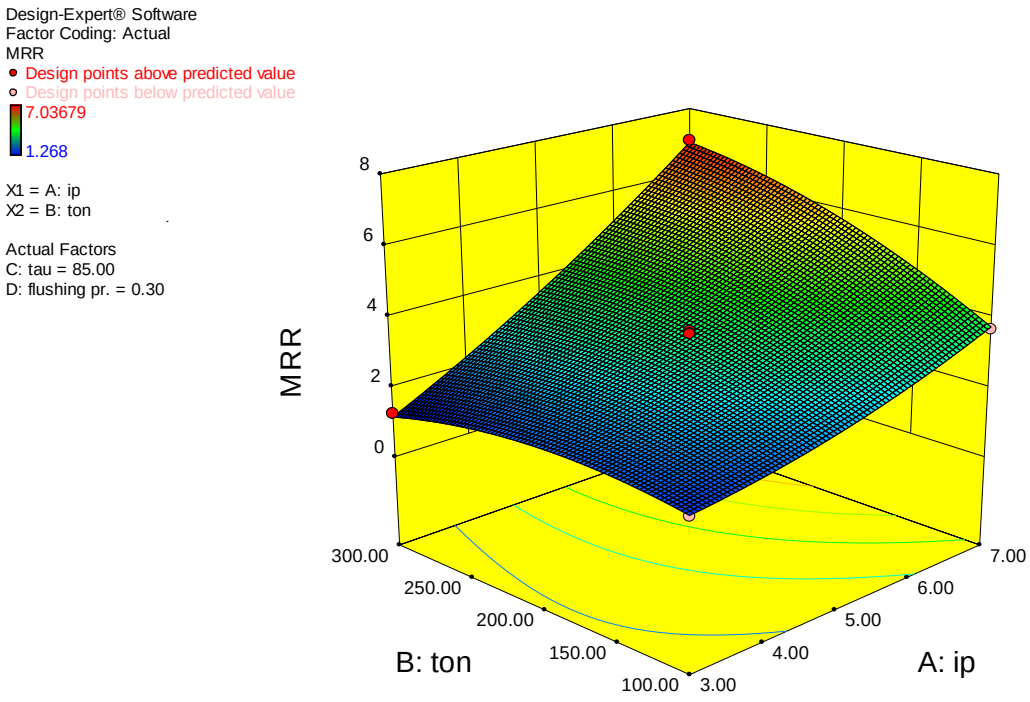

Figure 5.3. Surface plot for MRR using brass tool

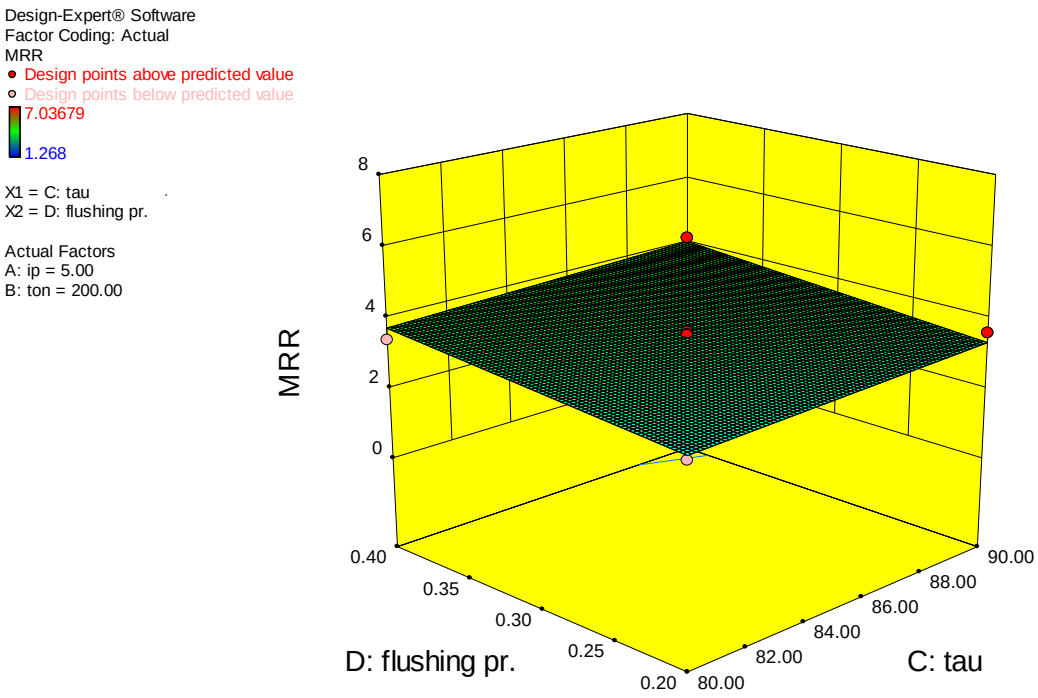

Figure 5.4. Surface plot For MRR using brass tool

Surface plot for MRR using copper tool in relation with discharge current (Ip) and pulse – on–time (Ton) is shown in Figure 5.5. It is observed that MRR tends to increase with Ip from 3A to 7A for any value of Ton due to more heat generation as a result of strong spark. The MRR increases slowly with increasing Ton from 100 µs to 200 µs and then drop off up to 300 µs for any value of Ip. This occurs due to increase of inter electrode gap (IEG). It is seen that Ip attains maximum at 7 A Ip and 100 µs Ton.

Figure 5.6 shows the surface plot for MRR using copper tool, in relation with duty factor (τ) and flushing pressure (Fp). It can be observed from the plot that MRR increases very slowly with increasing flushing pressure for any value of τ because this doesn't allow forming the carbon layer. MRR increases slightly with increasing τ for any value of flushing pressure because work piece gets less time to cool between two sparks. MRR reaches maximum at 90% τ and 0.4 bar Fp.

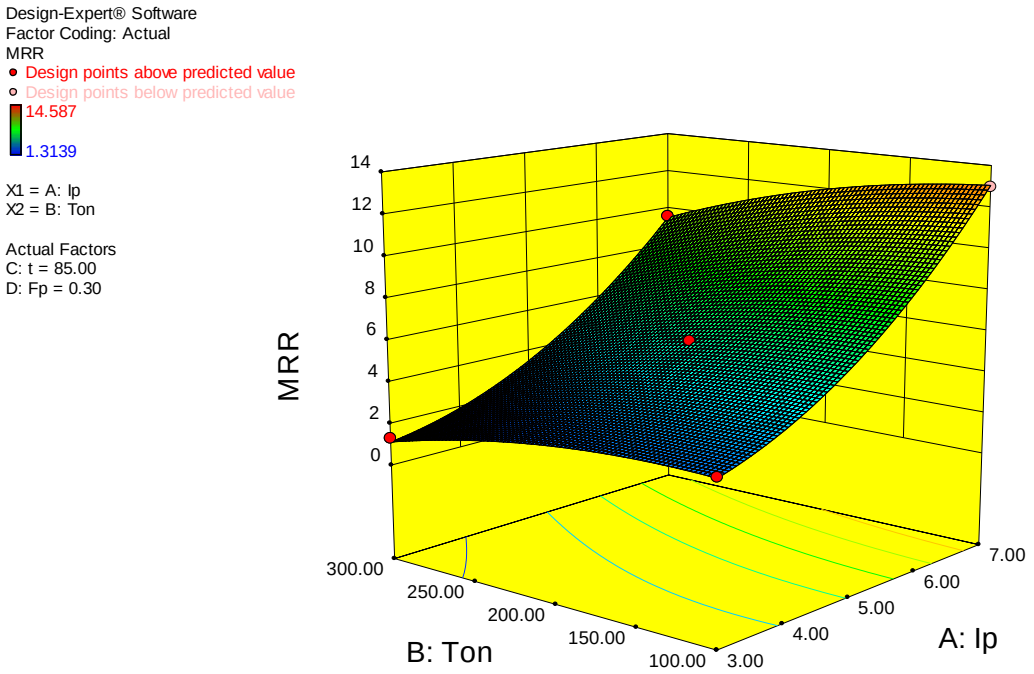

Figure 5.5. Surface plot for MRR using copper tool

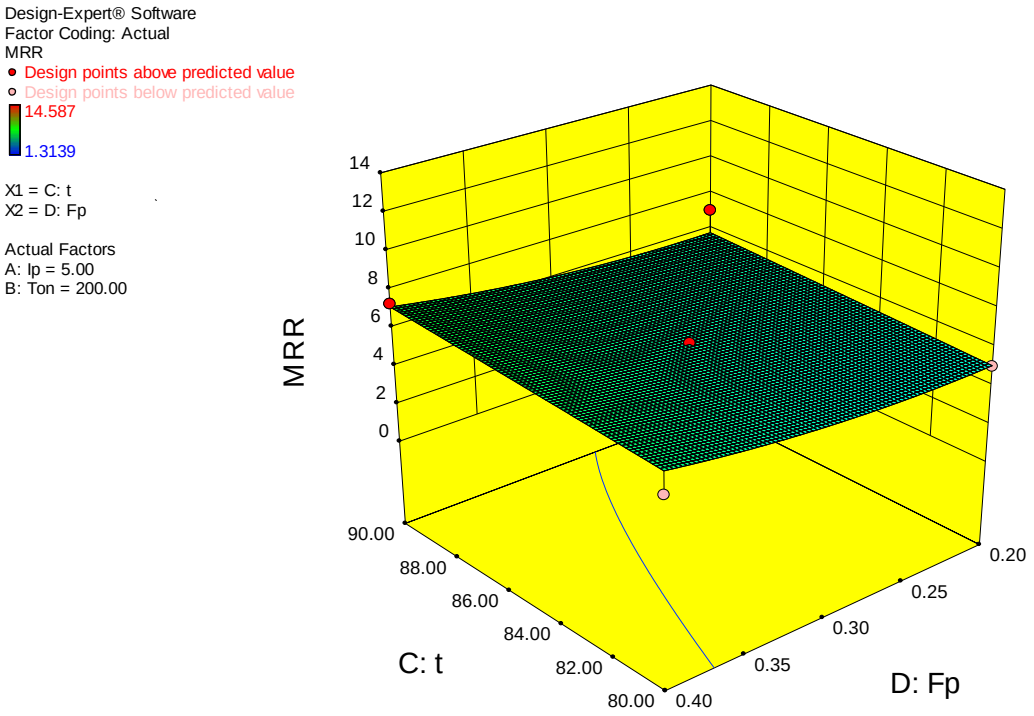

Figure 5.6. Surface plot for MRR using copper tool

5.2.2 Tool Wear Rate

In electric discharge machining process tool design is a difficult task, because the tool profile is transferred to the work piece. The heat generated in the spark is transferred to both tool as well as work piece. So tool is eroded during machining which affect the final product. It is impossible to avoid tool wear, but tool wear rate can be minimized. The tool wear rate of brass tool and copper tool is given in Table 5.4.

Table 5.4. Tool wear rate of brass and copper tool

Observation No	Ip (A)	Ton (μs)	T (%)	Fp (bar)	TWR of brass tool (mm^3/min)	TWR of copper tool (mm^3/min)
1	3	100	85	0.3	1.8428	0.0131
2	7	100	85	0.3	3.4851	0.0429
3	3	300	85	0.3	1.2493	0.0056
4	7	300	85	0.3	3.2652	0.0242
5	5	200	80	0.2	1.9031	0.0054
6	5	200	90	0.2	2.7700	0.0093
7	5	200	80	0.4	2.8250	0.0095
8	5	200	90	0.4	3.2555	0.0093
9	3	200	80	0.3	1.3038	0.0053
10	7	200	80	0.3	2.8177	0.0261
11	3	200	90	0.3	1.9031	0.0075
12	7	200	90	0.3	4.5437	0.0160
13	5	100	85	0.2	2.7496	0.0270
14	5	300	85	0.2	2.1930	0.0128
15	5	100	85	0.4	2.7807	0.0190
16	5	300	85	0.4	2.2378	0.0070
17	3	200	85	0.2	1.5937	0.0075
18	7	200	85	0.2	3.7945	0.0188
19	3	200	85	0.4	1.6793	0.0003
20	7	200	85	0.4	3.9949	0.0333
21	5	100	80	0.3	2.0199	0.0242
22	5	300	80	0.3	1.7007	0.0093
23	5	100	90	0.3	3.1524	0.0186
24	5	300	90	0.3	2.6912	0.0112
25	5	200	85	0.3	2.7087	0.0131
26	5	200	85	0.3	2.8157	0.0075
27	5	200	85	0.3	2.7574	0.0112

ANOVA of Response Surface Quadratic Model for TWR

The satisfactoriness of the model is checked by using the analysis of variance (ANOVA) technique. As per this technique, if the calculated value of the P value of the developed model

does not exceed the standard tabulated value of P for a desired level of confidence (say 95%), then the model is considered to be satisfactory within the confidence limit. ANOVA test results are presented in the Table 5.5 and Table 5.6.

ANOVA for TWR using brass tool, Table 5.5 shows that the factor Ip, Ton, τ, Fp, interaction of Ip and Fp, square term of Ton are the significant terms. Among these terms Ip has the highest effect on TWR with a contribution of 71.42%. Flushing pressure has the second highest effect on TWR with contribution 16.11%, Ton have 3.4% contribution, square of Ton have contribution 2.39%, but other interaction and main effect terms have very less contribution on TWR as compared to Ip contribution.

ANOVA for TWR using copper tool, Table 5.6 shows that the factor Ip, Ton, τ, Fp, interaction of Ip and Fp, square term of Ton are the significant terms. Among these terms Ip has the highest effect on TWR with a contribution of 71.42%. Flushing pressure has the second highest effect on TWR with contribution 16.11%, Ton have 3.4% contribution, square of Ton have contribution 2.39%, but other interaction and main effect terms have very less contribution on TWR as compared to Ip contribution.

Table 5.5. ANOVA for brass tool wear rate

Source	Sum of Squares	df	Mean Square	F Value	p-value Prob > F	% Contribution
Model	17.2911	14	1.23508	33.371	< 0.0001	97.4958
A-Ip	12.6672	1	12.6672	342.259	< 0.0001	71.4239
B-Ton	0.60449	1	0.60449	16.3328	<0.0016	3.4084
C- τ	0.22944	1	0.22944	6.19929	<0.0284	1.29369
D-Fp	2.85744	1	2.85744	77.2058	< 0.0001	16.1116
AB	0.03489	1	0.03489	0.94282	0.3507	0.19675
AC	0.00329	1	0.00329	0.08902	0.7705	0.01858
AD	0.31736	1	0.31736	8.57492	<0.0126	1.78945
BC	4.7E-05	1	4.7E-05	0.00127	0.9722	0.00026
BD	0.00504	1	0.00504	0.1362	0.7185	0.02842
CD	0.04761	1	0.04761	1.28642	0.2789	0.26846
A^2	0.00196	1	0.00196	0.05291	0.8219	0.01104
B^2	0.42514	1	0.42514	11.4871	<0.0054	2.39717
C^2	0.00189	1	0.00189	0.05114	0.8249	0.01067
D^2	0.04567	1	0.04567	1.23398	0.2884	0.25751
Residual	0.44413	12	0.03701			2.50421
Lack of Fit	0.43839	10	0.04384	15.2752	0.0630	2.47184
Pure Error	0.00574	2	0.00287			0.03236
Cor Total	17.7353	26				100
< Significant						

Table 5.6. ANOVA for copper tool wear rate

Source	Sum of Squares	df	Mean Square	F Value	p-value Prob > F	% of Contribution
Model	0.002331	14	0.000166	13.07474	< 0.0001	93.84762
A-Ip	0.001242	1	0.001242	97.54791	< 0.0001	50.01269
B-Ton	0.000465	1	0.000465	36.51011	< 0.0001	18.71868
C-t	5.79E-07	1	5.79E-07	0.045439	0.8348	0.023296
D-Fp	4.86E-06	1	4.86E-06	0.38179	0.5482	0.195743
AB	3.13E-05	1	3.13E-05	2.456168	0.1430	1.259274
AC	0.000117	1	0.000117	9.196468	< 0.0104	4.715017
AD	3.75E-05	1	3.75E-05	2.943769	0.1119	1.509267
BC	1.23E-06	1	1.23E-06	0.096846	0.7610	0.049653
BD	1.39E-05	1	1.39E-05	1.092021	0.3166	0.559878
CD	4.09E-06	1	4.09E-06	0.321235	0.5813	0.164697
A^2	0.000115	1	0.000115	9.038456	< 0.0109	4.634005
B^2	0.000222	1	0.000222	17.43569	<0.0013	8.939257
C^2	1.45E-06	1	1.45E-06	0.113944	0.7415	0.058419
D^2	1.11E-05	1	1.11E-05	0.871468	0.3690	0.446801
Residual	0.000153	12	1.27E-05			6.152385
Lack of Fit	0.000137	10	1.37E-05	1.684083	0.4294	5.499294
Pure Error	1.62E-05	2	8.11E-06			0.653091
Cor Total	0.002484	26				100
< Significant						

Normal plot

Normal plot is a graphical technique which shows whether the points are normally distributed or not. The data are plotted against Residuals in such a way that the points should lay in a straight line. If the points follow a straight line then the points are normally distributed. Normal plot Figure 5.7, show that the TWR data points except two are very close to the straight line. This indicates that the experimental data are normally distributed. The run order 9 and 13 have some distance below from the line due to higher tool wear rate. Figure 5.8, normal plot for TWR using copper tool shows that almost all points are nearer to straight line and looks like S-shape, which indicates that the points are normally distributed.

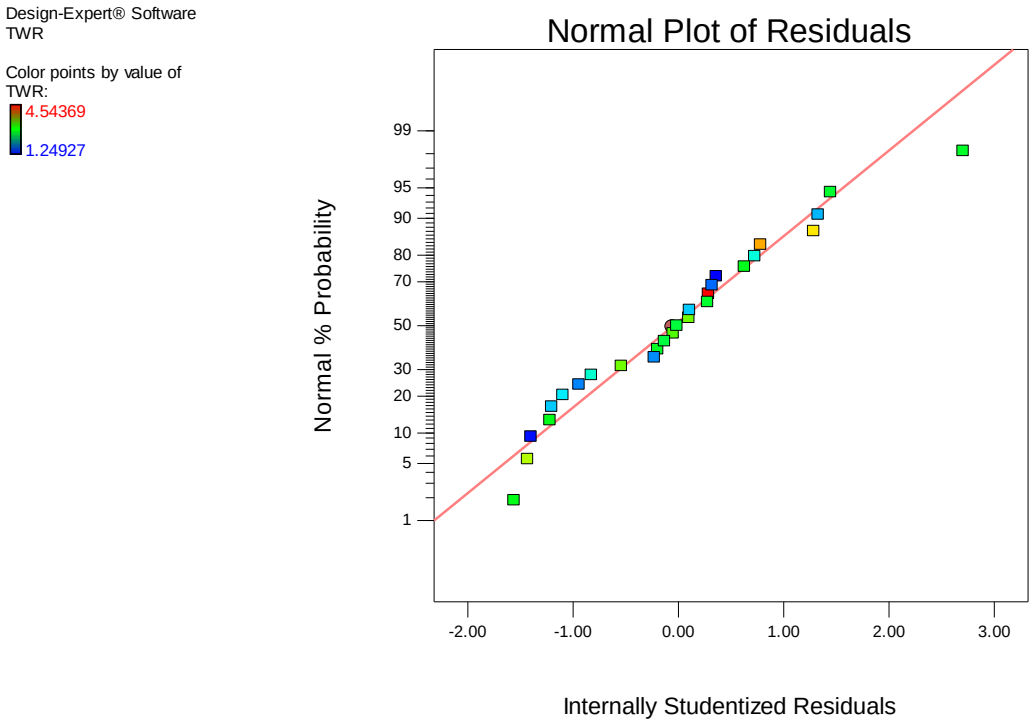

Figure 5.7. Normal plot of residuals for TWR using brass tool

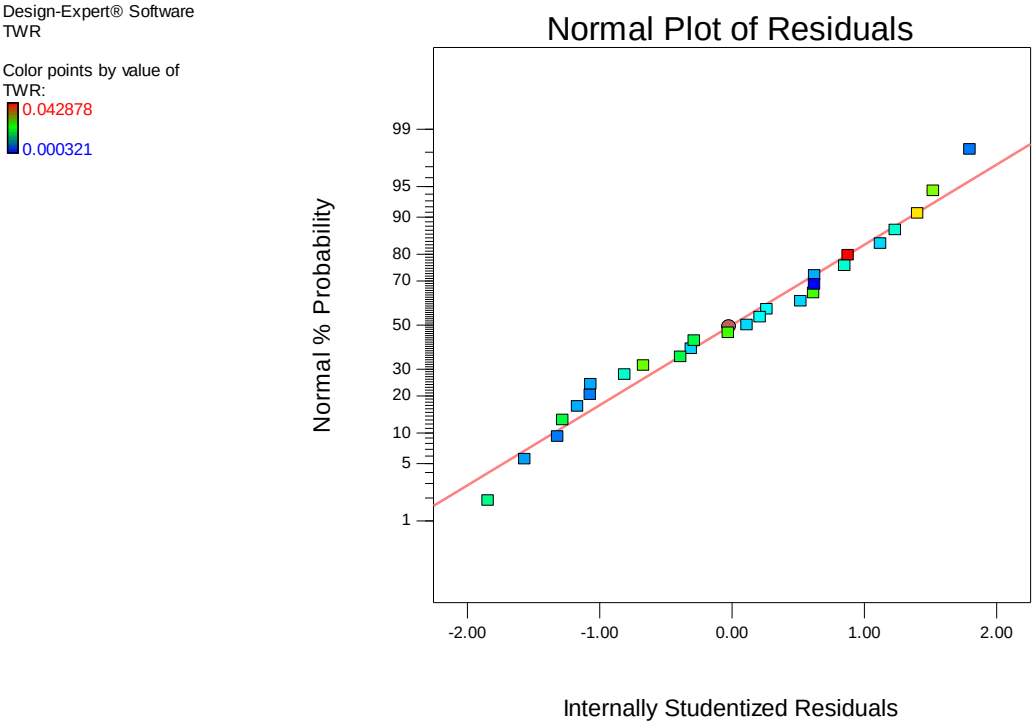

Figure 5.8. Normal plot of residuals for TWR using copper tool

Figure 5.9 shows surface plot for TWR of brass tool in relation with discharge current (Ip) and pulse-on-time (Ton). It can be observed that TWR increases steeply with increasing Ip from 3 A to 7 A for any value of Ton. This occurs due to melting and erosion of tool at high temperature as a result of strong spark. But TWR increases with increasing Ton up to 200 µs from 100 µs and then decreases up to 300 µs due to increase of inter electrode gap. This figure also shows that, minimum TWR can be achieved at 3 A discharge current and 100 µs pulse-on-time. Figure 5.10 shows the surface plot for TWR of brass tool in relation with duty factor and flushing pressure. It can be observed that TWR increases with increasing τ value from 80 % to 90% for any value of flushing pressure and also increases slowly with increasing flushing pressure from 0.2 to 0.4 bar for any value of duty factor. TWR increases with τ due to more time involvement of tool in spark generation. Although flushing pressure have not much effect but it does not allow carbon to deposit on tool face, so TWR increases. Minimum TWR is achieved at 80 % duty factor and 0.2 bar flushing pressure.

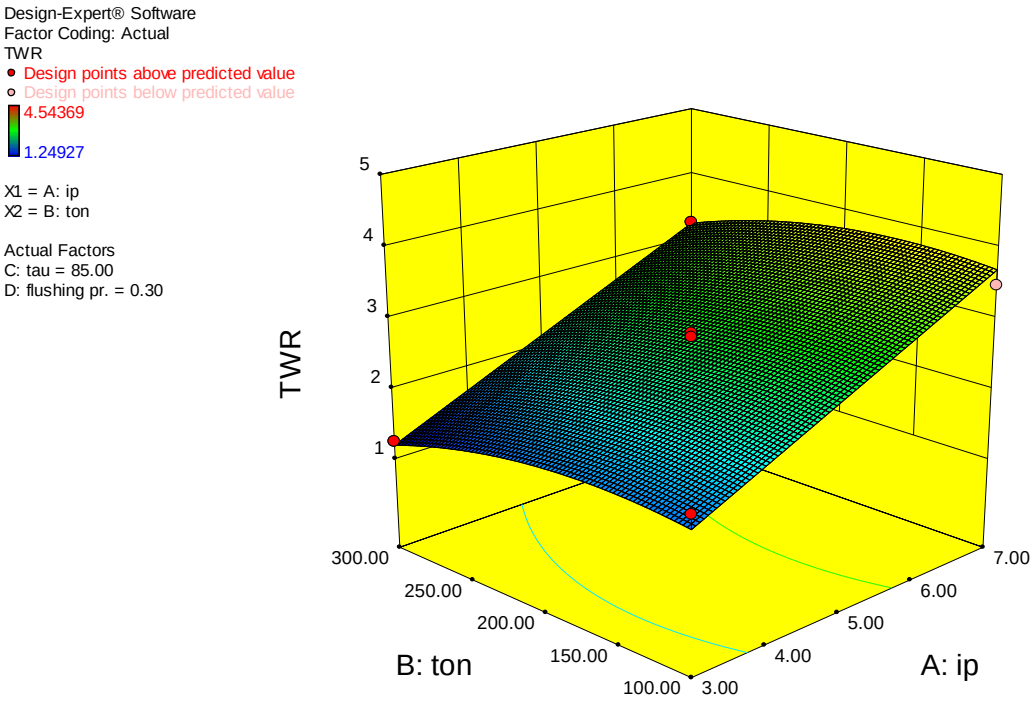

Figure 5.9. Surface plot For TWR using brass tool

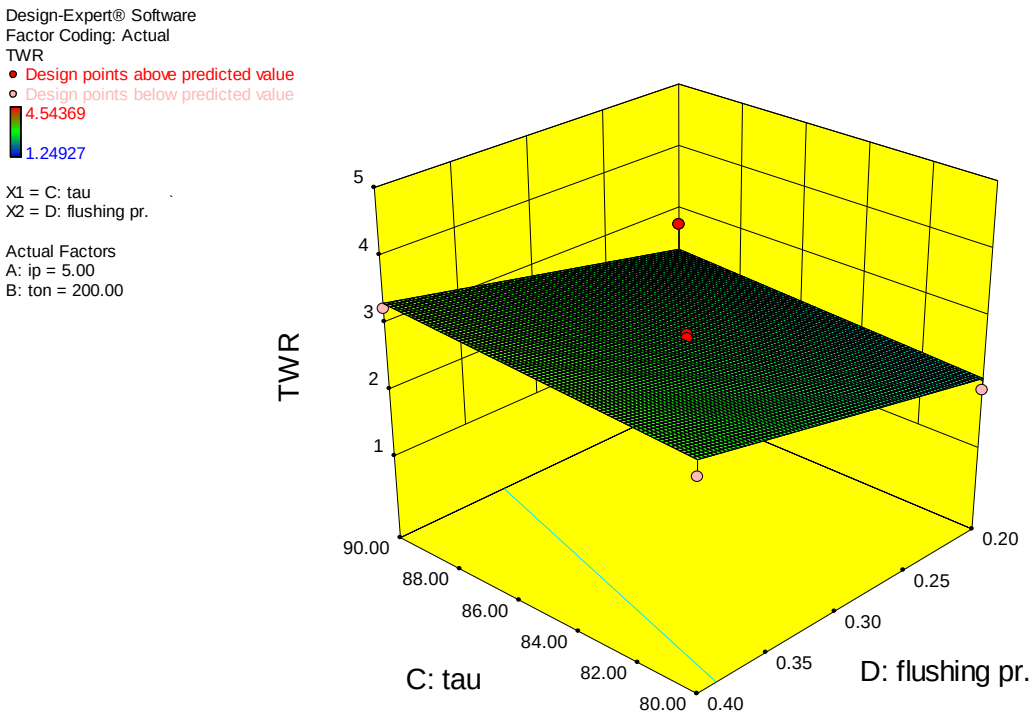

Figure 5.10.Surface plot For TWR using brass tool

Figure 5.11 shows the surface plot for TWR of copper tool in relation with discharge current and pulse-on-time. It is observed that TWR increases steeply with increasing Ip from 3 A to 7 A for any value of pulse-on-time. This occurs due to melting and erosion of tool at high temperature as a result of strong spark. But TWR decreases slightly with increasing Ton up to 200 µs from 100 µs and then increases slowly up to 300 µs for any value of discharge current due to carbon deposition. So minimum tool wear rate is achieved at 3 A discharge current and 200 µs pulse-on-time. Figure 5.12 shows the surface plot for TWR of copper tool in relation with duty factor and flushing pressure. It can be observed that TWR increases with increasing duty factor from 80 % to 90 % and also increases slowly with increasing flushing pressure from 0.2 bar to 0.4 bar for any value of duty factor. TWR increases with τ due to more time involvement of tool with respect to total time in spark generation. Although flushing pressure have not much effect but it does not allow carbon to deposit on tool face, so TWR increases.

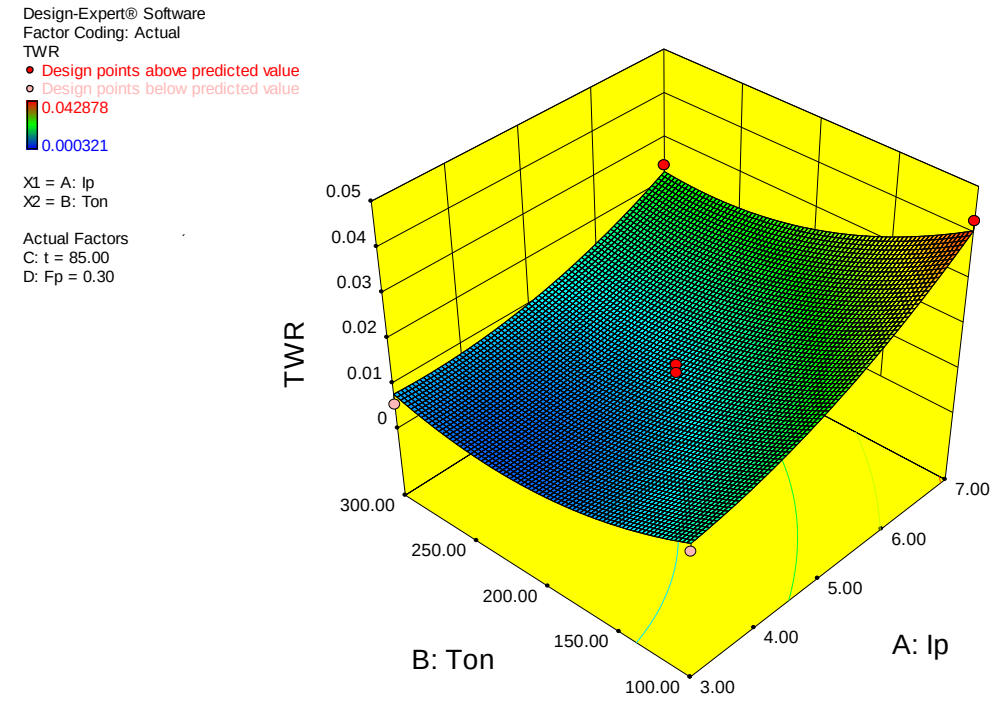

Figure 5.11.Surface plot for TWR using copper tool

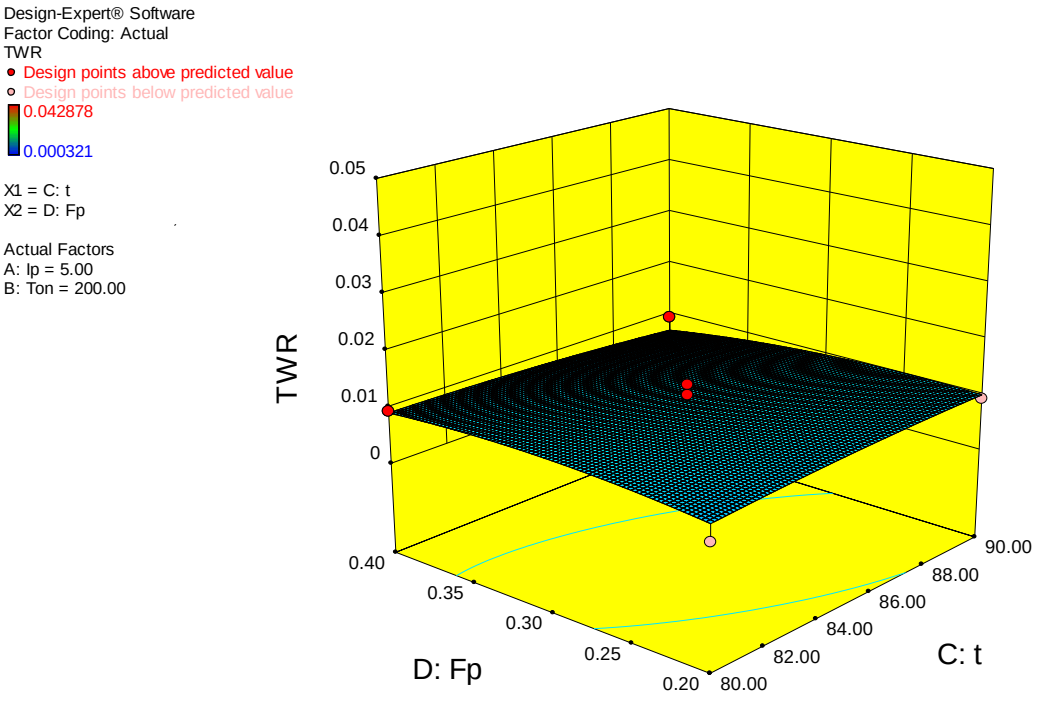

Figure 5.12.Surface plot for TWR using copper tool

5.2.3 Surface roughness (Ra)

Surface roughness is the measure of texture of a surface and an important objective of any precision machining process. Therefore, the controllable factors are to be optimized to minimize surface roughness. The Table 5.1 shows the experimental results for surface roughness (Ra) using brass and copper as electrode.

Table 5.7. Ra using Brass and Copper tool

Expt. No.	Ip (A)	Ton (μs)	τ (%)	Fp (bar)	Ra using brass tool (μm)	Ra using copper tool (μm)
1	3	100	85	0.3	3.93	3.61
2	7	100	85	0.3	4.57	6.38
3	3	300	85	0.3	4.65	2.6
4	7	300	85	0.3	7.59	4.3
5	5	200	80	0.2	6.52	4.33
6	5	200	90	0.2	6.15	4.6
7	5	200	80	0.4	6.4	5.1
8	5	200	90	0.4	5.93	4.52
9	3	200	80	0.3	5.17	3.42
10	7	200	80	0.3	6.47	6.11
11	3	200	90	0.3	4.55	2.83
12	7	200	90	0.3	5.48	5.38
13	5	100	85	0.2	5.49	4.78
14	5	300	85	0.2	7.35	3.92
15	5	100	85	0.4	5.07	5.54
16	5	300	85	0.4	7.46	3.22
17	3	200	85	0.2	5.27	3.11
18	7	200	85	0.2	7.73	5.45
19	3	200	85	0.4	4.69	3.21
20	7	200	85	0.4	6.83	6.33
21	5	100	80	0.3	4.28	5.42
22	5	300	80	0.3	8.51	4.27
23	5	100	90	0.3	4.47	4.67
24	5	300	90	0.3	7.79	3.64
25	5	200	85	0.3	6.21	3.8
26	5	200	85	0.3	5.77	4.24
27	5	200	85	0.3	5.8	4.52

ANOVA of Response Surface Quadratic Model for Ra

The satisfactoriness of the model is checked by using the analysis of variance (ANOVA) technique. As per this technique, if the calculated value of the P value of the developed model does not exceed the standard tabulated value of P for a desired level of confidence (say 95%),

then the model is considered to be satisfactory within the confidence limit. Analysis of variance (ANOVA) has been conducted on Ra values using brass tool and shown in Table 5.8. It is observed that the parameters such as Ip, Ton, τ, interaction of Ip and Ton, square of Ip and flushing pressure are the found to be significant for improving surface roughness. Ip and Ton have largely contribute to the surface roughness at 21 % and 49 % respectively. As the tool work piece contact time is more there is uneven inter electrode gap with heated atmosphere which results in uneven material rate and roughness is more. The coefficient of performance is found to be 92.77 %. Analysis of variance (ANOVA) has been conducted on Ra values using copper tool and shown in Table 5.9. It is observed that the parameters such as Ip, Ton, τ, are the found to be significant for improving surface roughness. Ip and Ton have largely contributed to the surface roughness at 66.75 % and 20.71 % respectively. This occurs due to high heat at large discharge current and as tool work piece contact time is more there is uneven inter electrode gap with heated atmosphere which results in uneven material rate and roughness is more. The coefficient of performance is found to be 94.71 %.

Table 5.8. ANOVA for Surface Roughness (Ra) using brass tool

Source	Sum of Squares	df	Mean Square	F Value	p-value Prob > F	% of contribution
Model	31.00029	14	2.21431	10.99749	< 0.0001	92.76955
A-Ip	7.06868	1	7.06868	35.10701	< 0.0001	21.15328
B-Ton	16.68521	1	16.68521	82.86812	< 0.0001	49.93113
C-τ	1.32003	1	1.32003	6.55603	< 0.0250	3.95025
D-Fp	0.30720	1	0.30720	1.52573	0.2404	0.91931
AB	1.31103	1	1.31103	6.51129	< 0.0254	3.92329
AC	0.16000	1	0.16000	0.79465	0.3902	0.47881
AD	0.05760	1	0.05760	0.28607	0.6025	0.17237
BC	0.19360	1	0.19360	0.96153	0.3462	0.57936
BD	0.00250	1	0.00250	0.01242	0.9131	0.00748
CD	0.00250	1	0.00250	0.01242	0.9131	0.00748
A^2	1.53606	1	1.53606	7.62893	< 0.0172	4.59672
B^2	0.05787	1	0.05787	0.28742	0.6017	0.17318
C^2	0.01356	1	0.01356	0.06733	0.7997	0.04057
D^2	1.04233	1	1.04233	5.17682	< 0.0420	3.11922
Residual	2.41616	12	0.20135			7.23044
Lack of Fit	2.29529	10	0.22953	3.79806	0.2263	6.86875
Pure Error	0.12087	2	0.06043			0.36170
Cor Total	33.41645	26				100
< Significant						

Table 5.9. ANOVA for Surface Roughness (Ra) using copper tool

Source	Sum of Squares	df	Mean Square	F Value	p-value Prob > F	% of contribution
Model	27.20597	14	1.94328	15.33600	< 0.0001	94.7067
A-Ip	19.17741	1	19.17741	151.34420	< 0.0001	66.7585
B-Ton	5.95021	1	5.95021	46.95782	< 0.0001	20.7133
C-t	0.04441	1	0.04441	0.35046	0.5648	0.1546
D-Fp	0.33668	1	0.33668	2.65697	0.1290	1.1720
AB	0.28623	1	0.28623	2.25883	0.1587	0.9964
AC	0.15210	1	0.15210	1.20034	0.2948	0.5295
AD	0.00490	1	0.00490	0.03867	0.8474	0.0171
BC	0.53290	1	0.53290	4.20554	0.0628	1.8551
BD	0.00360	1	0.00360	0.02841	0.8690	0.0125
CD	0.18063	1	0.18063	1.42546	0.2556	0.6288
A^2	0.01356	1	0.01356	0.10699	0.7492	0.0472
B^2	0.00005	1	0.00005	0.00036	0.9852	0.0002
C^2	0.26502	1	0.26502	2.09151	0.1737	0.9226
D^2	0.32122	1	0.32122	2.53503	0.1373	1.1182
Residual	1.52057	12	0.12671			5.2932
Lack of Fit	1.25710	10	0.12571	0.95428	0.6138	4.3761
Pure Error	0.26347	2	0.13173			0.9172
Cor Total	28.72654	26				100

Normal plot

Normal plot is a graphical technique which shows whether the points are normally distributed or not. The data are plotted against Residuals in such a way that the points should lay in a straight line. If the points follow a straight line then the points are normally distributed. Figure 5.13 shoes the normal probability plot for Ra using brass tool. It can be observed that about all points are close to the line having 'S' shape, which means the Ra values are normally distributed. Figure 5.14 shows the normal probability plot for Ra using copper tool. The Ra values are following the straight line. Therefore Ra using copper tool are normally distributed.

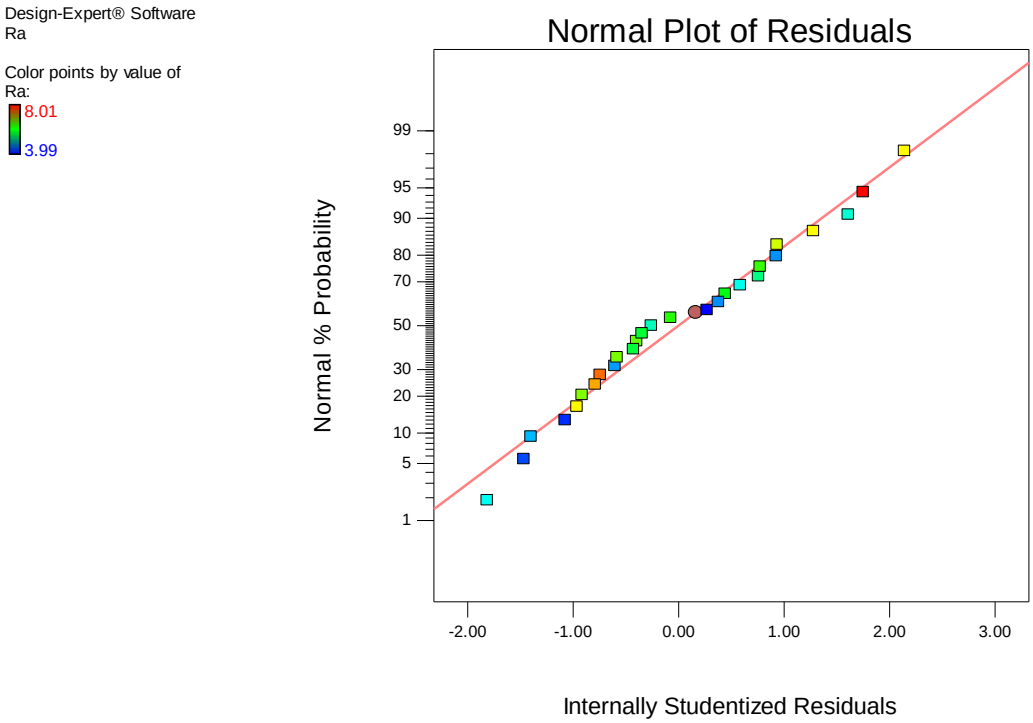

Figure 5.13. Normal probability of residuals for Ra using brass tool

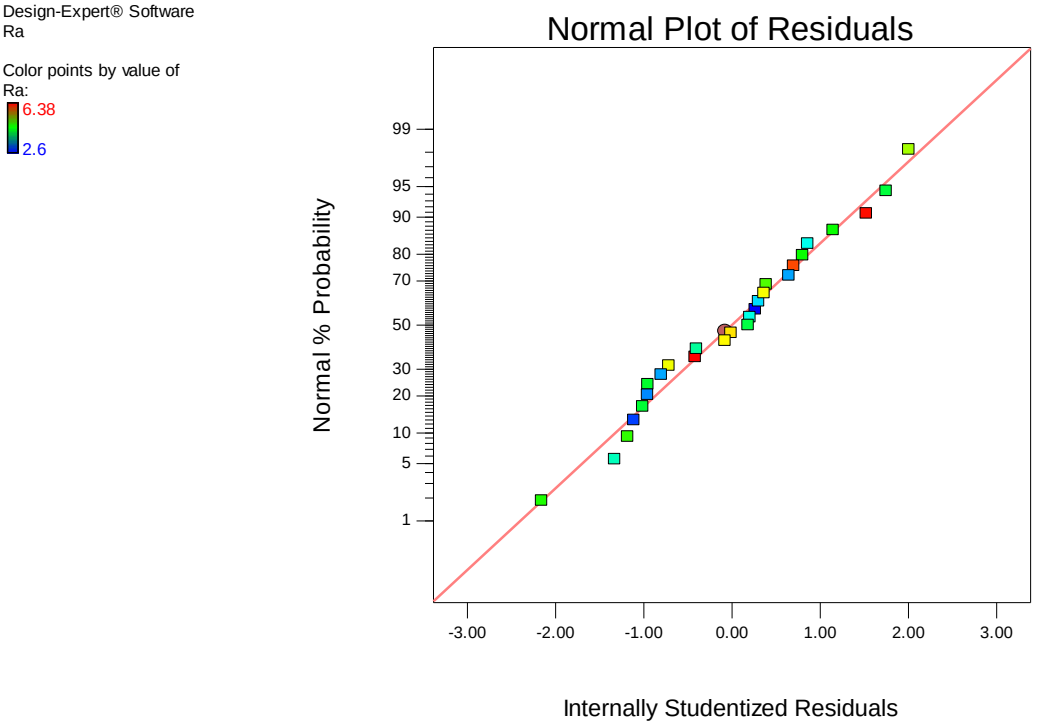

Figure 5.14. Normal probability of residuals for Ra using copper tool

Surface Plot

Figure 5.15 shows the surface plot for MRR using brass tool, in relation to the process parameters such as discharge current (Ip) and pulse-on-time (Ton). It can be observed that surface roughness value tends to increase with Ip up to 5A after that it is increasing but less as compared to previous one for any value of Ton due to more heat generation and more is the crater. Ra tends to increase with Ton from 100 µs to 300 µs as tool work piece contact time is more, there is uneven inter electrode gap with heated atmosphere which results in uneven material. Therefore better surface roughness is obtained at 3 A discharge current due to their dominant control over the input energy and 100 µs pulse-on-time.

Figure 5.16 shows the surface plot for Ra using brass tool, in relation to the process parameters such as duty factor and flushing pressure. Surface plot indicates that Ra decreases slowly with increasing τ from 80 % to 90 % for any value of flushing pressure. Ra decreases with increasing flushing pressure from 0.2 bar to 0.4 bar for any value of Ton as there is no material deposition on the surface. Also it can be observed that better roughness is achieved at 90 % τ and 0.4 bar flushing pressure.

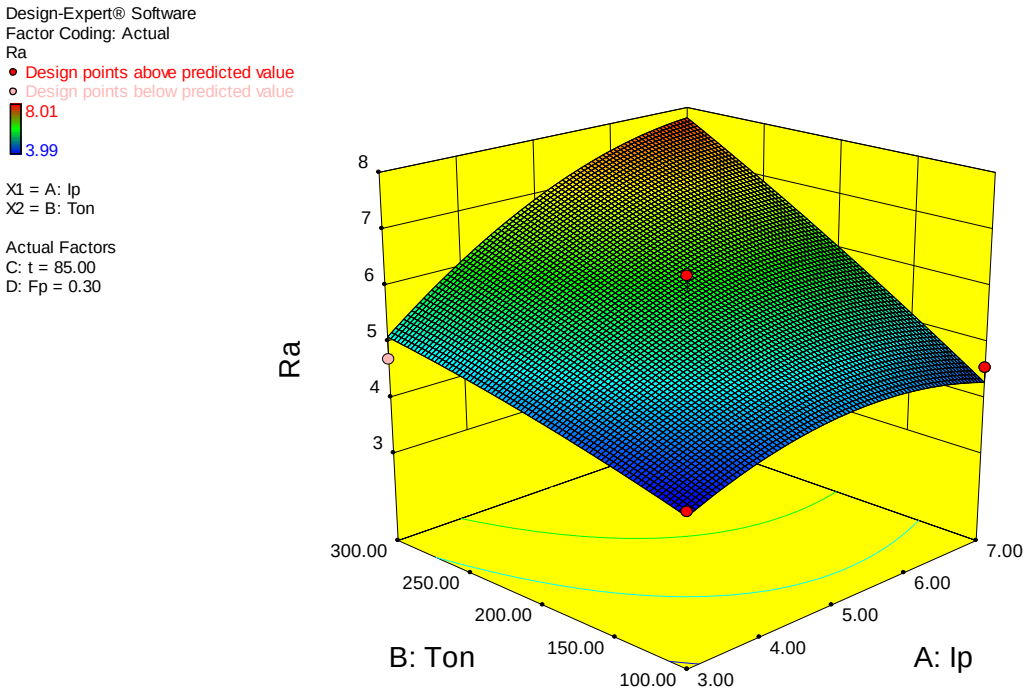

Figure 5.15. Surface plot for Ra using brass tool

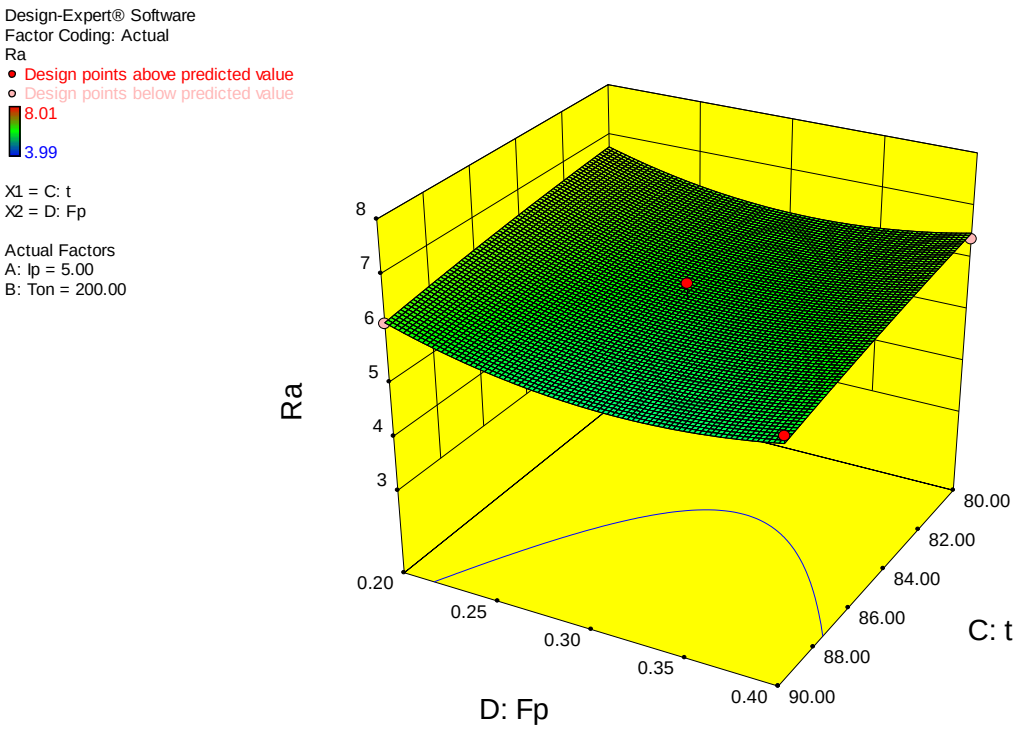

Figure 5.16. Surface plot for Ra using brass tool

Figure 5.17 shows the surface plot for Ra using copper tool, in relation to the process parameters such as discharge current (Ip) and pulse-on-time (Ton). It can be observed that surface roughness tends to increase with discharge current from 3 A to 7A due to more heat generation as a result of strong spark for any value of Ton. Surface roughness is decreasing with increasing pulse-on-time for any value of discharge current. It is clearly seen from the plot that better surface roughness is achieved at 3 A discharge current and 300 µs pulse-on-time.

Figure 5.18 shows the surface plot for Ra using copper tool, in relation to the process parameter such as duty factor and flushing pressure. It can be observed that the duty factor and flushing pressure doesn't have much effect on Ra. But minimum roughness is obtained at 90 % duty factor and 0.4 bar flushing pressure.

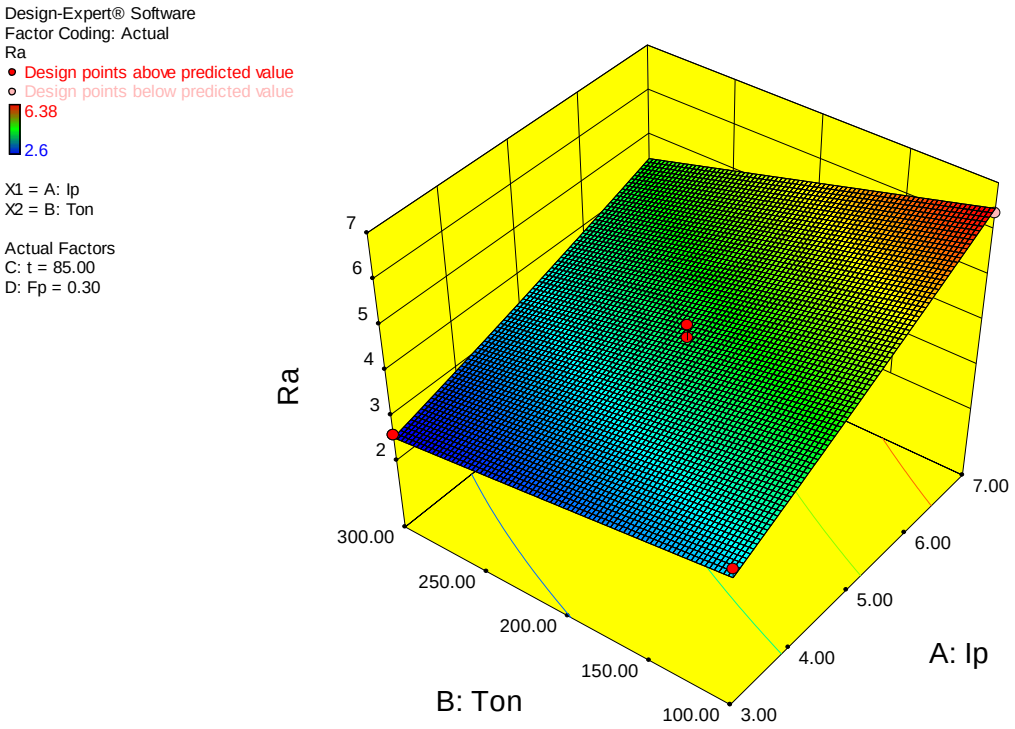

Figure 5.17. Surface plot for Ra using copper tool

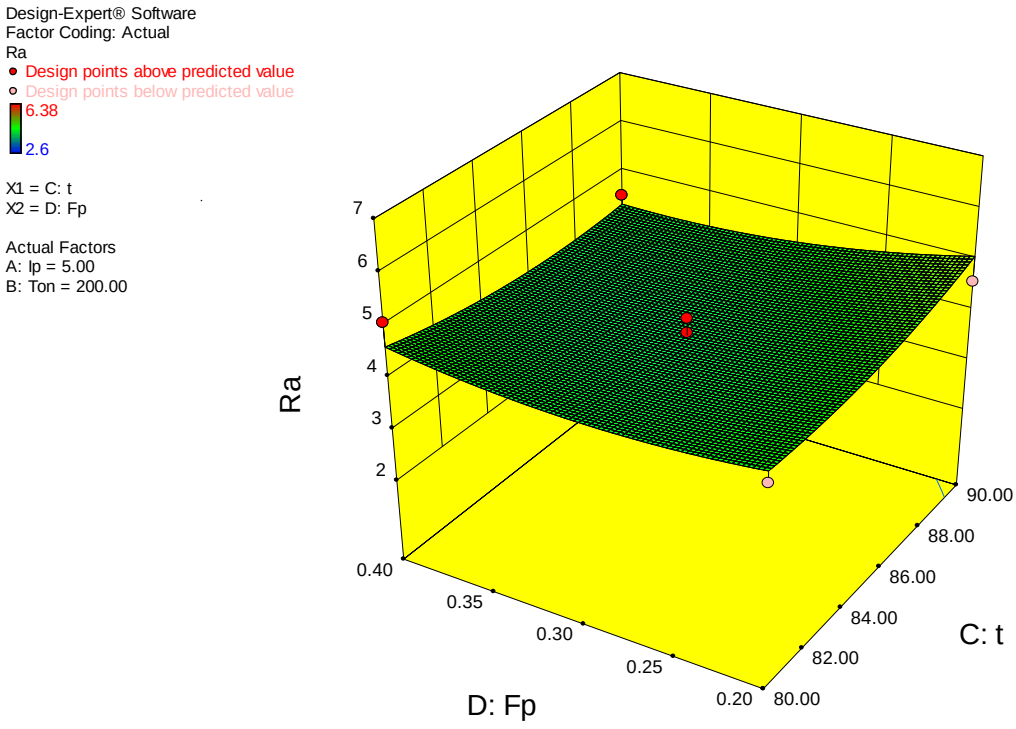

Figure 5.18. Surface plot for Ra using copper tool

5.2.4 Circularity

Electrical Discharge Machining is used for making complicated shape by transferring the tool profile to work piece. In case of cylindrical tool, circularity is the measure of transformation of tool profile to work piece. Circularity is measured by taking the ratio of minimum to maximum diameter and the circularity values are shown in Table 5.10 for brass and copper tool.

Table 5.10. Circularity using Brass and Copper tool

Expt. No	Ip (A)	Ton (μs)	τ (%)	Fp (bar)	Circularity using brass tool	Circularity using copper tool
1	3	100	85	0.3	0.8500	0.8403
2	7	100	85	0.3	0.8520	0.8437
3	3	300	85	0.3	0.8842	0.8180
4	7	300	85	0.3	0.8557	0.8415
5	5	200	80	0.2	0.8488	0.8437
6	5	200	90	0.2	0.8520	0.8437
7	5	200	80	0.4	0.8375	0.8350
8	5	200	90	0.4	0.8598	0.8412
9	3	200	80	0.3	0.8366	0.8211
10	7	200	80	0.3	0.8888	0.8442
11	3	200	90	0.3	0.8435	0.8402
12	7	200	90	0.3	0.8028	0.8469
13	5	100	85	0.2	0.8275	0.8524
14	5	300	85	0.2	0.8461	0.8355
15	5	100	85	0.4	0.8411	0.8351
16	5	300	85	0.4	0.8439	0.8453
17	3	200	85	0.2	0.8494	0.8397
18	7	200	85	0.2	0.8424	0.8446
19	3	200	85	0.4	0.8383	0.8400
20	7	200	85	0.4	0.8397	0.8402
21	5	100	80	0.3	0.8329	0.8392
22	5	300	80	0.3	0.8479	0.8451
23	5	100	90	0.3	0.8536	0.8443
24	5	300	90	0.3	0.8369	0.8344
25	5	200	85	0.3	0.8402	0.8400
26	5	200	85	0.3	0.8366	0.8531
27	5	200	85	0.3	0.8460	0.8467

ANOVA of Response Surface Quadratic Model for circularity

The satisfactoriness of the model is checked by using the analysis of variance (ANOVA) technique. As per this technique, if the calculated value of the P value of the developed model does not exceed the standard tabulated value of P for a desired level of confidence (say 95%),

then the model is considered to be satisfactory within the confidence limit. ANOVA test results are presented in the Table 5.11 and Table 5.12.

The experimental study ANOVA (Table 5.11), it is found that the factor Ip, Ton, τ and square of Ton, τ and Fp are significant terms. Ton largely affects the circularity having a contribution of 29.36 % as a result of more time of spark in between the tool and work piece. Therefore the total region of tool is heated and circular profile is transferred to the work piece. Ip has also significantly affects circularity with a contribution of 19.53 %. The other significant terms have very less effect on circularity. The coefficient of performance value (R^2) of the model is found to be 86.6%.

The experimental study ANOVA (Table 5.12), it is found that the factor Ip, interaction of Ton and τ are significant terms. Ip largely affects the circularity having a contribution of 21.08 % as a result of more time of spark in between the tool and work piece. Therefore the total region of tool is heated and circular profile is transferred to the work piece. Interaction of Ton and τ have the effect on circularity with a 12.2 % of contribution. The coefficient of performance value (R^2) of the model is found to be 86.4%.

Table 5.11. ANOVA for Circularity using brass tool

Source	Sum of Squares	df	Mean Square	F Value	p-value Prob > F	% of contribution
Model	0.0004	14	2.9E-05	5.44552	<0.0028	86.4003
A-Ip	9.1E-05	1	9.1E-05	17.23332	<0.0013	19.5307
B-Ton	0.00014	1	0.00014	25.90678	<0.0003	29.3604
C-t	3.3E-05	1	3.3E-05	6.24538	<0.0280	7.0779
D-Fp	3E-08	1	3E-08	0.00568	0.9411	0.0064
AB	1.2E-05	1	1.2E-05	2.24175	0.1602	2.5406
AC	1.8E-06	1	1.8E-06	0.35039	0.5649	0.3971
AD	2.3E-05	1	2.3E-05	4.41941	0.0573	5.0086
BC	7.6E-06	1	7.6E-06	1.44831	0.2520	1.6414
BD	5.8E-06	1	5.8E-06	1.09117	0.3168	1.2366
CD	1.7E-05	1	1.7E-05	3.29414	0.0946	3.7333
A^2	2.1E-05	1	2.1E-05	4.03969	0.0675	4.5782
B^2	6.1E-05	1	6.1E-05	11.48004	<0.0054	13.0104
C^2	2.5E-05	1	2.5E-05	4.80523	<0.0488	5.4458
D^2	2.8E-05	1	2.8E-05	5.36604	<0.0390	6.0814
Residual	6.3E-05	12	5.3E-06			13.5997
Lack of Fit	4.5E-05	10	4.5E-06	0.49331	0.8176	9.6766
Pure Error	1.8E-05	2	9.1E-06			3.9231
Cor Total	0.00047	26				100
< Significant						

Table 5.12. ANOVA for Circularity using copper tool

Source	Sum of Squares	df	Mean Square	F Value	p-value Prob > F	% of contribution
Model	0.001061	14	7.58E-05	2.032892	0.1125	70.35809
A-Ip	0.000318	1	0.000318	8.537635	<0.0128	21.08753
B-Ton	0.000103	1	0.000103	2.769784	0.1219	6.830239
C-t	2.43E-06	1	2.43E-06	0.065185	0.8028	0.161141
D-Fp	2.08E-06	1	2.08E-06	0.055886	0.8171	0.137931
AB	0.000101	1	0.000101	2.709406	0.1257	6.697613
AC	5.52E-06	1	5.52E-06	0.148142	0.7071	0.366048
AD	6.72E-05	1	6.72E-05	1.803722	0.2041	4.456233
BC	0.000184	1	0.000184	4.925162	<0.0465	12.20159
BD	6.24E-05	1	6.24E-05	1.674157	0.2201	4.137931
CD	9.61E-06	1	9.61E-06	0.25779	0.6208	0.637268
A^2	0.000165	1	0.000165	4.413452	0.0575	10.94164
B^2	7.52E-05	1	7.52E-05	2.016358	0.1811	4.986737
C^2	5.93E-06	1	5.93E-06	0.158986	0.6971	0.393236
D^2	5.56E-05	1	5.56E-05	1.491838	0.2454	3.687003
Residual	0.000447	12	3.73E-05			29.64191
Lack of Fit	0.000362	10	3.62E-05	0.842511	0.6553	24.00531
Pure Error	8.58E-05	2	4.29E-05			5.689655
Cor Total	0.001508	26				100

Normal plot

Normal plot is a graphical technique which shows whether the points are normally distributed or not. The data are plotted against Residuals in such a way that the points should lay in a straight line. If the points follow a straight line then the points are normally distributed. The normal probability plot for circularity using brass tool shown in Figure 5.19 indicates that about all points are close to a straight line and looks like 'S' shape. So the circularity values are normally distributed. The normal probability plot for circularity using copper tool shown in Figure 5.20 indicates that about all points are close to a straight line and looks like double 'S' shape. So the circularity values are normally distributed.

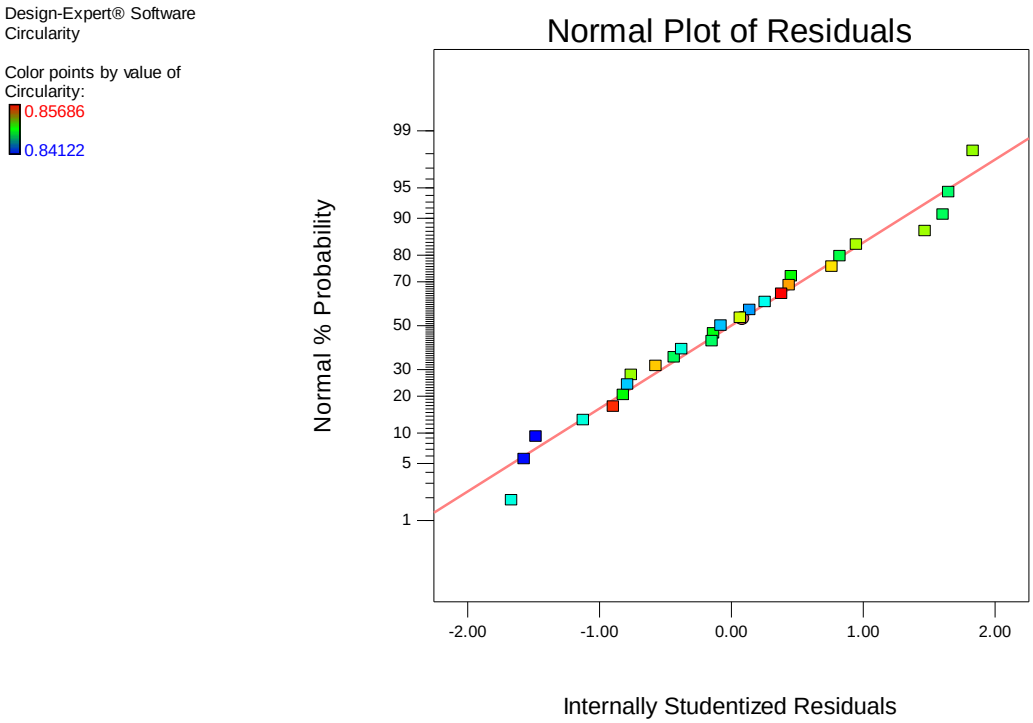

Figure 5.19. Normal probability plot of the residuals for circularity using brass tool

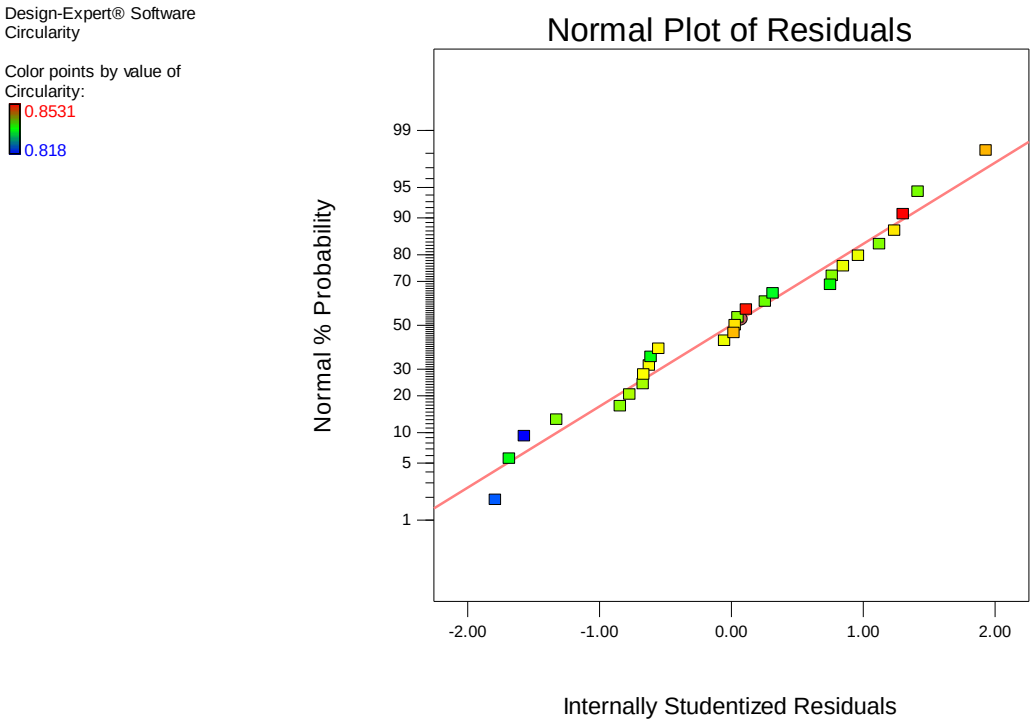

Figure 5.20. Normal probability plot of the residuals for circularity using copper tool

Surface plot

Figure 5.21 shows the surface plot for circularity using brass tool, in relation to the process parameters such as discharge current (Ip) and pulse-on-time (Ton). It can be observed that the circularity tends to increase with discharge current for any value of pulse-on-time due to concentration of spark. When tool moves downward as a result of more MRR the spark is concentrated and better circularity achieved. Circularity decreases slowly with increase Ton up to 200 µs and then tends to increase up to 300 µs for any value of discharge current. Due to the mutual effect the circularity seems to be very good. It is observed that best circularity is achieved at 7 A discharge current and 300 µs pulse-on-time.

Figure 5.22 shows the surface plot for circularity using brass tool, in relation with duty factor and flushing pressure. It can be observed that circularity initially decreases up to 85 % of duty factor, then increase slowly with increasing duty factor value from 85 % to 90 % for any value of flushing pressure. This occurs due to more time of contact of electrodes with respect to total cycle time and uniform heat distribution. Circularity is also initially decreases up to 3 bar, and then increases with increasing flushing pressure for any value of duty factor as this doesn't allow the eroded particle to interrupt in machining process. It is also seen that good circularity is achieved at 90 % duty factor and 0.4 bar flushing pressure.

Figure 5.23 shows the surface plot for circularity using coppr tool, in relation to the process parameters such as discharge current (Ip) and pulse-on-time (Ton). It can be observed that the circularity tends to increase with discharge current up to 5 A and then decreases for any value of pulse-on-time. Circularity decreases slowly with increase Ton for any value of discharge current. Due to the mutual effect the circularity seems to be very good. It is observed that best circularity is achieved at 7 A discharge current and 300 µs pulse-on-time.

Figure 5.24 shows the surface plot for circularity using copper tool, in relation with duty factor and flushing pressure. It can be observed that circularity decreases in very slower rate with increasing duty factor for any value of flushing pressure. This occurs due to more time of contact of electrodes with respect to total cycle time and uniform heat distribution. Circularity slowly increases with flushing pressure for any value of duty factor. It is also seen that good circularity is achieved at 90 % duty factor and 0.4 bar flushing pressure.

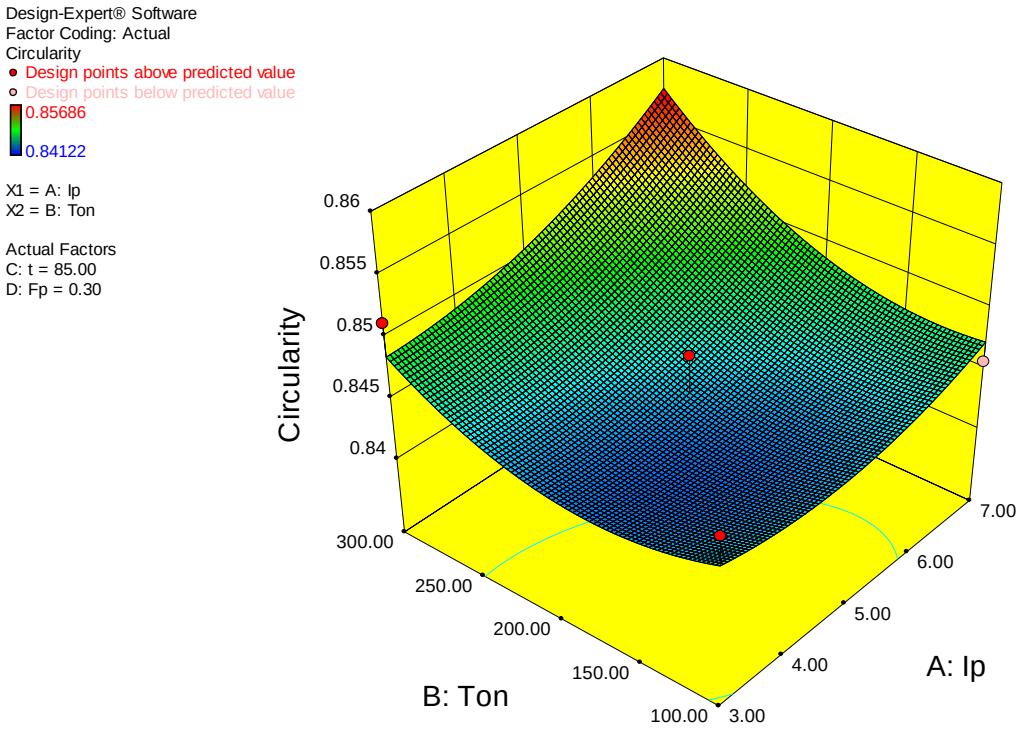

Figure 5.21. Surface plot for circularity using brass tool

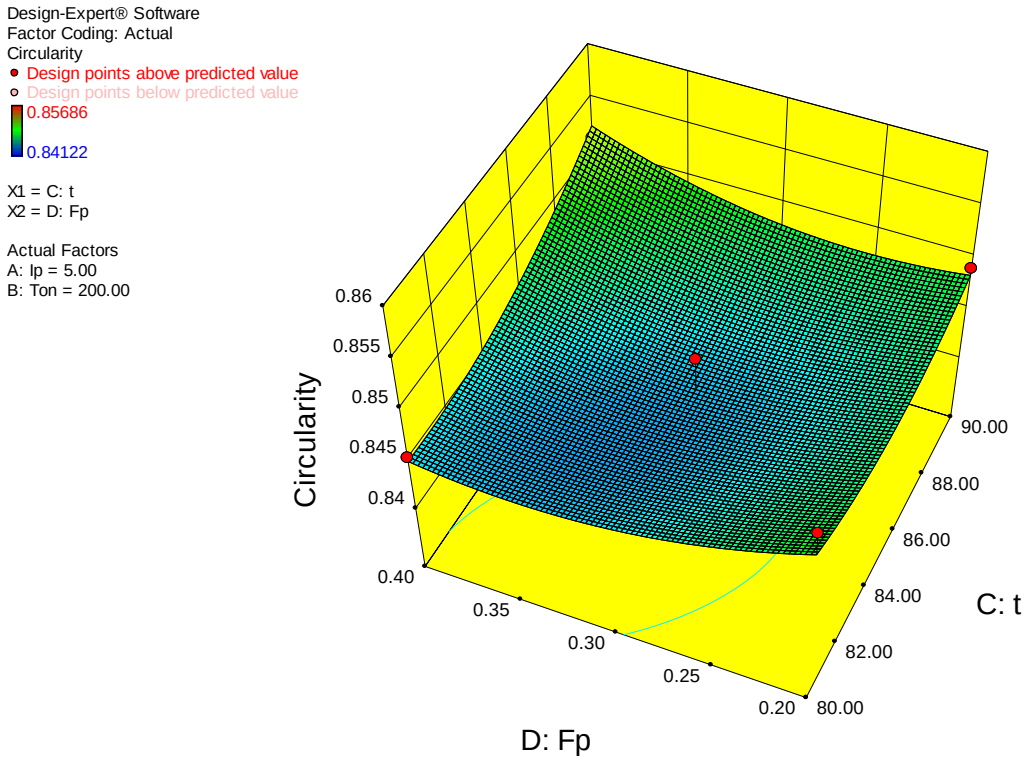

Figure 5.22. Surface plot for circularity using brass tool

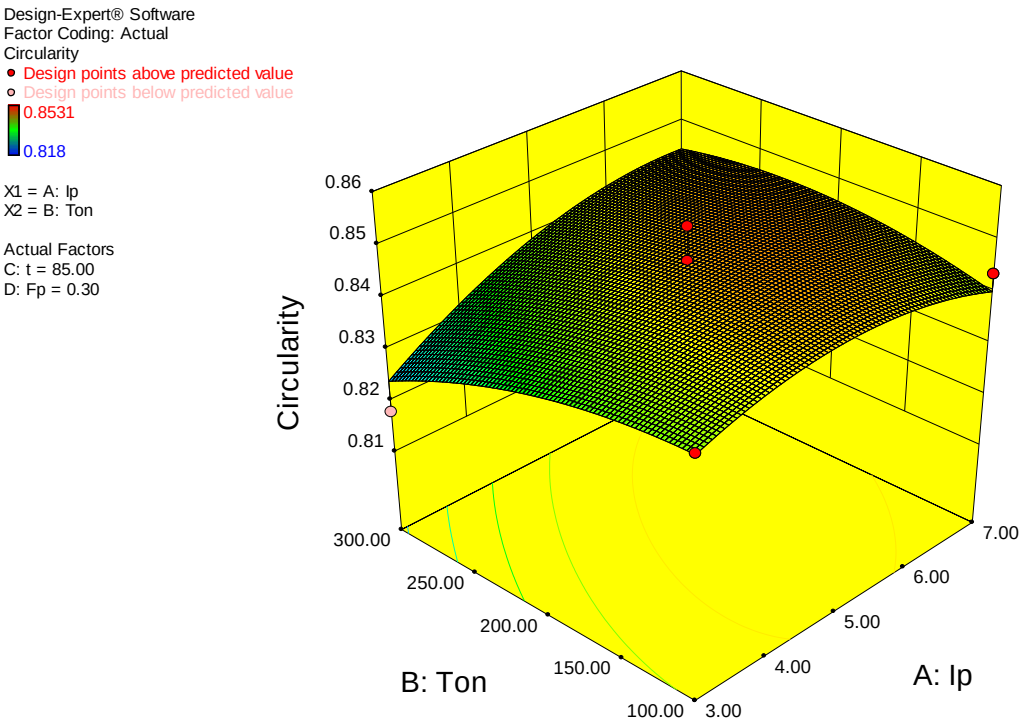

Figure 5.23. Surface plot for circularity using copper tool

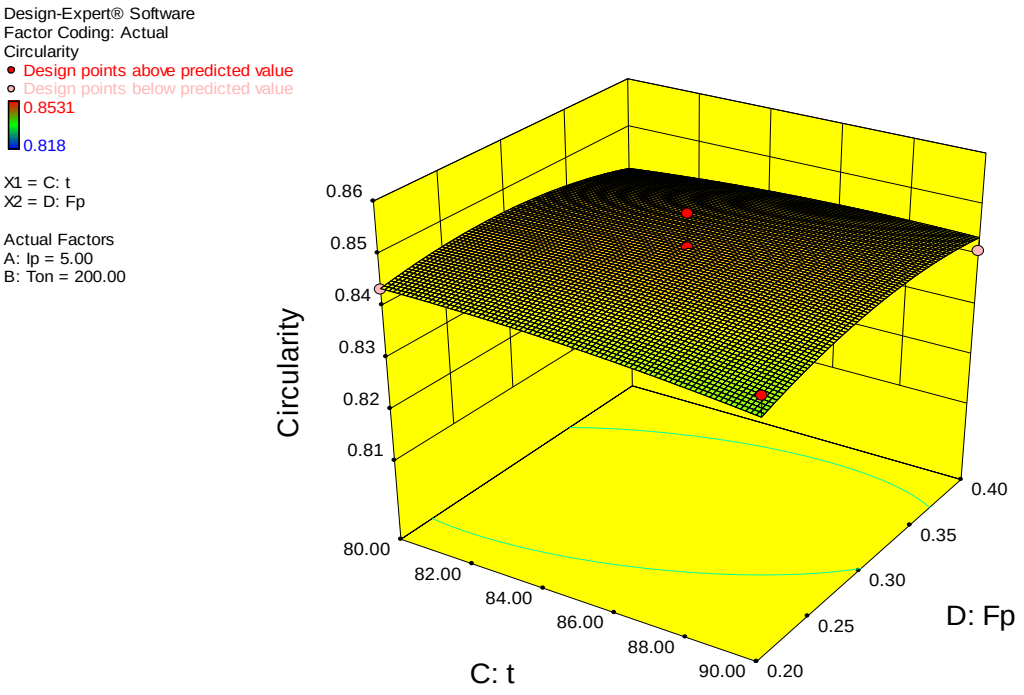

Figure 5.24. Surface plot for circularity using copper tool

The process models of four responses using brass and copper as tool materials (8 models) are obtained by regression analysis as given in equations below:

MRR (brass) = 9.76000 -1.02475*Ip -1.63867E-003*Ton -0.20600*τ +2.04408*Fp +4.55550E-003*Ip*Ton +2.49000E-003*Ip*τ +0.51950*Ip*Fp +1.73000E-005*Ton*τ +0.014502*Ton*Fp +0.023600*τ*Fp +0.074278*Ip*Ip -5.00525E-005*Ton*Ton +1.25450E-003*τ*τ -9.95750*Fp*Fp (5.1)

MRR(copper)=10.28928-4.09740*Ip +0.024741*Ton +0.044073*τ -49.59242*Fp-2.16450e-003*Ip*Ton+0.014395*Ip*τ+5.80000*Ip*Fp +3.46500e-005*Ton*τ -0.016210*Ton*Fp +0.067100*τ*Fp+0.38853*Ip*Ip-6.31158e-005*Ton*Ton-3.81333e-004*τ*τ+41.19542*Fp*Fp (5.2)

TWR (brass) = -1.67293 -0.19824*Ip +7.19683E-003*Ton -0.050700*τ +22.64712*Fp +4.67000E-004*Ip*Ton+2.87000E-003*Ip*τ+1.40838*Ip*Fp+6.85000E-006*Ton*τ -3.55000E-003*Ton*Fp -0.21820*τ*Fp-4.79062E-003*Ip*Ip-2.82337E-005*Ton*Ton+7.53500E-004*τ*τ-9.25375* Fp*Fp (5.3)

TWR (copper) = 0.065851 -0.045130*Ip -4.00746e-004*Ton +1.18213e-003*τ +0.29134*Fp -1.39813e -005*Ip*Ton +5.41075e-004*Ip*τ -0.015306*Ip*Fp +1.11050e-006*Ton*τ +1.86450e-004*Ton*Fp -2.02250e-003*τ*Fp +1.16135e-003*Ip*Ip +6.45204e-007*Ton*Ton-2.08633e-005*τ*τ -0.14425*Fp*Fp (5.4)

Ra (brass) = -19.93708 +2.67292*Ip +0.038296*Ton +0.47950*τ -27.37500*Fp +2.86250e-003*Ip*Ton -0.020000*Ip*τ +0.60000*Ip*Fp -4.40000e-004*Ton*τ +2.50000e-003*Ton*Fp -0.050000*τ*Fp -0.13417*Ip*Ip -1.04167e-005*Ton*Ton -2.01667e-003*τ*τ +44.20833* Fp* Fp (5.5)

Ra (copper) = 52.48135-0.83146*Ip+0.060679* Ton-1.32767* τ+20.00000* Fp-1.33750e-003 * Ip * Ton+0.019500*Ip* τ-0.17500*Ip*Fp-7.30000e-004*Ton* τ+3.00000e-003*Ton*Fp -0.42500*τ*Fp+0.012604*Ip*Ip+2.91667e-007*Ton*Ton+8.91667e-003*τ*τ +24.54167*Fp* Fp (5.6)

Circularity (brass) = 1.62695 -3.21458e-003*Ip -3.45708e-004*Ton -0.016026*τ -0.53163*Fp +8.62500e-006*Ip*Ton -6.75000e-005*Ip*τ +0.012125*Ip*Fp +2.80000e-006*Ton*τ -1.22500e-004*Ton*Fp+4.20000e-003*τ*Fp+4.96875e-004*Ip*Ip+3.37500e-007*Ton*Ton +8.75000e-005*τ*τ+0.23000*Fp*Fp (5.7)

Circularity (copper) = 0.69268 +0.027573*Ip -1.03804e-003*Ton +4.02583e-003*τ +0.11592*Fp +2.51250e-005*Ip*Ton -1.17500e-004*Ip*τ -0.020500*Ip*Fp +1.35500e-005*Ton*τ -3.95000e-004*Ton*Fp +3.10000e-003*τ*Fp -1.38854e-003*Ip*Ip -3.75417e-007*Ton*Ton -4.21667e-005*τ*τ -0.32292*Fp*Fp (5.8)

Genetic algorithm optimization technique is proposed to determine the optimal level for each parameter and the developed regression models are used as the fitness function in genetic algorithm (GA) optimization technique. The GA tool in Matlab 2009 is used to run the GA. The GA tool is run by changing population size, reproduction cross over fraction, migration fraction to minimize the fitness/objective function. In case of larger-the-best type of responses a unity negative factor is multiplied to fitness function to make them minimize type. The fitness vs generation/iteration is plotted at different generation and observed that about all curves are converges at generation 51 as shown in Figure 25-28. The optimal combination of process parameter and optimal value of responses are listed in Table 5.13.

Table 5.13. Optimal condition and optimal value

Response	Tool material	Ip (A)	Ton (μs)	τ (%)	Fp (bar)	Optimal value of response
MRR	Brass	6.997	299.998	90.000	0.398	7.706
	Copper	7.000	100.000	90.000	0.400	15.992
TWR	Brass	3.000	300.000	80.002	0.200	0.648
	Copper	3.648	255.155	80.000	0.200	0.271
Ra	Brass	3.000	100.000	80.000	0.332	3.729
	Copper	3.001	299.998	90.000	0.365	2.162
Circularity	Brass	7.000	299.999	89.997	0.400	0.868
	Copper	4.910	100.008	80.000	0.346	0.853

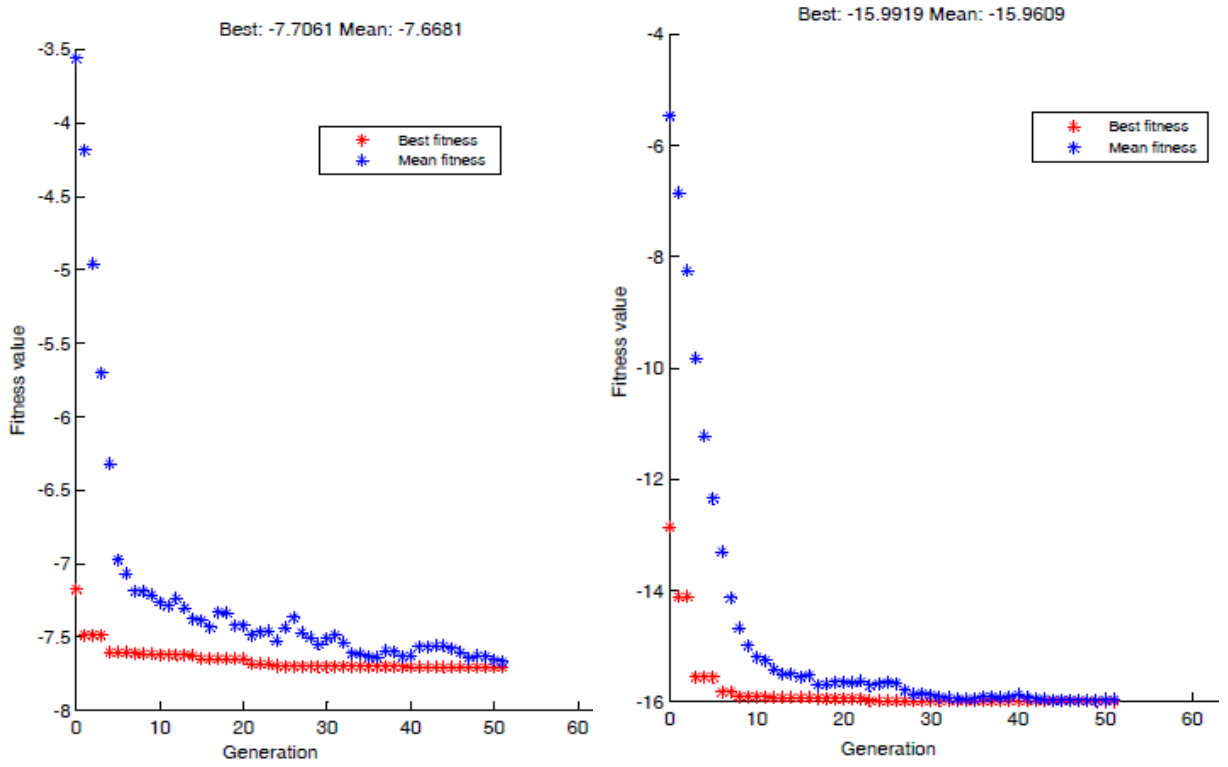

Figure 5.25. The convergence curve for MRR using brass and copper tool respectively

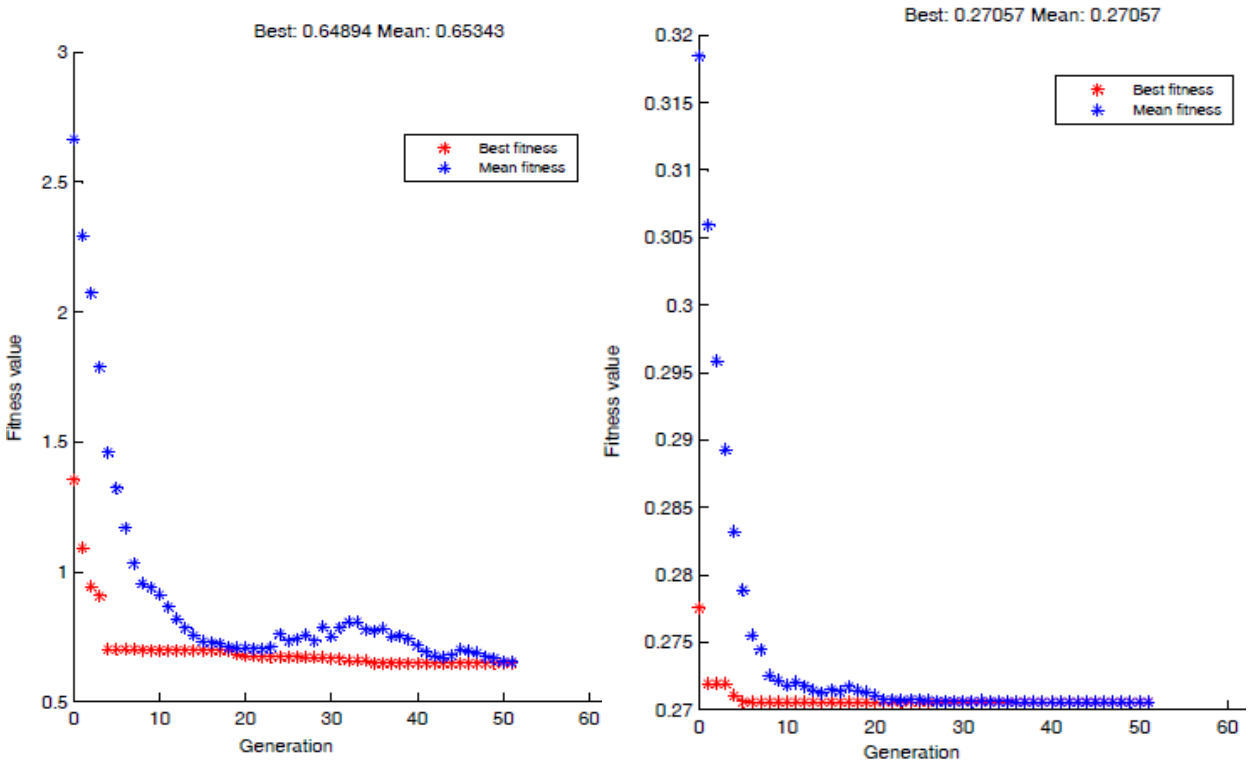

Figure 5.26. The convergence curve for TWR using brass and copper tool respectively

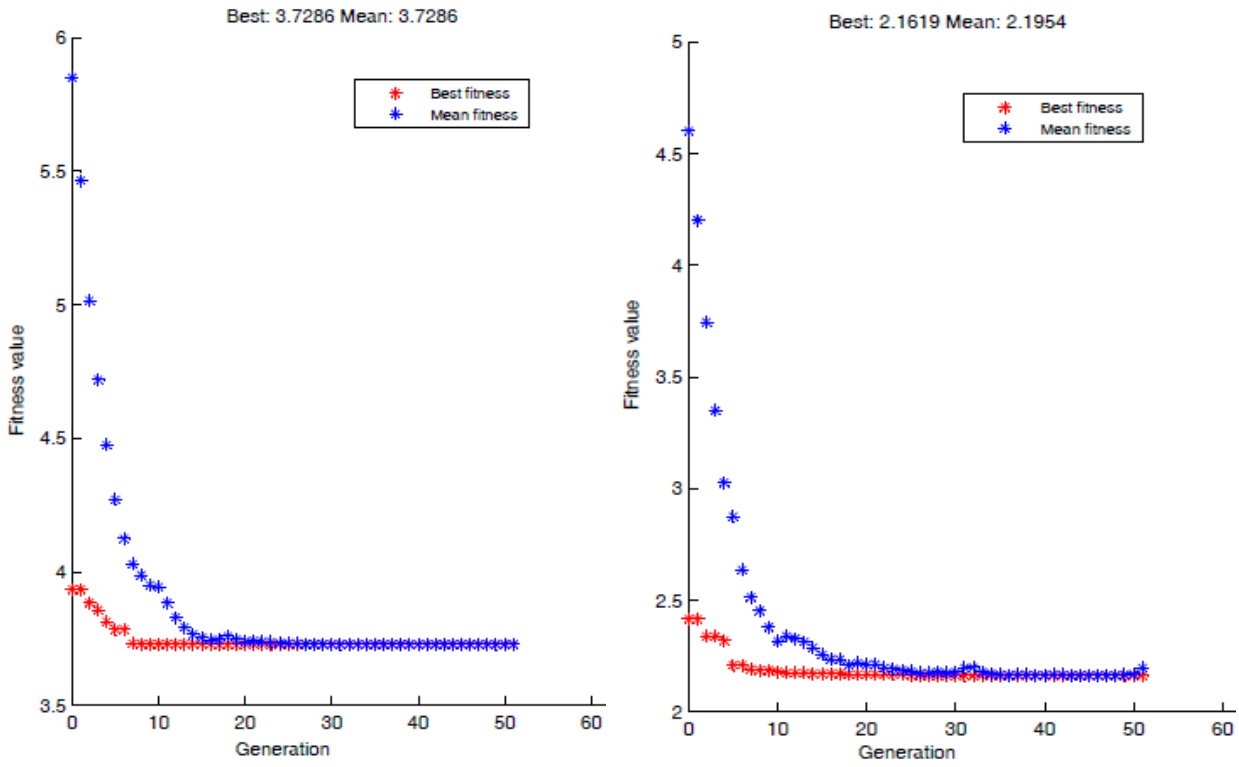

Figure 5.27. The convergence curve for Ra using brass and copper tool respectively

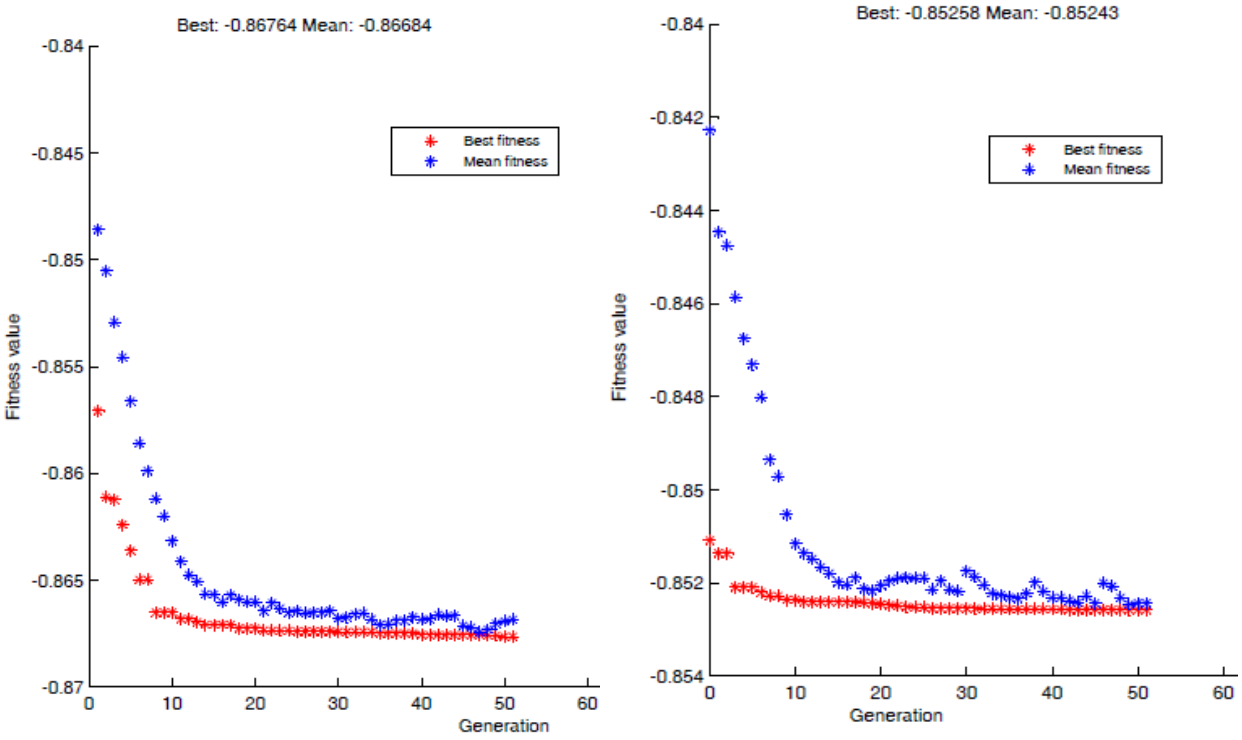

Figure 5.28. The convergence curve for circularity using brass and copper tool respectively

5.3. Multi-response optimization using neuro-fuzzy approach

The experiments have been conducted as per experimental plan shown in Table 3.6. Four responses are measured as explained in Chapter 3. Out of four responses, two responses such as MRR and circularity are to be maximized whereas two responses EWR and Ra are to be minimized. Since the responses are contradicting in nature, they are converted to S/N ratio to make them into same characteristic nature as explained Eq. 5.9 and Eq. 5.10.

The larger-the-best performance characteristic can be expressed as:

$$\text{S/N ratio} = -10\ \text{Log}_{10}(\ 1/n\ \ \Sigma\ 1/Y_i^2\ ) \tag{5.9}$$

The smaller-the-best performance characteristic can be expressed as:

$$\text{S/N ratio} = -10\ \text{Log}_{10}\ (1/n\ \ \Sigma Y_i^2\ ) \tag{5.10}$$

where Y_i is the i^{th} experimental data of response.

All the S/N ratio responses (X_{ij}) are normalized to obtain normalized response (Z_{ij}) so that they lie in the range, $0 \leq Z_{ij} \leq 1$. Normalization is carried out to avoid the scaling effect and minimize the variation of S/N ratio obtained at different scales. For responses of larger-the-better and smaller-the-better type, normalization is carried out using Eq. 5.11.

$$Z_{ij} = \frac{X_{ij} - \min\{X_{ij}, j = 1,2,.....,n\}}{\max\{X_{ij}, j = 1,2,.....,n\} - \min\{X_{ij}, j = 1,2,.....,n\}} \tag{5.11}$$

The S/N ratios of responses are shown in the Table 5.14. The S/N ratios exhibit large variation as evident from Table 5.14. Therefore, they are normalized using Eq. 5.11 and shown in the same Table 5.14. Then, a supervised learning BPN is modeled to find the membership function. These normalized data sets have been clustered by using fuzzy clustering into four fuzzy classes R_1, R_2, R_3, and R_4. There are twenty seven numbers of data sets as listed in Table 3, each of them comprising four responses or coordinates. They have been divided into four fuzzy classes R_1, R_2, R_3 and R_4 by using fuzzy clustering. The fuzzy partition matrix U gives an idea of the membership of each of data into four fuzzy classes. The matrix U is shown in Table 5.15 which gives an idea of the membership of each data into four fuzzy classes when the objective function of FCM is converged after thirty four iterations. The numbers for each cluster indicate the experiment number or run number.

R_1 = 4 8 10 12 14 16 18 20 22 24

R_2= 5 6 7 23 25 26 27

R_3= 2

R_4 = 1 3 9 11 13 15 17 19 21

Table 5.14. Signal-to-noise ratio and Normalized value

Sl. No.	Ip (A)	Ton (µs)	τ (%)	Fp (bar)	Signal-to-noise ratio				Normalized value			
					MRR	TWR	Ra	circularity	MRR	TWR	Ra	circularity
1	3	100	85	0.3	3.94	-5.31	-12.02	-1.44	0.126	0.698	1.000	0.4146
2	7	100	85	0.3	11.36	-10.84	-13.2	-1.46	0.624	5.609	0.805	0.2876
3	3	300	85	0.3	3.01	-1.93	-13.48	-1.4	0.000	1.000	0.758	0.6478
4	7	300	85	0.3	16.95	-10.28	-17.6	-1.35	1.000	0.255	0.077	0.9589
5	5	200	80	0.2	9.29	-5.59	-16.28	-1.4	0.485	0.674	0.295	0.6574
6	5	200	90	0.2	11.17	-8.85	-15.78	-1.42	0.611	0.383	0.379	0.5063
7	5	200	80	0.4	10.67	-9.02	-16.12	-1.46	0.578	0.368	0.322	0.2686
8	5	200	90	0.4	12.4	-10.25	-15.46	-1.40	0.694	0.258	0.431	0.6512
9	3	200	80	0.3	3.87	-2.3	-14.44	-1.44	0.121	0.966	0.600	0.4161
10	7	200	80	0.3	14.48	-9	-16.91	-1.42	0.834	0.370	0.191	0.4877
11	3	200	90	0.3	6.34	-5.59	-13.27	-1.48	0.287	0.674	0.792	0.1541
12	7	200	90	0.3	15.89	-13.15	-16.69	-1.37	0.928	0.000	0.228	0.8434
13	5	100	85	0.2	7.62	-8.79	-12.63	-1.46	0.373	0.389	0.899	0.2861
14	5	300	85	0.2	11.36	-6.82	-18.07	-1.42	0.624	0.564	0.000	0.4995
15	5	100	85	0.4	8.06	-8.88	-12.4	-1.43	0.403	0.380	0.936	0.4355
16	5	300	85	0.4	11.73	-7	-16.93	-1.34	0.649	0.548	0.189	1.0000
17	3	200	85	0.2	5.53	-4.05	-14.27	-1.5	0.232	0.811	0.628	0.0000
18	7	200	85	0.2	15.43	-11.58	-16.22	-1.39	0.898	0.139	0.306	0.6710
19	3	200	85	0.4	5.47	-4.5	-13.16	-1.46	0.228	0.770	0.811	0.2827
20	7	200	85	0.4	15.56	-12.03	-14.07	-1.38	0.906	0.099	0.661	0.7783
21	5	100	80	0.3	6.1	-6.11	-14.79	-1.47	0.271	0.627	0.542	0.1989
22	5	300	80	0.3	9.73	-4.61	-17.33	-1.37	0.515	0.761	0.123	0.8041
23	5	100	90	0.3	8.38	-9.97	-14.1	-1.44	0.424	0.283	0.656	0.4075
24	5	300	90	0.3	12.57	-8.6	-16.94	-1.39	0.705	0.405	0.187	0.7058
25	5	200	85	0.3	11.24	-8.66	-15.27	-1.44	0.616	0.400	0.463	0.3981
26	5	200	85	0.3	11.08	-8.99	-15.22	-1.47	0.606	0.370	0.470	0.1905
27	5	200	85	0.3	11	-8.81	-15.86	-1.5	0.600	0.386	0.365	0.0099

Table 5.15. Membership values from FCM

Expt. No.	Membership value of R_1	Membership value of R_2	Membership value of R_3	Membership value of R_4
1	0.0546	0.1098	0.0028	0.8328
2	0	0	1	0
3	0.1217	0.1883	0.0076	0.6824
4	0.7892	0.1494	0.0033	0.0580
5	0.349	0.449	0.0032	0.1988
6	0.1526	0.8095	0.0006	0.0373
7	0.0746	0.8773	0.0008	0.0473
8	0.6384	0.3088	0.0012	0.0516
9	0.074	0.1454	0.0037	0.7769
10	0.6028	0.3415	0.0016	0.0541
11	0.0277	0.0827	0.0012	0.8885
12	0.7546	0.1805	0.003	0.0619
13	0.1094	0.3215	0.0032	0.5659
14	0.4509	0.4248	0.0036	0.1206
15	0.1417	0.3438	0.0037	0.5108
16	0.6917	0.2075	0.0037	0.0971
17	0.0703	0.1876	0.0038	0.7384
18	0.8064	0.1547	0.0014	0.0375
19	0.0056	0.0141	0.0002	0.9801
20	0.5627	0.3126	0.0042	0.1205
21	0.0634	0.2492	0.0019	0.6855
22	0.4693	0.3369	0.0056	0.1881
23	0.1415	0.6276	0.0020	0.2288
24	0.8798	0.0977	0.0006	0.0219
25	0.0158	0.9749	0.0001	0.0091
26	0.0813	0.8300	0.0012	0.0876
27	0.1538	0.6585	0.0033	0.1844

Therefore, four neurons in input layer and four neurons in output later have been chosen. To determine the number of neurons in the hidden layer, various BPN models have been chosen to achieve performance error equal to 0.001. Six BPN models 4–5–4, 4–6–4, 4–7–4, 4–8–4, 4–9–4, 4–10–4 have been selected. Data set 1–18 are selected as training data and data set 19–27 have been used to test the performance of the selected neural network. Finally, BPN architecture 4-8-4 showed minimum root mean square error (RMSE). Learning and momentum parameters are set at 0.12 and 0.50. The number of epochs the BPN was run was 31250. In spite of higher number

of iterations to converge at a final value, low learning rate is used to ensure the neural network to escape from local optima.

Initial quasi-random weights have been assigned for all four layers. Thereafter, the data serial no. 1 with input co-ordinates x_1=0.125995, x_2= 0.698949, x_3 = 1 and x_4=0.4145741 with corresponding output membership 0.0546 (R_1), 0.1098(R_2), 0.0028(R_3) and 0.8328(R_4) is entered. The output of the network is computed and compared with the desired output to calculate the error. Using back propagation, initially assigned weights are repeatedly adjusted to minimize this error, until this error achieves the target 0.001 as shown in Figure3. Similarly, data set (2–18) are entered and weights are readjusted. Then, data set (19-27) are used to test the performance of the network. It has been observed that after 31250 iterations, the network achieves a satisfactory level of error as shown in Figure 5.29. The obtained adjusted membership values are shown in Table 5.16.

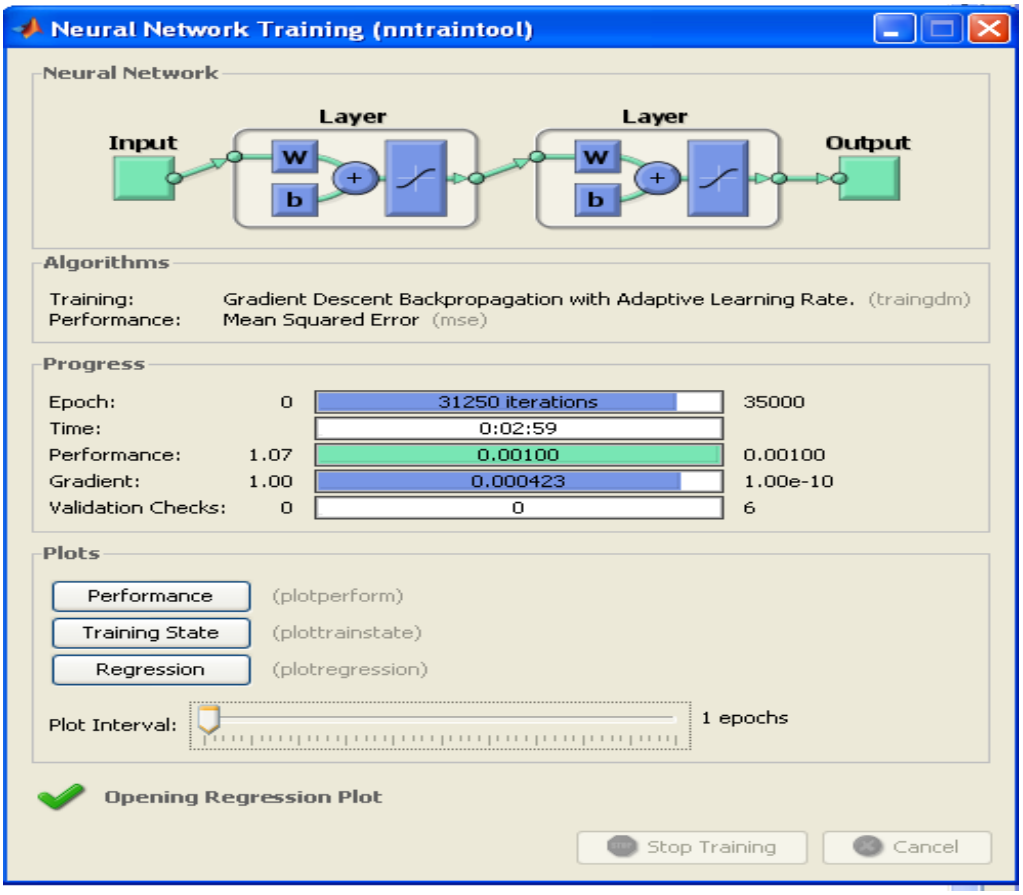

Figure 5.29. Training in neural network

Table 5.16. Adjusted membership value

Expt. No.	Membership value of R_1	Membership value of R_2	Membership value of R_3	Membership value of R_4
1	0.0594	0.1072	0.0022	0.8284
2	0.0126	0.0152	0.9915	0.0088
3	0.1203	0.1887	0.0006	0.6834
4	0.7582	0.1348	0.0040	0.0582
5	0.3447	0.4495	0.0008	0.1979
6	0.1531	0.7974	0.0010	0.0369
7	0.0760	0.8642	0.0026	0.0098
8	0.6454	0.3103	0.0014	0.0459
9	0.0693	0.1420	0.0006	0.7785
10	0.6088	0.3470	0.0093	0.0512
11	0.0535	0.0987	0.0074	0.8342
12	0.7698	0.1928	0.0045	0.0251
13	0.0969	0.3035	0.0094	0.5777
14	0.4513	0.4252	0.0018	0.1301
15	0.1445	0.3574	0.0025	0.5084
16	0.7130	0.2097	0.0013	0.1028
17	0.0532	0.1884	0.0091	0.7469
18	0.7651	0.1434	0.0084	0.0331
19	0.0722	0.1206	0.0015	0.8389
20	0.7971	0.0064	0.0030	0.0864
21	0.0700	0.6341	0.0009	0.3346
22	0.6089	0.1789	0.0011	0.3122
23	0.1831	0.4561	0.0007	0.2811
24	0.6752	0.1525	0.0019	0.1856
25	0.1223	0.8325	0.0016	0.0185
26	0.1072	0.8507	0.0068	0.0112
27	0.1228	0.8510	0.0171	0.0074

Regression curves are plotted in Figure 5.30 and Figure 5.31 between actual membership function and predicted membership function via neuro-fuzzy model for training data and testing data respectively. It can be observed that data are well fitted because a high degree of coefficient of determination (R^2) as 0.99897 for training and a high degree of coefficient of determination (R^2) as 0.99854 for testing data is obtained.

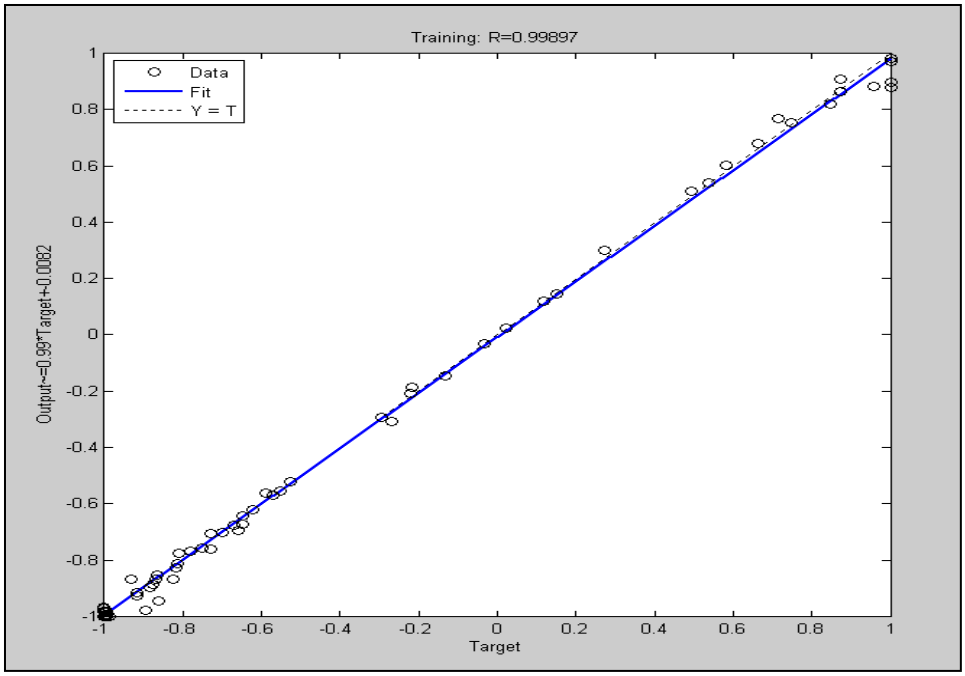

Figure 5.30. Regression plot for training data

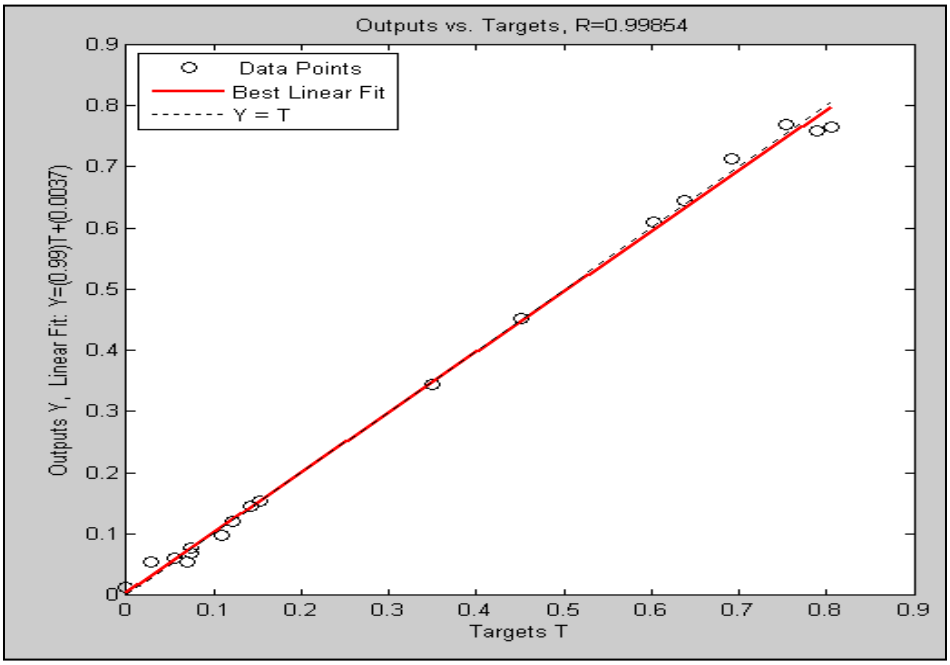

Figure 5.31. Regression plot for testing data

Figure 5.32 shows the membership functions for output predicted by neural network. After getting fuzzified value, it is needed to defuzzify them to get a crisp value containing the combined quality characteristic which can be used as higher the best criteria. This is done by center if area (COA) method. These defuzzified data are called MPCI, listed in Table 5.17.

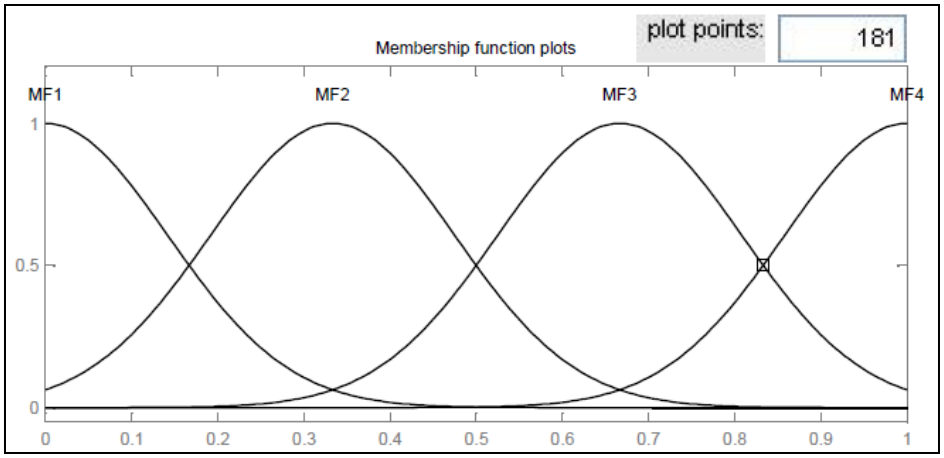

Figure 5.32. Membership function plot

Table 5.17. MPCI

Sl. No.	Ip (A)	Ton (µs)	τ (%)	Fp (kg/cm^2)	MPCI
1	-1	-1	0	0	0.42805
2	1	-1	0	0	0.89407
3	-1	1	0	0	0.63183
4	1	1	0	0	0.84881
5	0	0	-1	-1	0.60064
6	0	0	1	-1	0.41836
7	0	0	-1	1	0.36551
8	0	0	1	1	0.55886
9	-1	0	0	-1	0.47000
10	1	0	0	-1	0.66304
11	-1	0	0	1	0.21636
12	1	0	0	1	0.73710
13	0	-1	-1	0	0.32799
14	0	1	-1	0	0.58683
15	0	-1	1	0	0.41793
16	0	1	1	0	0.68113
17	-1	0	-1	0	0.17097
18	1	0	-1	0	0.73192
19	-1	0	1	0	0.34790
20	1	0	1	0	0.79249
21	0	-1	0	-1	0.48420
22	0	1	0	-1	0.70094
23	0	-1	0	1	0.32184
24	0	1	0	1	0.66965
25	0	0	0	0	0.41702
26	0	0	0	0	0.38558
27	0	0	0	0	0.40928

The MPCI values are considered now as single response and analyzed. From analysis of variance shown in Table 5.18, it is observed that the factors Ip, Ton, and τ and square terms Ip×Ip and Ton×Ton, and interaction Ip×τ re statistically significant. From percentage of contribution, it is said that Ip has the highest effect followed by Ton, Ton×Ton, Ip×Ip, Ip×τ and τ. Ip has highest effect because it directly contribute to the heat generation. As Ip increases the spark become stronger and more erosion arise. The process model is obtained by regression analysis as given in Eq. 5.12 and coefficient of determination (R^2) is found to be 82.7%.

Table 5.18. ANOVA for MPCI

Term	Coef	SE Coef	T	P
Constant	0.426	0.03032	14.051	0
Ip	0.20019	0.02626	7.625	0
Ton	0.10375	0.02626	3.952	0.001
τ	-0.03017	0.02626	-1.149	0.264
Ip×Ip	0.11189	0.03595	3.112	0.005
Ton×Ton	0.11946	0.03595	3.323	0.003
Ip×τ	0.08193	0.04548	1.801	0.087

$$MPCI=0.4260+0.2002\times Ip+0.1038\times Ton-.0302\times\tau+0.1119\times Ip\times Ip+0.1195\times Ton\times Ton +0.0819\times Ip\times\tau \text{ (in coded form)} \quad (5.12)$$

Figure 5.33 shows the response surface for MPCI in relation to the process parameters of discharge current and pulse on time. It can be seen from the figure that the MPCI tends to increase rapidly with increase in peak current for any value of pulse-on-time. The figure also indicates that maximum MPCI value is obtained at high peak current (7 A) and high pulse on time (300 μs). This is due to their principal control over the input spark energy. As the discharge current increases, it generates strong spark which produce the higher temperature as a result of more material is melted and eroded from the work piece. Figure 5.34 shows the response surface for MPCI in relation to the process parameters of discharge current and duty factor. It can be observed from the figure that MPCI increases as Ip increases for any value of τ.

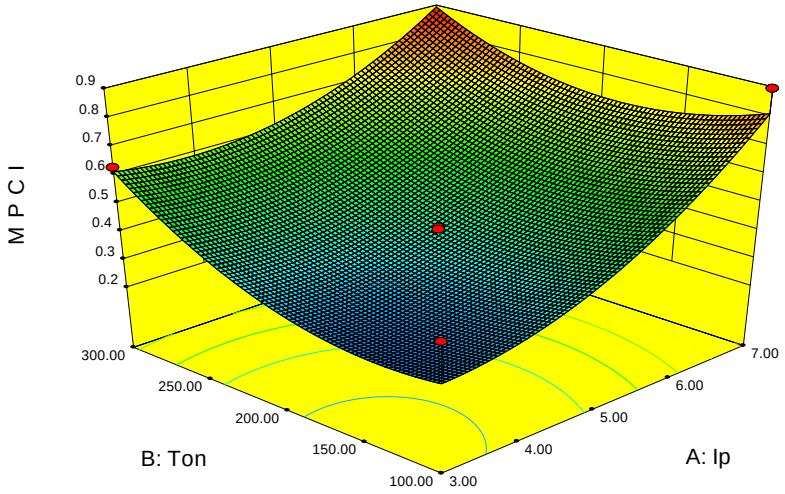

Figure 5.33. Surface plot of MPCI vs Ip, Ton

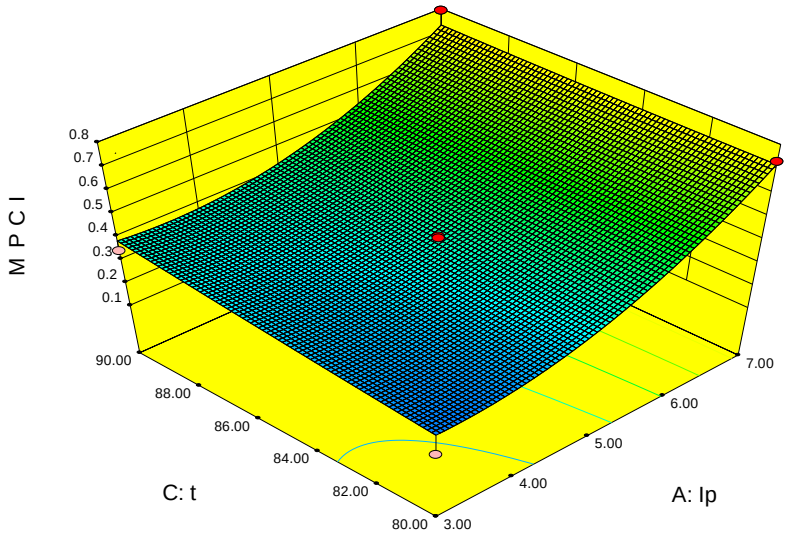

Figure 5.34. Surface plot of MPCI vs Ip, τ

Particle swarm optimization technique is proposed to determine the optimal parameter setting using the model shown in Eq. 5.12. The algorithm is coded in Visual C^{++} and run on Pentium IV machine. The algorithm is run for 100 iterations but converges at 59 iterations as shown in Figure 5.35. The optimal value of MPCI is obtained as 0.946074 at parametric values of Ip=0.962, Ton=0.987, τ= 0.112 in coded form. These values are decoded using Eq. 3.3 as

described in Chapter 3 and actual values of factors are found to be Ip=6.924 A, Ton=298.7 μs, τ=85.56 %.

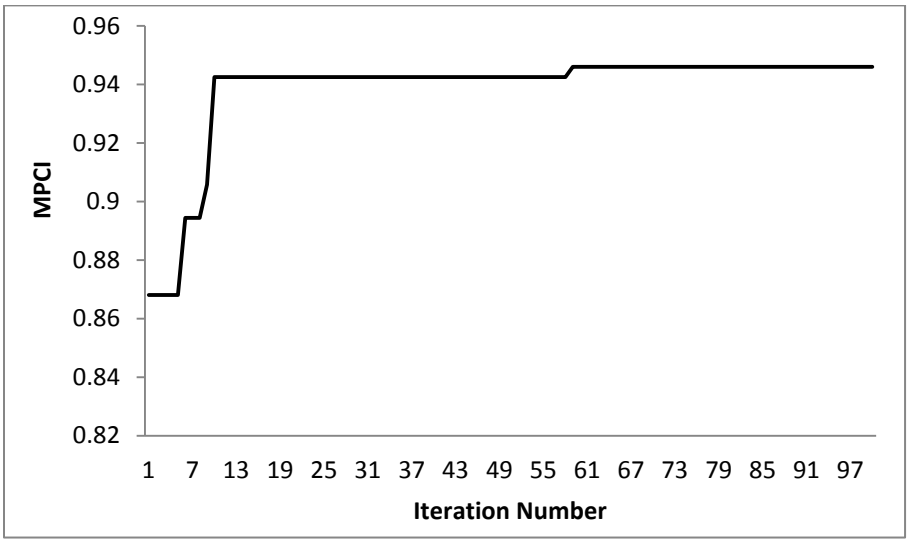

Figure 5.35. The convergence curve

The same neuro-fuzzy route is proposed to find optimal setting for the responses MRR, TWR Ra, circularity obtained using copper as tool material. The optimal parametric combination in actual form is found to be Ip = 6.87 A, Ton = 116.2 μs, τ = 80 %.

5.4. Multi-response optimization using non dominated sorting genetic algorithm (NSGA)

In the present study, the objectives are maximization of MRR, circularity and minimization of TWR, Ra which are functions of decision variables viz., discharge current (Ip), pulse on time (Ton), duty factor (τ) and flushing pressure (Fp). But there is no such mathematical equation, which relates these objectives with the decision variable. Thus empirical relation between input parameters and output parameters obtained from the RSM analysis is used as functional equations. Note that objectives are conflicting in nature. In order to convert the responses single characteristice, it is suitably modified. The objective functions are given below.

Objective 1 = - (MRR)

Objective 2 = TWR

Objective 3 = Surface Roughness (Ra)

Objective 4= - (Circularity)

There are four decision variables. The range and the step length of decision variables are different. Here, the range of discharge current (Ip) is between 3-7 A, pulse on time (Ton) is

between 100-300 μs, duty factor (τ) is between 80-90 %, flushing pressure (Fp) is between 0.2-0.4 bar. Matlab tool (optimtool ('gamultiobj')) is used for solving the multi-objective problem. Initially, the chromosomes are created randomly. An initial size of 100 populations is chosen. Simple crossover and bitwise mutation have been used with a crossover probability, Pc = 0.8, migration interval 20, migration fraction 0.2 and pareto fraction 0.35. Objective values are calculated from the RSM model as described earlier. Ranking and sorting of solutions have been done as it is mentioned in the NSGA-II algorithm. 100 non-dominated solutions are obtained at the end of 108 generation. The corresponding objective function values and the decision variables of selected non-dominated solution set are shown in Table 5.19. Figure 5.36 and Figure 5.37 shows the pareto-optimal solution front for responses MRR, TWR and Ra, Circularity respectively. This shows the formation of the pareto-optimal front leading to the final set of solutions. Since none of the solutions in the pareto-optimal front is absolutely better than any other, any one of them is an acceptable solution. The choice of one solution over the other depends on the requirement of the process engineer.

Table 5.19. Pareto Optimal solution set and corresponding variable settings

Sl. No.	Ip (A)	Ton (μS)	τ (%)	Fp (bar)	MRR (mm^3/min)	TWR (mm^3/min)	Ra (μm)	circularity
1	6.9689	287.6651	89.8221	0.3964	7.5433	4.1215	7.2351	0.8655
2	6.9576	282.9828	89.2089	0.3963	7.4514	4.1318	7.2709	0.8639
3	6.3316	281.6500	80.6657	0.3341	5.8229	3.2327	7.9634	0.8524
4	6.9571	282.7784	80.0158	0.3958	7.0986	4.0167	8.5979	0.8568
5	4.8205	246.0264	82.2590	0.3430	3.6752	2.6323	6.5820	0.8452
6	3.0460	283.0952	80.4193	0.2160	0.9469	0.8904	5.8656	0.8520
7	6.7066	281.4000	80.6657	0.3966	6.6864	3.8697	8.4294	0.8554
8	6.9576	283.1078	89.2401	0.3963	7.4541	4.1316	7.2676	0.8640
9	6.6260	270.0997	82.4138	0.3741	6.4296	3.7642	7.8382	0.8536
10	6.5259	282.1139	80.8575	0.3892	6.3723	3.7031	8.3002	0.8543
11	4.6818	241.8751	81.8282	0.3953	3.6277	2.7590	6.7127	0.8451
12	3.1145	257.0338	80.7411	0.2236	1.3189	1.1426	5.6888	0.8496
13	6.5973	281.4312	80.6970	0.2716	5.9063	2.9040	8.0424	0.8540
14	6.1916	269.6910	82.0395	0.3752	5.7440	3.4954	7.7502	0.8516
15	6.5120	265.2738	82.5515	0.3719	6.2066	3.7088	7.7020	0.8527
16	6.4304	282.9966	81.0996	0.3348	6.0011	3.2938	7.9715	0.8529
17	6.9571	282.7784	80.0158	0.3958	7.0986	4.0167	8.5979	0.8568
18	5.9947	273.9215	82.6449	0.3961	5.5582	3.4547	7.8106	0.8519
19	6.5166	261.7889	81.6577	0.3629	6.1232	3.6629	7.7003	0.8520
20	5.0904	256.7973	80.9818	0.3926	4.1512	2.9362	7.2205	0.8468

21	6.9605	195.4649	89.6421	0.3890	6.2832	4.4435	5.8508	0.8571
22	5.0633	238.2708	82.2666	0.3515	3.9687	2.8507	6.6577	0.8455
23	6.8103	252.8930	82.7219	0.3898	6.6183	4.0705	7.6589	0.8540
24	6.1456	279.9306	83.1241	0.3696	5.7437	3.3854	7.7258	0.8524
25	6.7130	264.0038	84.2647	0.3812	6.6023	3.9205	7.5709	0.8547
26	4.8155	225.0956	82.7662	0.3440	3.6197	2.7353	6.3000	0.8444
27	6.6208	276.5871	81.3257	0.3060	6.1251	3.2362	7.8529	0.8530
28	6.5529	277.0494	81.2208	0.3728	6.3275	3.6554	8.0692	0.8536
29	6.9643	249.8267	86.9139	0.3928	6.9903	4.2571	7.0976	0.8576
30	6.5551	265.8930	84.9494	0.3833	6.4032	3.8300	7.4958	0.8547
31	3.2680	248.1609	83.9896	0.2691	1.7891	1.5356	5.3346	0.8458
32	4.2827	225.2354	84.3440	0.3987	3.2124	2.5872	6.1020	0.8450
33	6.7568	209.1346	88.2383	0.3985	6.1973	4.3087	6.3381	0.8560
34	6.7136	279.0062	83.5886	0.3900	6.7448	3.8754	7.9624	0.8559
35	3.1085	283.2827	80.1693	0.3410	1.5202	1.3294	5.4279	0.8441
36	6.5120	265.0238	82.5515	0.3719	6.2045	3.7102	7.6980	0.8527
37	3.1659	214.2010	81.3885	0.3695	2.0501	1.8474	5.0067	0.8415
38	6.5059	280.0064	82.1310	0.3809	6.3305	3.6656	8.0436	0.8540
39	3.5267	126.5512	85.1870	0.3437	2.0615	2.1754	4.4241	0.8438
40	6.6421	205.4448	84.0586	0.3340	5.6167	3.7926	6.4105	0.8488
41	6.7407	263.9586	84.5922	0.3810	6.6568	3.9420	7.5305	0.8550
42	6.8719	232.6433	84.4105	0.3616	6.4209	4.0403	6.9379	0.8523
43	6.7907	279.2445	80.8506	0.3700	6.7099	3.7674	8.2007	0.8548
44	6.3556	258.1096	86.0041	0.3577	5.9735	3.6284	7.0614	0.8529
45	6.0270	267.7529	84.6297	0.3680	5.5394	3.3990	7.3226	0.8517
46	5.9995	223.3485	89.3988	0.3757	5.3611	3.7061	6.2142	0.8539
47	5.6961	274.2029	82.6452	0.3636	5.0012	3.1025	7.4719	0.8499
48	6.9571	282.8431	80.0158	0.3825	7.0474	3.9264	8.4941	0.8564
49	3.4321	226.7327	80.9908	0.3884	2.2765	1.9949	5.4821	0.8418
50	4.5640	203.4894	82.0734	0.3737	3.3058	2.7662	6.0406	0.8435
51	3.0001	111.0658	83.5648	0.3203	1.6834	1.7953	3.9364	0.8443
52	6.1441	281.7437	80.5407	0.3497	5.5968	3.2220	7.9552	0.8518
53	6.7488	230.7229	86.3499	0.3875	6.3814	4.1558	6.8258	0.8544
54	6.3382	264.5740	82.9661	0.3994	6.0418	3.7577	7.7879	0.8531
55	6.9571	282.8097	80.0939	0.2708	6.4744	3.0424	8.2173	0.8558
56	4.9567	277.8829	81.7995	0.3844	4.0015	2.6852	7.2617	0.8476
57	6.8326	283.3109	89.2557	0.2869	6.6945	3.4475	6.9097	0.8581
58	6.9466	282.0338	80.6239	0.3909	7.0718	3.9859	8.4638	0.8565
59	5.5504	211.2700	84.0622	0.3596	4.4385	3.3029	6.4075	0.8463
60	6.4923	206.4058	80.2149	0.3396	5.3534	3.6723	6.7821	0.8488
61	4.2807	244.7531	81.7253	0.3434	3.0409	2.3142	6.2158	0.8440
62	4.9288	267.8218	80.8302	0.3656	3.8798	2.6542	7.1041	0.8466
63	6.6880	282.3546	84.5361	0.3892	6.7594	3.8443	7.8732	0.8567
64	6.1923	221.6003	88.8176	0.3819	5.5873	3.8477	6.3202	0.8540
65	6.0508	246.0594	83.3313	0.3685	5.3822	3.5109	7.1699	0.8496

66	5.7827	267.9517	80.8833	0.3649	5.0592	3.1812	7.6137	0.8495
67	5.9491	223.1114	88.4778	0.3432	5.1448	3.5176	6.1763	0.8509
68	6.7290	277.3360	81.7688	0.3428	6.5000	3.5702	7.9086	0.8538
69	6.6696	275.5220	83.4602	0.3275	6.3688	3.4780	7.6095	0.8534
70	6.8155	282.3427	82.3058	0.3855	6.8819	3.8796	8.1771	0.8560
71	5.2917	282.9625	80.1593	0.3441	4.2972	2.6670	7.5249	0.8487
72	5.1806	251.4427	81.1670	0.2257	3.5634	2.0877	7.2538	0.8496
73	6.1916	281.9615	82.3345	0.2786	5.3617	2.8080	7.7235	0.8521
74	5.4139	237.2952	81.2286	0.3487	4.3583	3.0355	6.8994	0.8463
75	6.8181	284.6349	89.7485	0.3947	7.2462	4.0293	7.1805	0.8642
76	5.1085	248.4753	81.8236	0.3873	4.1537	2.9756	7.0211	0.8465
77	6.9390	276.1812	80.8774	0.3950	7.0282	4.0458	8.3593	0.8562
78	6.8076	249.6728	88.7637	0.2944	6.3896	3.6339	6.5069	0.8541
79	3.1126	181.0954	83.6537	0.3538	2.0528	1.9067	4.6056	0.8421
80	6.6595	266.4564	84.0045	0.3756	6.5095	3.8369	7.5968	0.8542
81	4.7284	227.3257	81.3834	0.3814	3.5929	2.8080	6.5128	0.8444
82	3.3138	208.0326	84.6758	0.3166	2.1501	1.8870	4.9344	0.8431
83	4.3428	232.2641	82.5874	0.3442	3.1240	2.4259	6.0834	0.8437
84	3.0460	283.0952	80.4193	0.2160	0.9469	0.8904	5.8656	0.8520
85	6.8439	279.7541	86.4637	0.3739	7.0125	3.9096	7.4804	0.8581
86	3.7692	281.0214	81.5442	0.3137	2.2279	1.6788	6.0773	0.8458
87	3.8911	211.9571	84.3172	0.3404	2.6878	2.2550	5.4538	0.8431
88	6.9148	287.2052	88.5464	0.3067	6.9434	3.5663	7.0632	0.8586
89	3.1778	244.4651	82.9448	0.3774	2.0049	1.7177	5.2197	0.8426
90	5.7359	272.9939	82.1580	0.3682	5.0579	3.1522	7.5496	0.8499
91	3.6511	222.9683	86.2731	0.3205	2.4747	2.0596	5.2444	0.8446
92	6.3708	276.5871	81.3257	0.3060	5.7347	3.1030	7.7832	0.8521
93	6.9571	283.0597	80.1564	0.2708	6.4776	3.0430	8.2141	0.8558
94	3.4321	226.8577	80.7408	0.3884	2.2717	1.9948	5.4918	0.8418
95	3.2941	111.4408	84.0296	0.3323	1.8020	1.9848	4.1354	0.8440
96	5.7586	274.2654	82.3952	0.3636	5.0861	3.1380	7.5300	0.8500
97	5.9917	222.9093	83.3898	0.3387	4.9954	3.4019	6.6873	0.8474
98	5.7495	223.5985	89.3988	0.3132	4.8224	3.2921	6.0099	0.8503
99	6.9576	282.7328	89.2089	0.3963	7.4492	4.1334	7.2674	0.8639
100	5.2440	238.9719	82.9181	0.3619	4.2412	3.0110	6.7504	0.8463

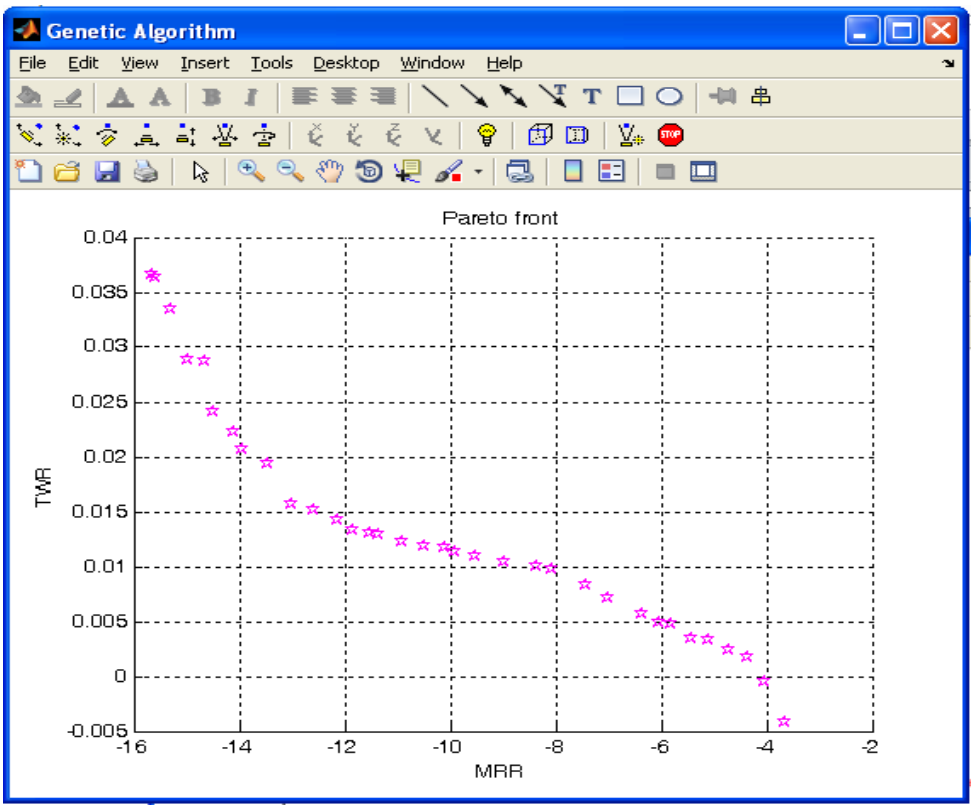

Figure 5.36. Pareto-optimal front for objectives MRR and TWR

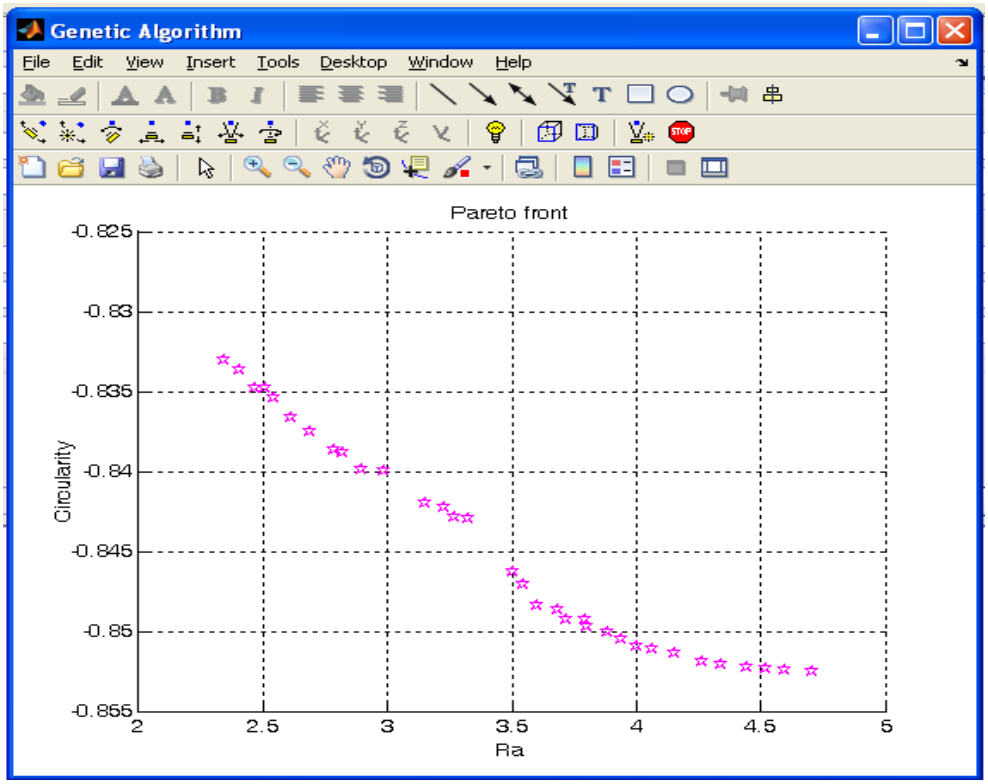

Figure 5.37. Pareto-optimal front for objectives Ra and Circularity

The proposed route multi-response optimization using non-dominated sorting genetic algorithm (NSGA) is followed for the responses obtained using copper as tool material in electric discharge machining. An initial size of 100 populations is chosen. Simple crossover and bitwise mutation have been used with a crossover probability, Pc = 0.8, migration interval 20, migration fraction 0.2 and pareto fraction 0.35. Objective values are calculated from the RSM model as described earlier. Ranking and sorting of solutions have been done as it is mentioned in the NSGA-II algorithm. 100 non-dominated solutions are obtained at the end of 123 generation. The corresponding objective function values and the decision variables of selected non-dominated solution set are shown in Table 5.20. Figure 5.38 and Figure 5.39 shows the pareto-optimal solution front for responses MRR, TWR and Ra, Circularity respectively. This shows the formation of the pareto-optimal front leading to the final set of solutions. Since none of the solutions in the pareto-optimal front is absolutely better than any other, any one of them is an acceptable solution. The choice of one solution over the other depends on the requirement of the process engineer.

Table 5.20. Pareto Optimal solution set and corresponding variable settings

Sl. No.	Ip(A)	Ton(μs)	τ(%)	Fp(bar)	MRR (mm^3/min)	TWR (mm^3/min)	Ra(μm)	circularity
1	5.5351	119.1320	82.0902	0.2735	7.3425	0.0234	5.0330	0.8490
2	6.9642	119.4133	88.7668	0.3214	13.6171	0.0383	6.7244	0.8363
3	3.0168	279.4258	87.0141	0.2056	2.6061	-0.0003	2.9042	0.8249
4	3.0200	276.4820	85.6742	0.2063	2.5861	0.0008	2.9436	0.8242
5	4.1949	137.6921	88.0478	0.2986	4.7864	0.0111	4.2735	0.8422
6	5.5405	119.0570	80.5773	0.3197	7.7127	0.0220	4.9817	0.8512
7	6.9884	115.7624	89.1673	0.3725	14.9948	0.0358	6.7713	0.8340
8	3.0035	277.5294	89.1828	0.3729	1.5848	0.0030	2.3659	0.8320
9	3.0637	279.3555	87.1948	0.3110	1.6482	0.0044	2.4985	0.8305
10	4.4347	131.0068	87.7621	0.3346	5.4767	0.0128	4.4054	0.8443
11	5.6338	167.3074	88.5583	0.2948	8.0224	0.0181	5.1539	0.8449
12	5.5721	128.9747	86.7570	0.2688	7.7429	0.0232	5.3768	0.8436
13	3.0356	276.3570	85.7367	0.2063	2.5924	0.0007	2.9504	0.8244
14	3.0035	277.5294	89.1203	0.3729	1.5815	0.0031	2.3684	0.8320
15	6.9877	113.8193	89.9057	0.3849	15.4092	0.0355	6.9100	0.8321
16	3.0168	279.4258	87.0453	0.2056	2.6075	-0.0004	2.9039	0.8249
17	6.9995	113.8662	89.9584	0.3653	14.9588	0.0374	6.9422	0.8326
18	4.4462	131.0200	87.7621	0.3190	5.3952	0.0133	4.4397	0.8438
19	5.4626	114.6460	89.2279	0.3342	8.4154	0.0224	5.5482	0.8411
20	3.4991	132.2536	86.5254	0.2868	3.6250	0.0098	3.7127	0.8401
21	5.1796	168.4988	88.2924	0.3008	6.8022	0.0140	4.7513	0.8452

22	6.7478	117.5080	87.7091	0.3801	13.9500	0.0313	6.3460	0.8376
23	6.1615	145.4457	89.3929	0.3046	10.0989	0.0259	5.8899	0.8416
24	4.9790	253.2869	83.2574	0.2565	4.5089	0.0083	3.9545	0.8430
25	4.7811	162.4285	86.2305	0.3100	5.7974	0.0122	4.3392	0.8462
26	6.9230	126.6892	87.3546	0.3938	14.9676	0.0303	6.3600	0.8369
27	5.0972	134.4022	87.0566	0.3066	6.7956	0.0176	4.8676	0.8450
28	4.6270	144.0095	85.5613	0.2588	5.3171	0.0141	4.4729	0.8440
29	3.0077	277.1712	86.2820	0.3167	1.5739	0.0054	2.5287	0.8293
30	6.8250	134.3964	87.9742	0.3000	12.4234	0.0347	6.3687	0.8401
31	5.5771	119.1546	80.5175	0.2916	7.4957	0.0227	5.0013	0.8510
32	3.0168	279.4258	86.9985	0.2056	2.6054	-0.0003	2.9043	0.8249
33	6.9046	135.6046	89.9401	0.3896	14.9577	0.0306	6.5597	0.8348
34	4.7892	148.5991	87.2110	0.3464	6.3041	0.0126	4.4723	0.8459
35	3.8416	269.7997	82.2144	0.3190	2.3254	0.0082	3.3366	0.8325
36	4.9062	268.7027	87.8341	0.3720	5.1363	0.0081	3.5480	0.8419
37	6.7138	155.9761	86.1960	0.3750	13.1321	0.0247	5.7658	0.8419
38	4.4177	156.5823	87.5781	0.3342	5.2859	0.0098	4.1711	0.8450
39	5.5639	119.1490	80.5348	0.2972	7.5182	0.0226	4.9903	0.8511
40	4.0321	175.0079	80.8312	0.2316	3.9464	0.0090	3.9389	0.8415
41	6.5079	132.2824	89.7686	0.3435	12.2128	0.0298	6.2847	0.8384
42	6.1788	134.8454	87.2564	0.2813	9.7238	0.0278	5.8091	0.8430
43	5.2108	168.5242	88.3236	0.3145	7.0107	0.0139	4.7385	0.8455
44	3.2051	277.8920	88.9136	0.2941	1.9589	0.0021	2.5747	0.8332
45	4.6270	144.0408	85.5642	0.2646	5.3301	0.0141	4.4501	0.8443
46	6.5693	118.8459	87.1897	0.3537	12.5236	0.0309	6.1222	0.8404
47	3.0168	279.4258	87.0141	0.2056	2.6061	-0.0003	2.9042	0.8249
48	6.9096	117.2831	89.7395	0.3964	15.3150	0.0329	6.7720	0.8328
49	5.5042	236.2144	89.4635	0.3294	7.0938	0.0119	4.3038	0.8467
50	6.7141	118.0119	85.5374	0.3010	11.8942	0.0345	6.1309	0.8425
51	5.5673	131.3959	87.2478	0.3574	8.8389	0.0197	5.2077	0.8447
52	6.8538	172.3406	86.6076	0.3696	13.4138	0.0247	5.7245	0.8418
53	5.5123	152.8727	86.2139	0.3216	7.9120	0.0178	4.9192	0.8467
54	4.0389	219.0780	84.9847	0.2858	3.6328	0.0059	3.5066	0.8414
55	6.3839	212.5165	88.0323	0.3006	9.7845	0.0209	5.1451	0.8469
56	5.7636	129.2632	86.8453	0.3103	8.7657	0.0236	5.3975	0.8445
57	4.1603	169.6543	87.1539	0.3211	4.5631	0.0079	3.8818	0.8443
58	3.0168	279.4258	87.0155	0.2056	2.6061	-0.0003	2.9042	0.8249
59	3.9331	124.1373	86.0480	0.2733	4.2228	0.0131	4.0881	0.8415
60	3.9203	159.1534	89.7337	0.3837	4.7100	0.0042	3.9155	0.8430
61	6.9999	113.8505	89.9486	0.3966	15.7908	0.0347	6.9282	0.8314
62	6.4013	182.5371	88.1120	0.3772	11.7379	0.0198	5.3934	0.8428
63	5.7804	122.0629	83.0767	0.3635	9.3429	0.0218	5.2111	0.8480
64	6.2038	160.4813	86.8812	0.3366	10.3785	0.0220	5.3910	0.8451
65	5.8433	123.1914	89.8630	0.3372	9.7175	0.0245	5.8610	0.8400
66	5.2020	208.5971	87.2371	0.3399	6.6589	0.0105	4.2522	0.8462

67	6.9062	125.1459	88.7073	0.3628	14.2577	0.0337	6.5223	0.8366
68	3.9338	225.1033	88.5347	0.2865	3.6213	0.0032	3.4460	0.8410
69	6.8848	169.6248	88.5833	0.3720	13.8558	0.0265	5.9491	0.8400
70	6.8137	138.7099	88.0594	0.3811	14.1051	0.0287	6.2008	0.8384
71	3.7866	274.7030	87.2040	0.3211	2.4783	0.0053	2.8976	0.8370
72	4.4038	245.8278	86.4405	0.3013	3.9214	0.0063	3.4969	0.8425
73	5.3183	170.1273	85.5327	0.2736	6.7141	0.0153	4.7072	0.8468
74	5.0336	267.5796	82.4218	0.2236	4.2386	0.0075	4.0559	0.8411
75	4.7061	210.0210	85.2336	0.2848	4.9152	0.0086	3.9669	0.8452
76	3.3135	199.7309	88.8234	0.2710	3.2586	0.0009	3.3169	0.8364
77	5.4367	199.5727	88.2387	0.2928	7.0385	0.0136	4.6532	0.8465
78	6.4569	159.6711	86.5984	0.3753	12.0809	0.0221	5.5653	0.8429
79	3.1555	276.7165	89.1088	0.3191	1.8400	0.0023	2.4910	0.8335
80	3.0224	183.9154	86.9784	0.2546	3.1881	0.0024	3.2138	0.8337
81	6.9874	119.7785	89.7884	0.3981	15.7057	0.0333	6.8155	0.8323
82	6.6472	133.5673	87.7022	0.3706	13.1528	0.0283	6.0815	0.8399
83	5.0939	223.4606	83.4095	0.2827	5.3806	0.0098	4.1290	0.8456
84	6.5132	117.3250	87.3548	0.3776	12.8561	0.0290	6.1132	0.8396
85	6.5343	118.2847	88.2053	0.3352	12.1034	0.0323	6.2541	0.8393
86	5.4713	210.6299	86.6299	0.3053	6.9494	0.0128	4.4393	0.8471
87	4.4174	215.2488	84.9974	0.2721	4.2738	0.0071	3.7888	0.8433
88	3.5682	199.0648	89.5343	0.3103	3.4706	0.0016	3.3949	0.8400
89	4.9430	241.1191	88.9447	0.3518	5.6828	0.0077	3.8275	0.8450
90	6.7524	144.1759	86.4676	0.3575	13.0580	0.0279	5.9263	0.8419
91	6.7738	134.6294	86.3086	0.3235	12.5019	0.0315	6.0519	0.8423
92	4.7580	148.6099	87.2110	0.3611	6.3794	0.0120	4.4482	0.8459
93	3.0040	269.3453	89.5870	0.2081	2.8502	-0.0033	2.9949	0.8270
94	6.9058	125.9612	88.7257	0.3961	15.1039	0.0309	6.5175	0.8351
95	6.8784	117.2831	89.7395	0.3964	15.1714	0.0325	6.7449	0.8330
96	5.5863	119.1764	80.5378	0.2660	7.2862	0.0232	5.0373	0.8504
97	3.0168	279.4493	86.9828	0.2271	2.3257	0.0009	2.7745	0.8265
98	5.5405	119.0570	80.5773	0.2884	7.3667	0.0226	4.9796	0.8509
99	6.9956	113.8193	89.9057	0.3536	14.6455	0.0382	6.9471	0.8330
100	6.9311	164.9897	88.8850	0.3843	14.4630	0.0268	6.0754	0.8385

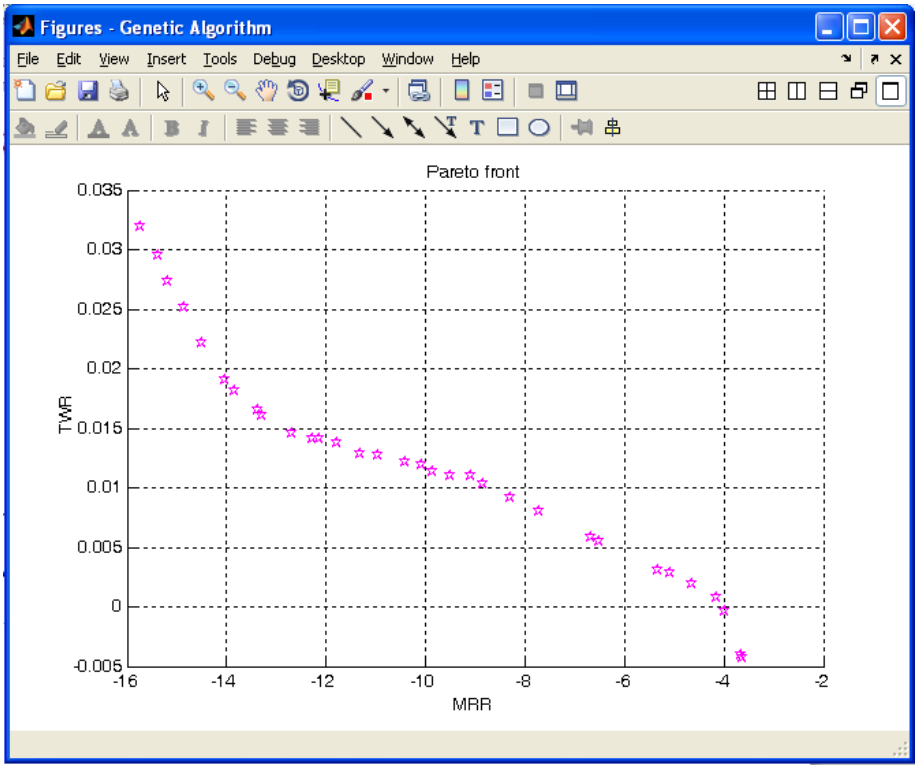

Figure 5.38. Pareto-optimal front for objectives MRR and TWR

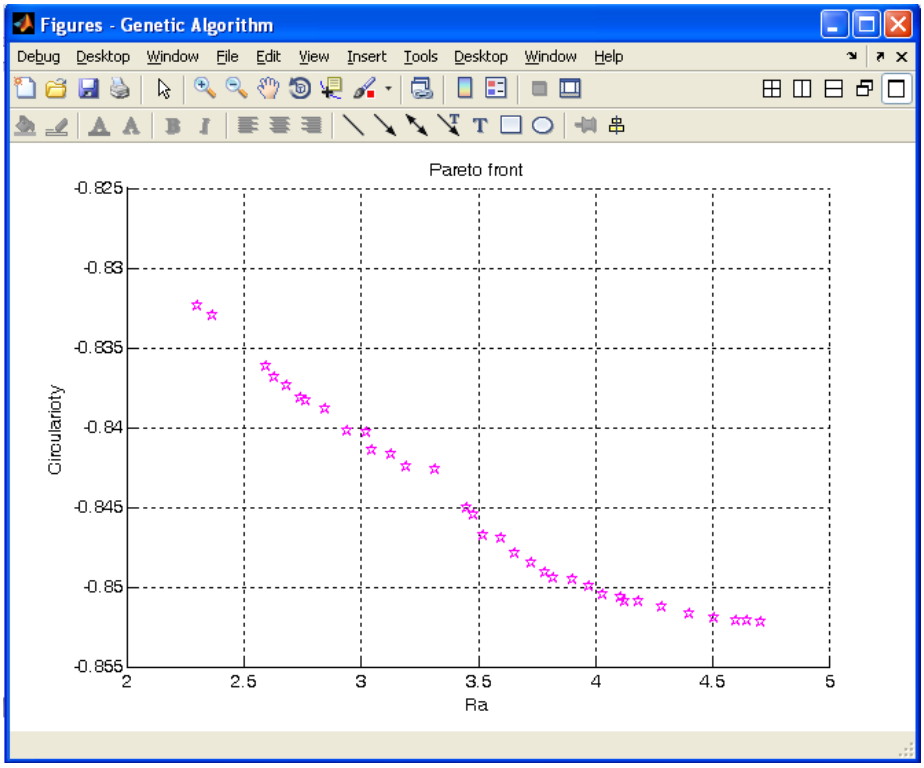

Figure 5.39. Pareto-optimal front for objectives Ra and Circularity

5.5. Comparison of responses using brass and copper tool

Experiment is conducted in electric discharge machining, of AISI D2 steel using two tool such as brass tool and copper tool. Responses such as MRR, TWR, Ra, circularity are obtained in both cases. It is observed that responses are different for different tool material. A comparison is described below to obtain the better tool material. Table 5.21 shows the optimal response values and corresponding optimal process parameters, optimized by genetic algorithm individually. Table 5.21 shows that the optimal MRR obtained by copper tool is twice of time of MRR obtained by brass tool. The tool wear rate of copper tool is very less as compared to brass tool. Minimum surface roughness is obtained by machining copper tool. The circularity is nearly equal in both cases. Therefore copper as tool material should be preferred rather than brass.

Table 5.21. Optimal solution for individual responses and corresponding variable

Response	Tool material	Ip (A)	Ton (μs)	τ (%)	Fp (bar)	Optimal value of response
MRR (mm^3/min)	Brass	6.997	299.998	90.000	0.398	7.706
	Copper	7.000	100.000	90.000	0.400	15.992
TWR (mm^3/min)	Brass	3.000	300.000	80.002	0.200	0.648
	Copper	3.648	255.155	80.000	0.200	0.271
Ra (μm)	Brass	3.000	100.000	80.000	0.332	3.729
	Copper	3.001	299.998	90.000	0.365	2.162
Circularity	Brass	7.000	299.999	89.997	0.400	0.868
	Copper	4.910	100.008	80.000	0.346	0.853

The optimal setting using neuro-fuzzy and PSO model is exposed in Table 5.22. From table, observed that better MRR, TWR and Ra are achieved by using copper tool with less pulse-on-time and duty factor. Discharge current is almost same in both cases. The circularity is nearly equal in both cases. Therefore copper tool can be preferred rather than brass tool.

Table 5.22. Condition for optimal EDM performance using neuro-fuzzy model

Tool material	Optimal process parameter				MPCI	Optimal value of response			
	Ip (A)	Ton (μs)	τ (%)	Fp (bar)		MRR (mm^3/min)	TWR (mm^3/min)	Ra (μm)	Circularity
brass	6.924	298.7	85.56	0	0.9465	4.1676	0.0347	11.737	0.8741
copper	6.87	116.2	80	0	0.8579	10.0912	0.0303	8.135	0.8245

5.6. White layer thickness and crack analysis

In EDM total eroded material can't be removed from surface due to improper flushing. The un-flushed material recrystallizes on the machined surface forming a white layer. Hence white layer modifies the machined surface. The machined material is cut in transvers section to study the white layer for experiment number 11, 12, 14, 15, 17, 18, 19, 20 by as shown in Figure 40-47 and the measured white layer value is listed in Table 5.23. Table 5.23 indicates that the white layer thickness increases with increasing discharge current due to more material removed as a result of strong spark. White layer thickness increases with decreasing pulse-on-time with same duty factor. This occurs because, as pulse-on-time is less there is much time for recrystallization formation. White layer thickness is decreases with increasing flushing pressure due to effectively removal of eroded material.

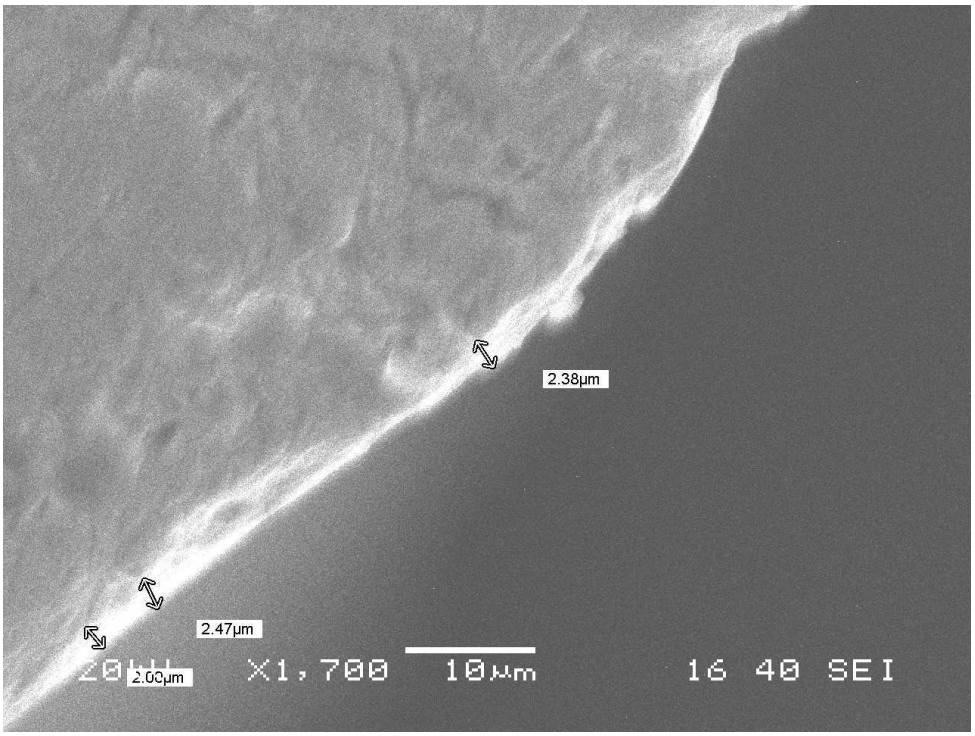

Figure 5.40. White layer at Ip=3A, Ton =200µs, τ =90%,Fp=0.3bar

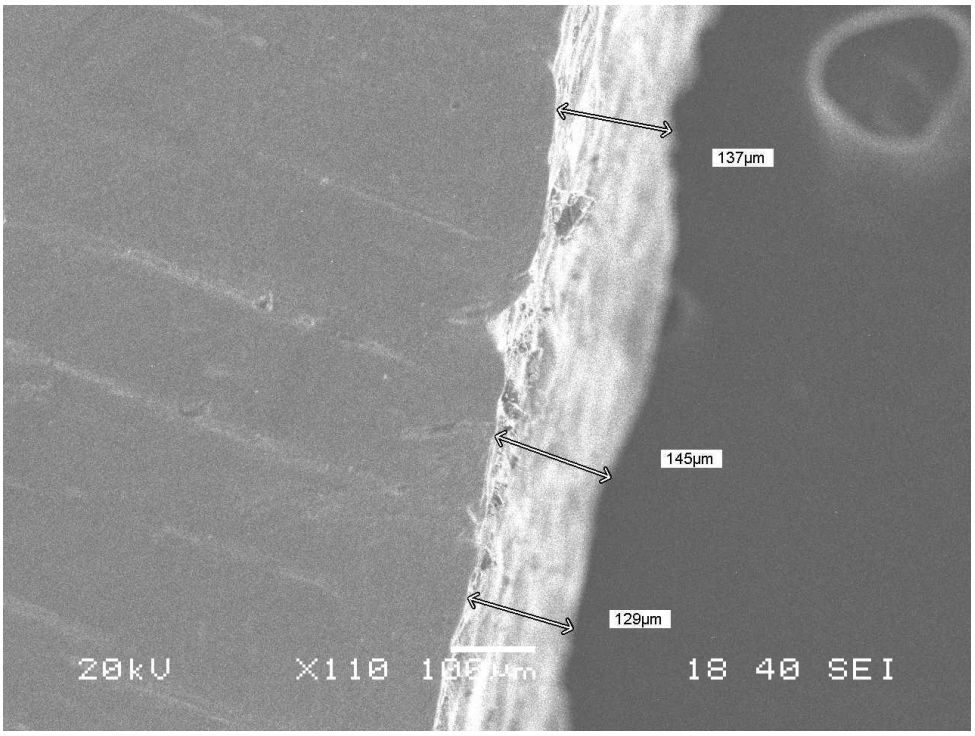

Figure 5.41. White layer at Ip=7A, Ton=200µs, τ =90%, Fp=0.3bar

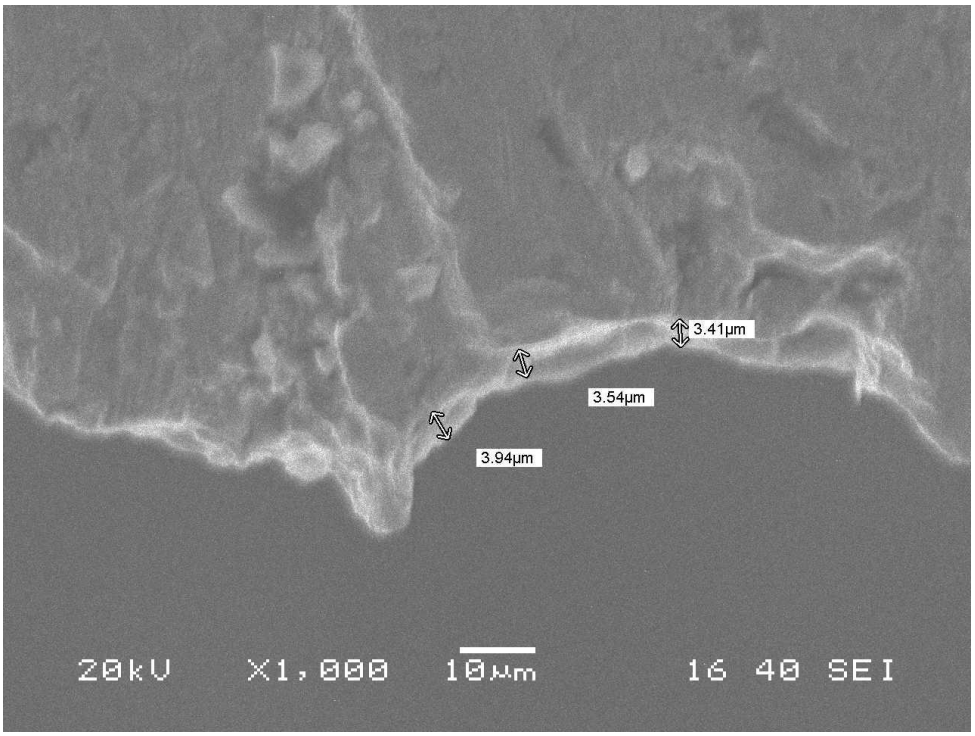

Figure 5.42. White layer at Ip=5A, Ton=300µs, τ =85%, Fp= 0.2bar

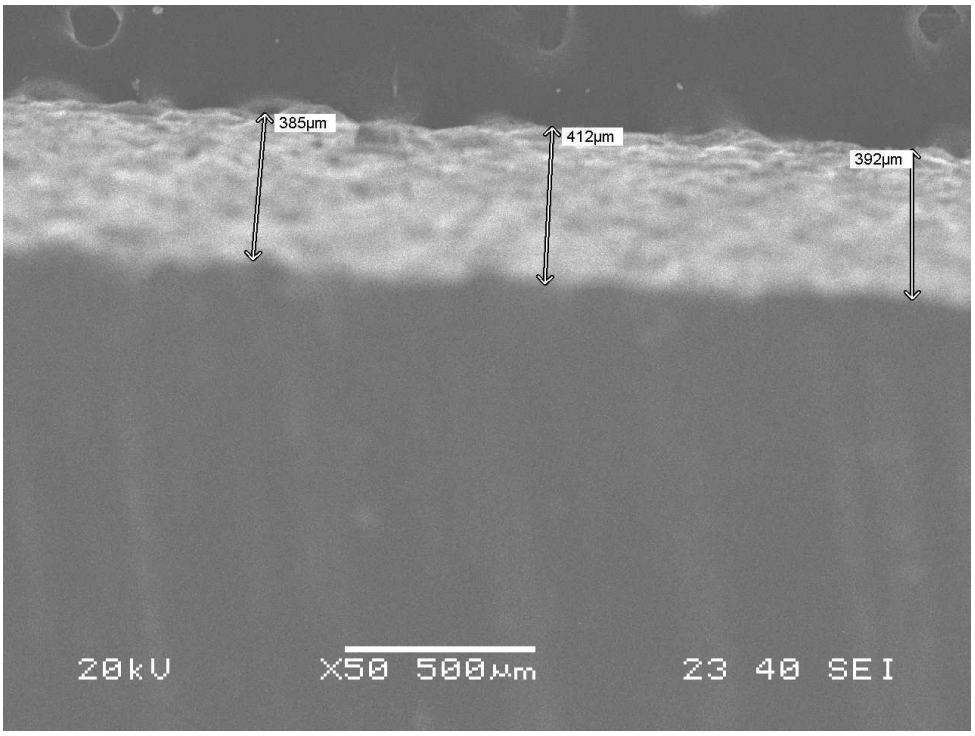

Figure 5.43. White layer at Ip=5A, Ton=100µs, τ =85%, Fp=0.4bar

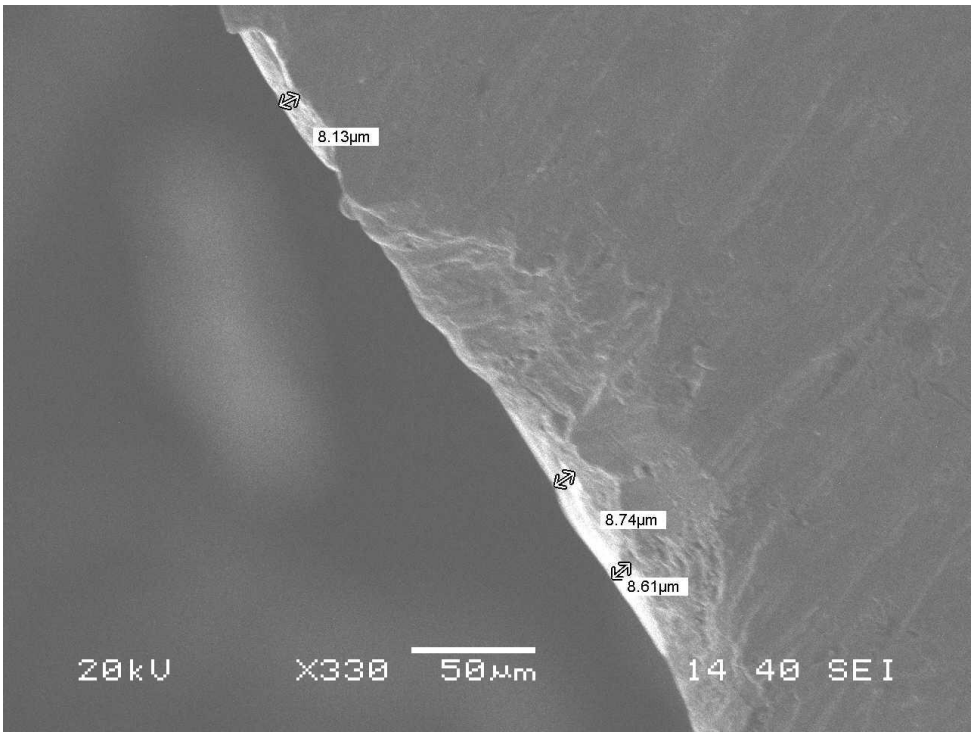

Figure 5.44. White layer at Ip=7A, Ton=200 µs, τ =85%, Fp=0.2bar

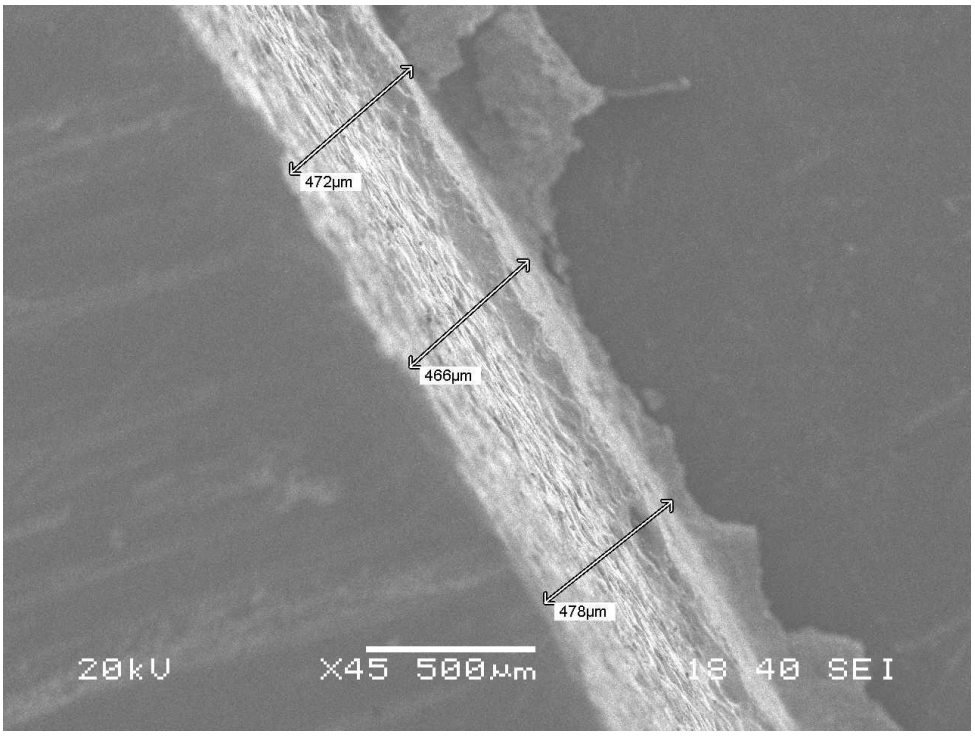

Figure 5.45. White layer at Ip=3A,Ton=200µs, τ =85%, Fp=0.2bar

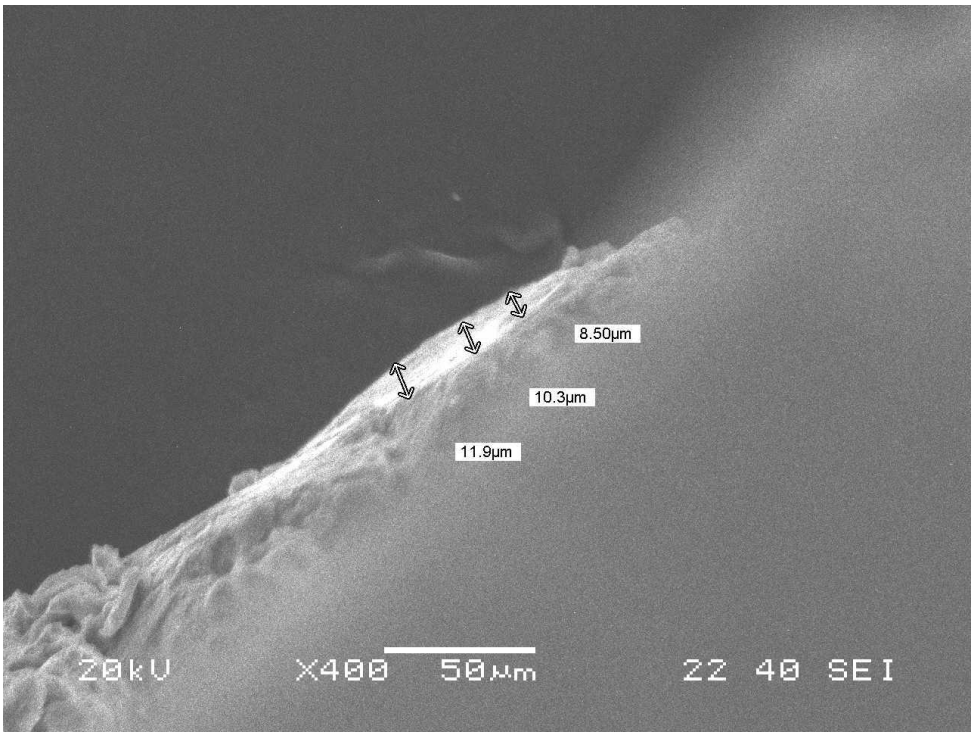

Figure 5.46. White layer at Ip=3A, Ton=200µs, τ =85%, Fp=0.4bar

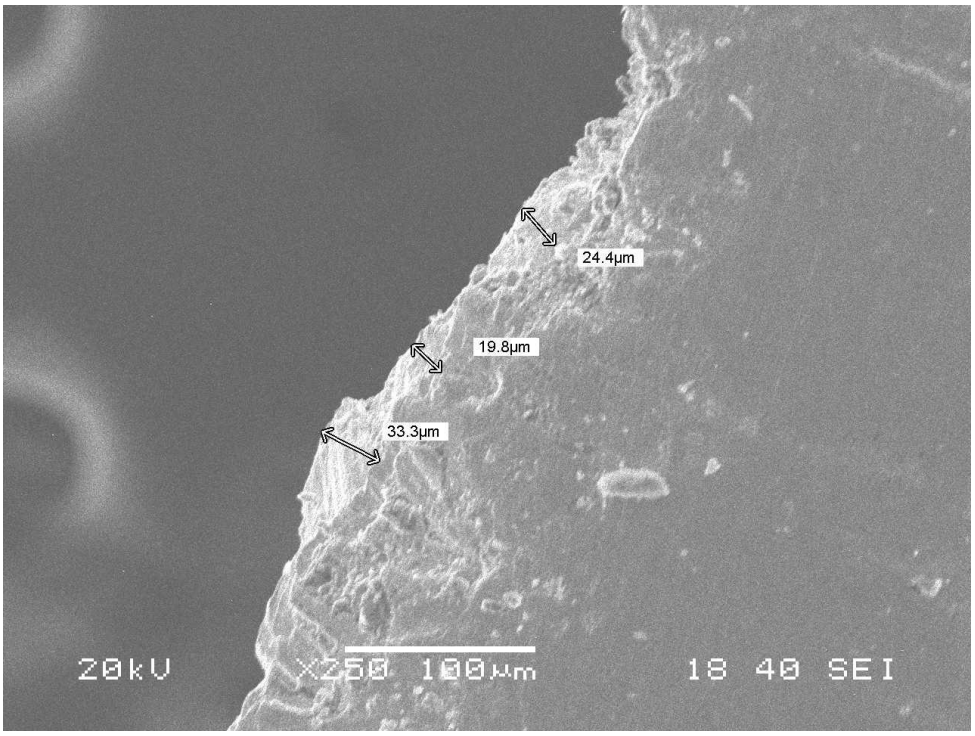

Figure 5.47. White layer at Ip=7A, Ton=200µs, τ=85%, Fp=0.4bar

Table 5.23. White layer thickness

Experiment No.	Ip	Ton	τ	Fp	White layer thickness
11	3	200	90	0.3	2.28
12	7	200	90	0.3	137.00
14	5	300	85	0.2	3.63
15	5	100	85	0.4	396.33
17	3	200	85	0.2	8.49
18	7	200	85	0.2	472.00
19	3	200	85	0.4	10.23
20	7	200	85	0.4	25.83

The machined surface of experiment numbers 22 (Ip = 5 A, Ton = 300 µs, τ = 80%, Fp=0.3 bar) and 23 (Ip=5A, Ton =100µs, τ =90%, Fp=0.3bar) is analysed under scanning electron microscope at 1000 magnification (Model JEOL JSM-6480LV). Figure 5.48 shows pores and micro cracks for experiment number 22 whereas Figure 5.49 shows the same for experiment number 23. It can be observed that few larger pores and small number of micro cracks are present in Figure 5.48. In Figure 5.49, more number of small pores and more number of micro cracks are present. It can be deduced that increase of pulse-on-time causes pores and cracks to be larger.

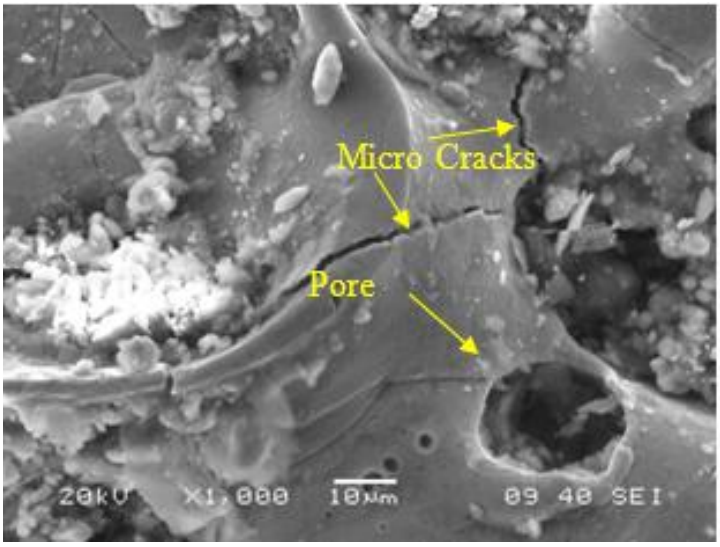

Figure 5.48. SEM picture showing pores and cracks for experiment number 22

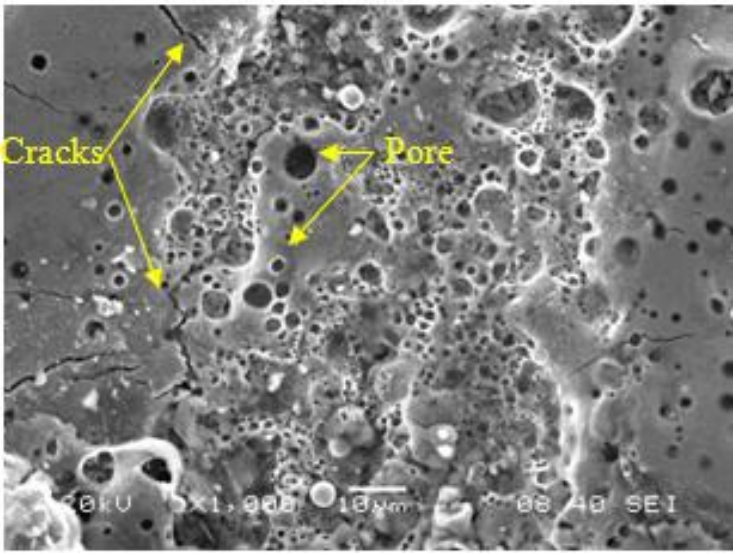

Figure 5.49. SEM picture showing pores and cracks for experiment number 22

3.11. Conclusions

The chapter describes the optimal setting for single response as well as multi-response (equivalent single response of multi-response). NSGA is proposed to obtain 100 pareto optimal solution and corresponding input variables instead of single optimal solution. By comparing it is concluded that copper tool giver better EDM performance that brass tool. The machined surface and its transverse section are studied under scanning electron microscope to analyse cracks and white layer thickness respectively. The model is validated using finite element thermal modelling in the next chapter.

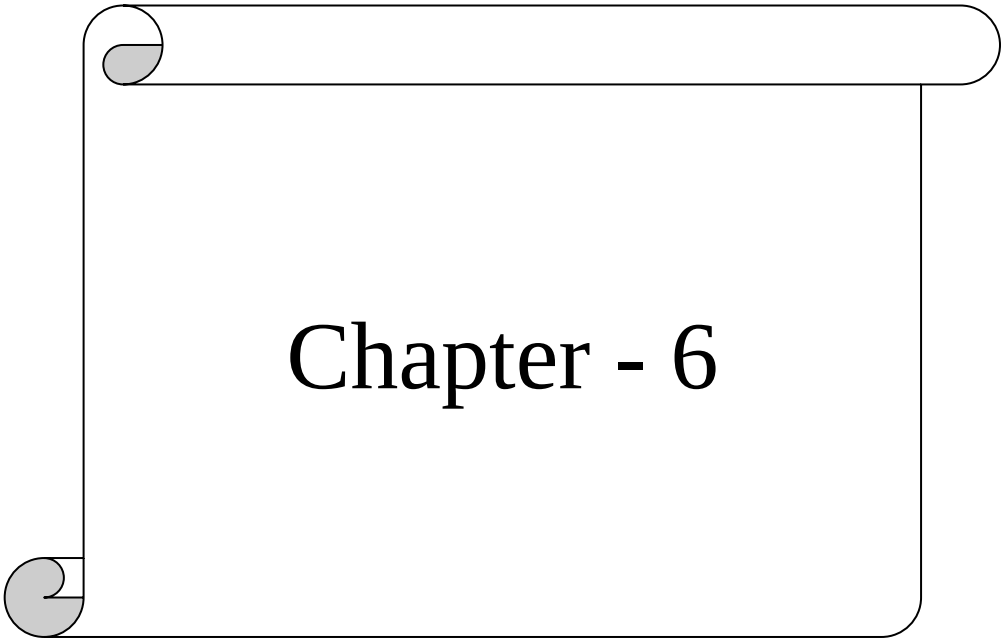
Chapter - 6

Chapter 6

TRHERMO-PHYSICAL MODELLING

6.1. Introduction

Electrical discharge machining EDM contributes a prime share in the manufacture of complex-shaped dies, mould, and critical parts used in automobile, aerospace, and other industrial applications [84, 85]. It is, thus, important to improve the process productivity and finishing capability to produce complex part shapes accurately in the shortest possible lead times. The physics of the EDM spark (plasma) is so complicated that, it is difficult to observe the process experimentally and quantify the mechanism of material removal [86, 87]. Researchers worldwide are developing models for accurate prediction of crater shapes, material removal rate (MRR), and tool wear rate (TWR). The present study describes an intelligence technique for thermo-physical modelling to validate the model developed by empirical relation and neuro-fuzzy system.

6.2. Thermal analysis of the EDM process

During EDM process, the dielectric medium ionizes due to high potential as a result plasma arc produced. The primary mechanism of material removal is spark erosion process which produces large heat and melted the work piece as well as tool material. For thermal analysis conduction is thus considered as primary mode of heat transfer. In the present study flourier heat conduction equation is used as governing equation (Eq. 6.1) [85]. Transient nonlinear analysis of the single spark operation of EDM process has been carried out in ANSYS 10 software.

$$\frac{1}{r}\frac{\partial}{\partial r}\left(K_t r \frac{\partial T}{\partial r}\right) + \frac{\partial}{\partial z}\left(K_t r \frac{\partial T}{\partial r}\right) = \rho C_p \frac{\partial T}{\partial t} \tag{6.1}$$

Where r and z are the coordinates of cylindrical work domain, T is temperature, K_t is thermal conductivity, ρ is density, C_p is specific heat capacity of work piece.

A small cylindrical portion of the work piece around the spark is chosen for analysis. Figures 6.1 show the two-dimensional axisymmetric process continuum and Figures 6.2 shows the mode of heat transfer in the work piece.

6.2.1. Assumptions

The following assumptions have been made during the thermal analysis.

1. Homogeneity in tool and work piece material which are temperature dependant.
2. Heat transfer is only due to conduction, not by convection and radiation.
3. Spark channel is cylindrical column and spark radius a function of discharge current and time.
4. Flushing efficiency is 100%.
5. Only fraction of heat is conducted to the work piece, rest goes to the dielectric.

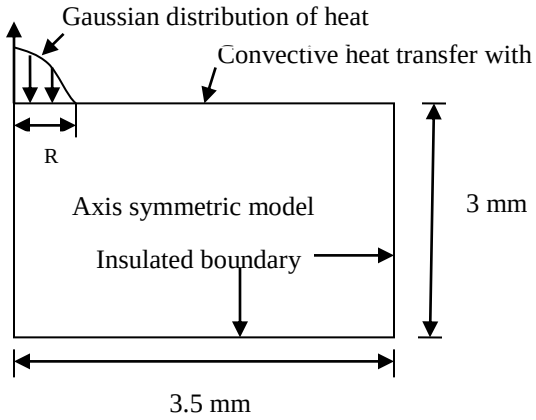

Figure 6. 1. Two-dimensional axisymmetric model

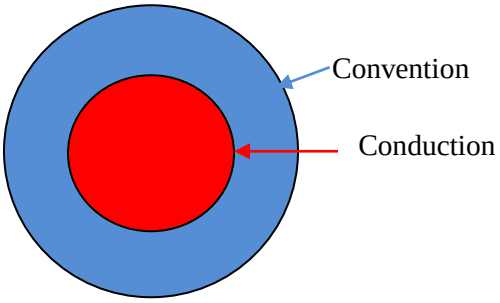

Figure 6. 2. Mode of heat transfer in the work piece

6.2.2. Heat input, spark radius and boundary condition

The heat conduction equation used is shown in Eq. 6.2 and the spark radius is calculated by the empirical formula Eq. 6.3.

$$q_w(r) = q_o \exp\{-4.5(\frac{r}{R})^2\} \quad (6.2)$$

Where q_w is the heat enters to the work piece. The maximum heat flux is $q_o = \frac{4.56 F_C VI}{R}$, Fc is Fraction of heat going to cathode. V discharge voltage (V), I discharge current (A), R is spark radius in μs.

$$R = (2.04e^{-3})I^{0.43}T_d^{0.44} \quad (6.3)$$

Where I is discharge current, T_d pulse-on-time.

The boundary of work piece is immersed in dielectric medium having ambient temperature (Ta) and heat flux is applied on the top surface of the work piece at the spark region.

6.2.3. Solution methodology

The governing equation (Eq. 6.1) with boundary conditions is solved by Finite Element Method to predict the temperature distribution. ANSYS^{TM} 10.0, an FEM solver was used. The 2-D continuum (size 0.35×0.3 mm) was considered for the analysis. An axisymmetric, four-noded, thermal solid element (PLANE 55) was used for discretization of the continuum. Isometric material properties, thermal conductivity were employed and following steps are followed to find crater and temperature distribution.

Step 1. Model geometry is created and meshing is done using PLANE 55 thermal solid element.

Step 2. Material property such as thermal conductivity, density, heat capacity is given along with initial and bulk temperature as 300 K .

Step 3. The heat flux location equation is imported Eq 6.2 and applied to the spark location.

Step 4. Temperature distribution is obtained.

Step 5. The node having temperature more than melting point temperature is identified and killed to eliminate from mesh.

Step 6. The MRR and TWR are calculated using coordinate data of the craters of work and tool material for the optimal setting obtained from empirical combined with GA model and neuro-fuzzy model.

6.3. Results and comparison of models

The optimal conditions from empirical model combined with GA and neuro-fuzzy model, i.e input process parameter for ANSYS are listed in Table 6.1.

Table 6.1. Process parameter for ANSYS

Response	Tool material	Ip (A)	Ton (μs)	τ (%)
Optimal setting from empirical model combined with GA				
MRR (mm^3/min)	Brass	6.997	299.998	90.000
	Copper	7.000	100.000	90.000
TWR (mm^3/min)	Brass	3.000	300.000	80.002
	Copper	3.648	255.155	80.000
Optimal setting from Neuro-fuzzy model				
MRR (mm^3/min) (MPCI)	Brass	6.924	298.700	85.56
	Copper	6.870	116.200	80.000
TWR (mm^3/min) (MPCI)	Brass	6.924	298.700	85.56
	Copper	6.870	116.200	80.000

Radius is calculated using Eq. 6.3 and the transient heat transfer problem was solved by applying the heat flux at the spark location (Eq. 6.2). The discharge duration is used as the time step for the analysis. Figure 6.3 shows the results for a typical problem showing the temperature contour plots. The results are for work material AISI D2 tool steel with machining conditions, discharge current 3 A, pulse-on-time 300 μs and duty cucle 80 %. The nodes showing temperature more than melting point were selected and eliminated from the complete mesh of the work domain for further analysis. A typical crater cavity generated by this analysis is shown in Figure 6.4.

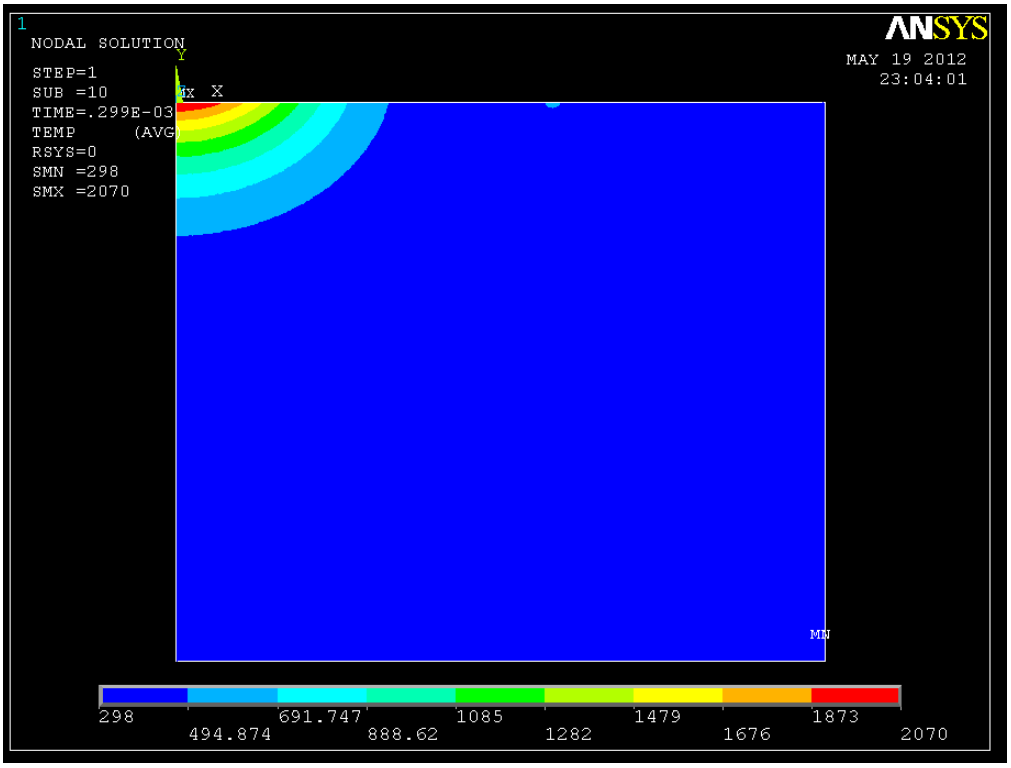

Figure 6. 3. Temperature distribution

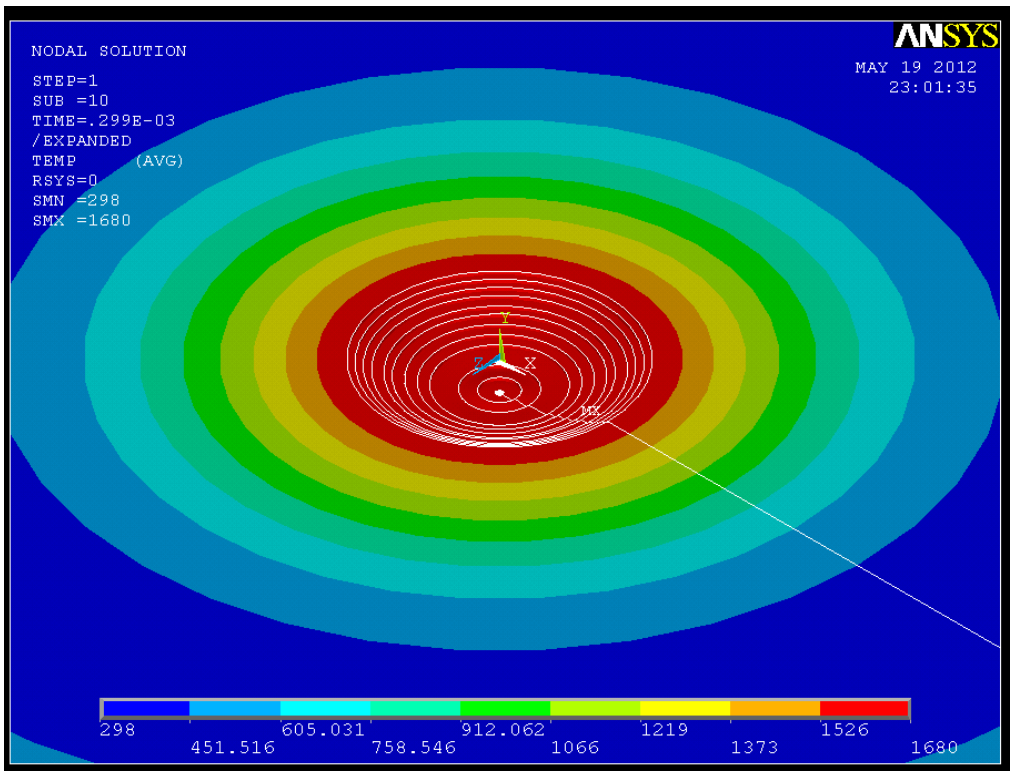

Figure 6. 4. Predicted bowl shaped crater using the FEM analysis

The material removal rate due to single spark discharge is calculated by dividing the cavity volume into number of cylindrical discs Figure 6.5.

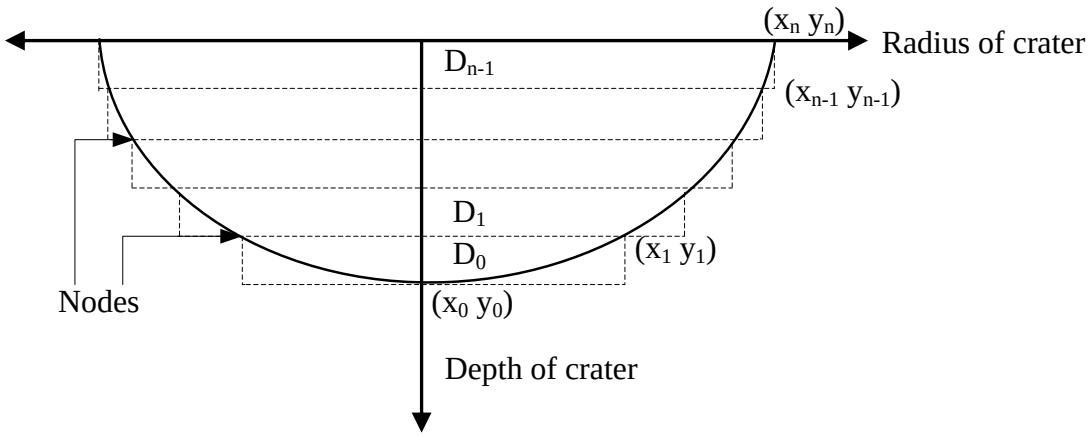

Figure 6. 5. Calculation of crater volume

Total crater volume C_v (μm^3) is given by Eq. 6.4

$$C_v = \sum_{i=0}^{n-1} D_i \tag{6.4}$$

Where D_i is given by Eq. 6.5

$$D_i = \pi\left(\frac{x_i + x_{i+1}}{2}\right)^2 (y_{i+1} - y_i) \tag{6.5}$$

where x and y are the coordinates of nodes and n is the number of nodes.

The material removal rate in mm^3/min is calculated assuming all sparks are equally effective using Eq. 6.6. The similar procedure is followed to calculate tool wear rate putting tool material properties instead of work piece material. The MRR, TWR results are listed in Table 6.2 with results from AI model for comparison.

$$MRR = \frac{60 \times C_v}{Ton + Toff} \tag{6.6}$$

Table 6.2. Comparison of AI and thermo-physical model

Response	Tool material	Optimal parametric value			AI model response value	Thermo-physical model response value
		Ip (A)	Ton (μs)	τ (%)		
Single response optimization using GA						
MRR (mm^3/min)	Brass	6.997	299.998	90.000	7.706	7.22000
	Copper	7.000	100.000	90.000	15.992	15.05724
TWR (mm^3/min)	Brass	3.000	300.000	80.002	0.648	0.709874
	Copper	3.648	255.155	80.000	0.271	0.304146
Multi-response optimization using Neuro-fuzzy model						
MRR (mm^3/min)	Brass	6.924	298.700	85.560	4.1676	4.266725
	Copper	6.870	116.200	80.000	10.0912	10.12844
TWR (mm^3/min)	Brass	6.924	298.700	85.560	0.0347	0.034185
	Copper	6.870	116.200	80.000	0.0303	0.034535

From Table 6.2, it is observed that the response obtained in thermo-physical model is very close to the optimal response obtained from AI model. Therefore the model is validated within and beyond the boundary of process parameter.

6.4. Conclusions

In the present study a non-linear, transient, thermo-physical model of die-sinking EDM process has been developed using the FEM and thermal analysis of the process is carried out. The results obtained from the numerical model are compared with results of AI model. It is observed that the MRR values predicted by our model are closer to the results of AI model, which validate the model.

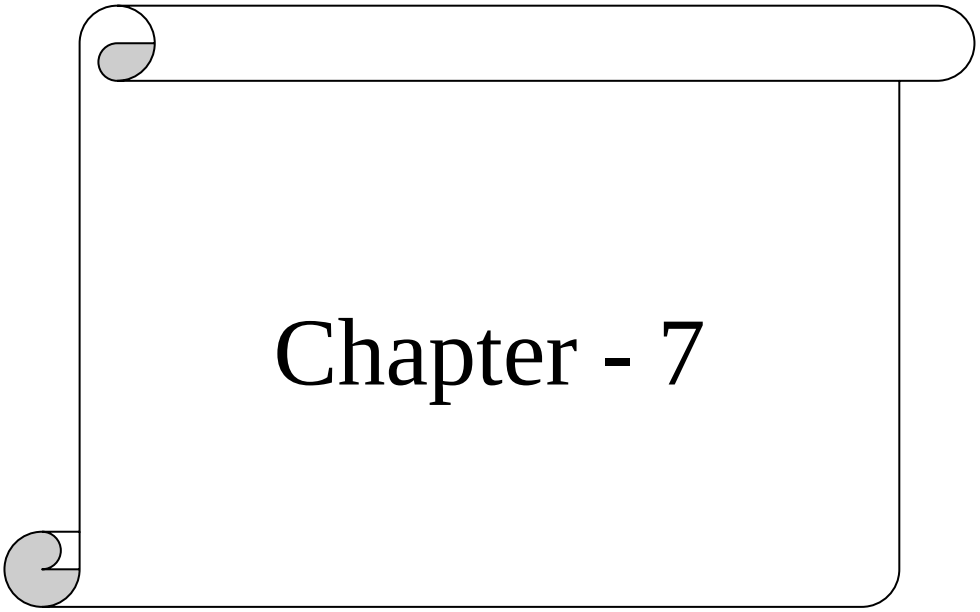
Chapter - 7

Chapter 7

CONCLUSIONS

7.1. Introduction

Electric discharge machining (EDM) is one of the non-traditional machining processes to manufacture complex shape in conductive material irrespective of hardness. EDM has significant advantage in terms of elimination of multi pass manufacturing, the flexibility and the possibility of producing very complex parts and shapes. The present study describes a solution to solve one challenge faced by EDM user, i.e. improvement of quality and productivity of parts produced, which is allied with the accurate application of the specified performance.

7.2. Summary of findings

The understandings generated in this work not only properly explain the complex build mechanism but also present in detail the processing parameter effect on output responses. The comparison of EDM performance using copper and brass as tool material. The development of an artificial intelligence model to optimize process parameters for better performance. The optimization of the process parameters for MRR, TWR, Ra, circularity has been performed individually for both brass and copper tool. The optimal results are shown in Table 7.1.

Table 7.1. Optimal condition and optimal value

Response	Tool material	Ip (A)	Ton (μs)	τ (%)	Fp (bar)	Optimal value of response
MRR	Brass	6.997	299.998	90.000	0.398	7.706
	Copper	7.000	100.000	90.000	0.400	15.992
TWR	Brass	3.000	300.000	80.002	0.200	0.648
	Copper	3.648	255.155	80.000	0.200	0.271
Ra	Brass	3.000	100.000	80.000	0.332	3.729
	Copper	3.001	299.998	90.000	0.365	2.162
Circularity	Brass	7.000	299.999	89.997	0.400	0.868
	Copper	4.910	100.008	80.000	0.346	0.853

It is concluded from the table that copper tool has better performance than brass tool as the optimal value of response in case of copper tool are found to be larger. The responses are optimized simultaneously using neuro-fuzzy model and the results are shown in Table 7.2. In this case flushing pressure is found to be insignificant and better performance is achieved using copper tool.

Table 7.2. Condition for optimal EDM performance using neuro-fuzzy model

Tool material	Optimal process parameter				MPCI	Optimal value of response			
	Ip (A)	Ton (μs)	τ (%)	Fp (bar)		MRR (mm^3/min)	TWR (mm^3/min)	Ra (μm)	Circularity
brass	6.924	298.7	85.56	-	0.9465	4.1676	0.0347	11.737	0.8741
copper	6.870	116.2	80.00	-	0.8579	10.0912	0.0303	8.135	0.8245

The analytical model is validated by a non-linear, transient, thermo-physical model. The results obtained using analytical and thermo-physical models are shown in Table 7.3. From Table 6.2, it is observed that the response obtained in thermo-physical model is very close to the optimal response obtained from analytical model. Therefore the model is validated within and beyond the boundary of process parameter.

Table 7.3. Comparison of AI and thermo-physical model

Response	Tool material	Optimal parametric value			AI model response value	Thermo-physical model response value
		Ip (A)	Ton (μs)	τ (%)		
Single response optimization using GA						
MRR (mm^3/min)	Brass	6.997	299.998	90.000	7.706	7.22000
	Copper	7.000	100.000	90.000	15.992	15.05724
TWR (mm^3/min)	Brass	3.000	300.000	80.002	0.648	0.709874
	Copper	3.648	255.155	80.000	0.271	0.304146
Multi-response optimization using Neuro-fuzzy model						
MRR (mm^3/min)	Brass	6.924	298.700	85.560	4.1676	4.266725
	Copper	6.870	116.200	80.000	10.0912	10.12844
TWR (mm^3/min)	Brass	6.924	298.700	85.560	0.0347	0.034185
	Copper	6.870	116.200	80.000	0.0303	0.034535

7.3. Limitation of the study

In spite of several advantages obtained through proposed study, the following may be treated as limitations of the study since they have not been addressed in study.

- Heat affected zone is not been considered.
- The effect of process parameter on white layer thickness and crack density has not been studied.
- The present study mainly develops empirical model, numerical model and soft computing technique but mathematical approach must be developed to study the effect of process parameters on various responses.
- In this work, only EDM process has been considered limiting the scope of improving other non-traditional machining process.

7.4. Future scope

- White layer thickness and crack density can be considered as a response with lower-the-better criteria.
- Heat affected zone can be considered as a response with lower-the-better criteria.
- Mathematical approach can be developed to study the effect of process parameters on various responses.
- The model can be used in other field for optimization purpose.

BIBLIOGRAPHY

1. El-Hof HA–G. Advance machining process. McGraw-Hill, production Engineering Department, Alexandria University, Egypt; 2005.
2. Benedict GF. Nontraditional Manufacturing Process. Marcel Dekker, New York; 1987.
3. Ramakrishnan R, Karunamoorthy L. Multi response optimization of wire EDM operations using robust design of experiments. *International Journal of Advanced Manufacturing Technology*. 2006; 29:105-112.
4. Sanchez JA, Rodil JL, Herrero A, Lacalle LNL, Lamikiz A. On the influence of cutting speed limitation on the accuracy of wire-EDM corner-cutting. *Journal of Materials Processing Technology*. 2007; 182:574-579.
5. Schumacher B M. After 60 years of EDM the discharge process remains still disputed. *Journal of Material Process and Technology*. 2004; 149:376–381.
6. Anders A. Tracking down the origin of arc plasma science, I. Early pulsed and oscillating discharges. *IEEE Transaction on Plasma Science*. 2003; 31(4):1052–1059.
7. Priestley J. Experiments on the circular spots made on pieces of metal by large electrical explosions. The history and present state of electricity with original experiments. 1775; vol. II, 3rd ed., London.
8. Dibner B, Volta G. A controversy that led to the discovery of useful electricity. CT: Burndy Library, Norwalk (1952).
9. Anders A. Tracking down the origin of arc plasma science, II. Early continuous discharges. *IEEE Transaction on Plasma Science*. 2003; 31(4), 1060–1069.
10. Lazarenko BR. About the inversion of metal erosion and methods to fight ravage of electric contacts, WEI-Institute, Moscow (in Russian) (1943).
11. Germer LH, Haworth FE. Erosion of electrical contacts on make. *Journal of Applied Physics*. 1949; 20(11):1085–1109.
12. Cobine JD, Burger EE. Analysis of electrode phenomena in the high-current arc. *Journal Applied Physics*. 1955; 26(7):895–900.
13. Zingerman AS. The effect of thermal conductivity upon the electrical erosion of metals. *Soviate Physics-Technical Physics*. 1956; 1:1945–1958.

14. Kobayashi K. The present and future developments of EDM and ECM. *Proceedings of the 11th International Symposium for Electro Machining (ISEM-11)*. 1995:29–47 (Lausanne, Switzerland).
15. Lottgen R. EDM die-sinking - state of the art. *Proceedings of the 12th International Symposium for Electro Machining (ISEM-12)*. 1998; 341–350 (Aachen, Germany).
16. Ho KH, Newman ST. State of the art electrical discharge machining (EDM). *International Journal of Machine Tools and Manufacture*. 2003; 43(13):1287–1300.
17. Ho KH, Newman ST, Rahimifard S, Allen RD. State of the art in wire electrical discharge machining (WEDM). *International Journal of Machine Tools and Manufacture*. 2004; 44(12-13):1247–1259.
18. Walder G. New technologies and EDM. *Proceedings of the 12th International Symposium for Electro Machining (ISEM-12)*. 1998; 331–340 (Aachen, Germany).
19. Singh A. Ghosh A. A thermo-electric model of material removal during electric discharge machining. *International Journal of Machine Tools and Manufacture*. 1999; 39:669-682.
20. Williams EM. Theory of Electric Spark Machining. A.I.E.E. Transactions. 1952; 71(II).
21. J Marafona, C Wykes. A new method of optimising material removal rate using EDM with copper–tungsten electrodes. *International Journal of Machine Tools and Manufacture*. 2000; 40:153-164.
22. Chen Y, Mahdivian SM. Analysis of electro-discharge machining process and its comparison with experiments. *Journal of Material Processing Technology*. 2000; 104:150-157.
23. Yadav V, Jain VK, Dixit PM. Thermal stresses due to electrical discharge machining. *International Journal of Machine Tools and Manufacture*. 2002; 42:877-888.
24. Marafona J, Chousal JA. A finite element model of EDM based on the Joule effect. *International Journal of Machine Tools and Manufacture*. 2006; 46:595-602.
25. Mahardika M, Tsujimoto T, Mitsui K. A new approach on the determination of ease of machining by EDM processes. *International Journal of Machine Tools and Manufacture*. 2008; 48:746-760.
26. Das S, Klotz M, Klocke F. EDM simulation: finite element-based calculation of deformation, microstructure and residual stresses. *Journal of Materials Processing Technology*. 2003; 142:434-451.

27. Schulze H, Herms R, Juhr H, Schaetzing W, Wollenberg G. Comparison of measured and simulated crater morphology for EDM. *Journal of Materials Processing Technology*. 2004; 149:316-322.
28. Kansal HK, Singh S, Kumar P. Numerical simulation of powder mixed electric discharge machining (PMEDM) using finite element method. *Mathematical and Computer Modelling*. 2008; 47:1217-1237.
29. Joshi SN, Pande SS. Development of an intelligent process model for EDM. *International Journal of Advance Manufacturing Technology*. 2009; 300-317.
30. Joshi SN, Pande SS. Thermo-physical modelling of die-sinking EDM process. *Journal of Manufacturing Processes*. 2010; 12(1):45-56.
31. Pradhan M. Process Simulation, modelling and estimation of Temperature and residual Stresses Electrical Discharge Machining of AISI D2 steel. *Journal of Applied Physics*. 2012; 1-9.
32. Habib SS. Study of the parameters in electrical discharge machining through response surface methodology approach. *Applied Mathematical Modelling*. 2009; 33(12):4397-4407.
33. Chattopadhyay KD, Verma S, Satsangi PS, Sharma PC. Development of empirical model for different process parameters during rotary electrical discharge machining of copper – steel (EN-8) system. *Journal of Materials Processing Technology*. 2009; 209:1454-1465.
34. Selc YK. An experimental study for determination of the effects of machining parameters on surface roughness in electrical discharge machining (EDM). *Journal of Engineering for Industry*. 2006:1118-1121.
35. Lee SH, Li XP. Study of the effect of machining parameters on the machining characteristics in electrical discharge machining of tungsten carbide. *Journal of Material processing Technology*. 2001; 115:344-358.
36. Salem SB. Parametric approach model for determining electrical discharge machining (EDM) conditions: effect of cutting parameters on the surface integrity. *The Arabian Journal for Science and Engineering Science*. 2009; 34(1):101-114.
37. Pradhan MK, Biswas CK. Modeling and Analysis of process parameters on Surface Roughness in EDM of AISI D2 tool Steel by RSM Approach. *World Academy of Science, Engineering and Technology*. 2009;814-819.

38. Helmi MH, Azuddin M, Abdullah W. Investigation of Surface Roughness and Material Removal Rate (MRR) on Tool Steel Using Brass and Copper Electrode for Electrical Discharge Grinding (EDG) Process. *International Journal of Integrated Engineering*. 2009:31-40.
39. Press AI. Reliable multi-objective optimization of high-speed WEDM process based on Gaussian process regression. *International Journal of Machine Tool and Manufacturer*. 2008; 48:47-60.
40. Prabhu S, Vinayagam BK. Analysis of surface characteristics of AISI D2 tool steel material using Electric Discharge Machining process with Single wall carbon nano tubes. *International Journal of Engineering and Technology*. 2010; 2(1):35-41.
41. Abbas NM, Solomon DG, Bahari F. A review on current research trends in electrical discharge machining. *International Journal of Machine Tool and Manufacturer*. 2007; 47:1214-1228.
42. Kansal HK, Singh S, Kumar P. Parametric optimization of powder mixed electrical discharge machining by response surface methodology. *Journal of Materials Processing Technology*. 2005; 169:427-436.
43. Selc YK. An experimental study for determination of the effects of machining parameters on surface roughness in electrical discharge machining (EDM). *Journal of Engineering For Industry*. 2006:1118-1121.
44. Su CT, Tong LI. Multi-response robust design by principal component analysis. *Total Quality Management*. 1997; 8:409–416.
45. Tong L, Wang C, Chen C, Chen C. Dynamic multiple responses by ideal solution analysis. *European Journal of Operational Research*. 2004; 156:433-444.
46. Road TH. Optimizing multi-response problems in the Taguchi method by fuzzy multiple attribute. *Quality and Reliability Engineering*. 1997; 13:25-34.
47. Tarng YS, Yang WH, Juang SC. The Use of Fuzzy Logic in the Taguchi Method for the Optimisation of the Submerged Arc Welding Process. *International Journal of Advanced Manufacturing Technology*. 2000; 16:688-694.
48. Lin YC, Yan BH, Huang FY. Surface improvement using a combination of electrical discharge machining with ball burnish machining based on the Taguchi method. *International Journal of Advanced Manufacturing Technology*. 2001a; 18(9):673-682.

49. Lin YC, Yan BH, Huang FY. Surface modification of Al-Zn-Mg aluminum alloy using the combined process of EDM with USM. *Journal of Materials Processing Technology*. 2001b; 115(3):359-366.
50. Lin JL, Lin CL. The use of grey-fuzzy logic for the optimization of the manufacturing process. *Journal of Materials Processing Technology*. 2005; 160(1):9-14.
51. Wang K, Gelgele HL, Wang Y, Yuan Q, Fang M A. Hybrid intelligent method for modeling the EDM process. *International Journal of Machine Tools and Manufacture*. 2003; 43(10):995-999.
52. Su JC, Kao JY, Tarng YS. Optimization of the electrical discharge machining process using a GA based neural networks. *International Journal of Advanced Manufacturing Technology*. 2004; 24(2):81-90.
53. Kuriakose S, Shunmugam MS. Multi-objective optimization of wire electro discharge machining process by non-dominated sorting genetic algorithm. *Journal of Materials Processing Technology*. 2005; 170(1-2):133-141.
54. Mandal D, Pal SK, Saha P. Modeling of EDM process using BP neural network and multi-objective optimization using non-dominating sorting GA. *Journal of Materials Processing Technology*. 2007; 186(1-3):154-162.
55. Liao HC. Using PCR-TOPSIS to optimize Taguchi's multi-response problem. *International Journal of Advanced Manufacturing Technology*. 2003; 22:649-55.
56. Tarang YS, Yang WH. Application of the Taguchi method to the optimization of the submerged arc welding process. *Materials and Manufacturing Processes*. 1998; 13(3):455-67.
57. Reddy PBS, Nishina K, Babu AS. Unification of robust design and goal programming for multiresponse optimization - a case study. *Quality and Reliability Engineering International*. 1997; 13:371-83.
58. Antony J, Bardhan AR, Kumar M, Tiwari MK. Multiple response optimization using Taguchi methodology and neuro-fuzzy based model. *Journal of Manufacturing Technology Management*. 2006; 17(7):908-925.
59. Panda DK, Bhoi RJ. Artificial neural network prediction of material removal rate in EDM. *Materials and Manufacturing Processes*. 2005; 20(4):645-672.

60. Yang SH, Srinivas J, Mohana S, Lee DK, Balaji S. Optimization of electric discharge machining using simulated annealing. *Journal of Materials Processing Technology*. 2009; 209(9):4471-4475.
61. Somashekhar KP, Ramachandran N, Mathew Jose. Optimization of material removal rate in micro-EDM using artificial neural network and genetic algorithms. *Materials and Manufacturing Processes*. 2010; 25(6):467-475.
62. Tang JG, Zhang XM, Deng YL, Du YX, Chen ZY. Texture decomposition with particle swarm optimization method. *Computational Material Science*. 2006; 38:395–399.
63. Mahdavinejad RA. Modeling and Optimization of Electrical Discharge Machining of SiC Parameters , Using Neural Network and Non-dominating Sorting Genetic Algorithm (NSGA II). *Material Science and Applications*. 2011; 2011(June):669-675.
64. Kuriakose S, Shunmugam M. Multi-objective optimization of wire-electro discharge machining process by Non-Dominated Sorting Genetic Algorithm. *Journal of Materials Processing Technology*. 2005; 170(1-2):133-141.
65. Kansal HK, Singh S, Kumar P. Parametric optimization of powder mixed electrical discharge machining by response surface methodology. *Journal of Materials Processing Technology*. 2005; 169:427-436.
66. Abbas NM, Solomon DG, Bahari F. A review on current research trends in electrical discharge machining. *International Journal of Machine Tools and Manufacture*. 2007; 47:1214-1228.
67. Singh P, Kumar A, Beri N, Kumar V. Influence of electrical parameters in powder mixed elecric discharge machining (PMEDM) of hastelloy. *Journal of Engineering Research and Studies*. 2010; I(II): 93-105.
68. http://www.lindquiststeels.com/documentation/d2.pdf
69. Jeff Wu CF, Hamada M. Experiments: Planning, Analysis, and Parameter Design Optimization. John Wiley & Sons, New York, 2002.
70. Montgomery DC. Design and Analysis of Experiments. John Wiley & Sons, Singapore; 2003.
71. Kumara S, Singh R, Singh T P, Sethi B L. Surface modification by electrical discharge machining: A review. *Journal of Materials Processing Technology*. 2009; 209:3675-3687.

72. Montgomery DC. Design and Analysis of Experiments. John Wiley & Sons, New York; 1991.
73. Kansal HK, Singh S, Kumara P. Parametric optimization of powder mixed electrical discharge machining by response surface methodology. *Journal of Materials Processing Technology*. 2005; 169(3):427-436.
74. Biswas R, Kuar AS, Biswas SK, Mitra S. Artificial neural network modelling of Nd:YAG laser microdrilling on titanium nitride-alumina composite. *Proceedings of Institution of Mechanical Engineering Journal of Engineering Manufacture Part B*. 2009; 224:473-482.
75. Bezdek JC. Pattern recognition with fuzzy objective function algorithms. Plenum press, New York; 1981.
76. Yang YK, Shie J-R, Liao H-T, Wen J-L, Yang R-T. A Study of Taguchi and Design of Experiments Method in Injection Molding Process for Polypropylene Components. *Journal of Reinforced Plastics and Composites*. 2008; 27(8):819-834.
77. Timothy J.R. Fuzzy Logic with Engineering Applications. Third Edition, John Wiley & Sons, University of New Mexico, USA; 2010.
78. Bojadziev G, Bojadziev M. Fuzzy Sets, Fuzzy Logic and Applications. World Scientific, London; 1995.
79. Singh P, Beri N, Kumar A. Some Studies On Electric Discharge Machining Of Hastlealloy Using Powder Metallurgy Electrode. *International Journal of Advanced Manufacturing Technology*. 2010; 1:16-27.
80. Clerc M, Kennedy JF. The Particle Swarm: Explosion, Stability and Convergence in a Multi-Dimensional Complex Space. *IEEE Transaction on Evolutionary Computation*. 2002; 6(1):58-73.
81. Subbaiah KV, Mouli KVV, Srinivas JC. Particles Swarm Optimization for production planning problems. *Journal of Decision and Mathematical Sciences*. 2005; 10:101-112.
82. Wang X, Sun J, Xu W. A Parallel QPSO Algorithm Using Neighbourhood Topology Model. *World Congress on Computer Science and Information Engineering*. 2009; 4:831-835.
83. Deb K, Pratap A, Agarwal S, Meyarivan T. A fast and elitist multiobjective genetic algorithm: NSGA-II. *IEEE Transactions on Evolutionary Computation*. 2002; 6(2):182-197.
84. Ho KH, Newman ST. State of the art in electrical discharge machining (EDM). *International Journal of Machine Tools Manufacturing*. 2003; 43:1287–1300.

85. Joshi SN, Pande SS. Development of an intelligent process model for EDM. *International Journal of Advanced Manufacturing Technology*. 2009; 300-317.
86. Descoeudres A. Characterization of electrical discharge machining plasmas. Ph.D. Thesis. EPFL Lausanne; 2006.
87. Joshi SN. Pande SS. Intelligent process modeling and optimization of die-sinking electric discharge machining. *Applied Soft Computing*. 2010; 11(2): 2743-2755.

PUBLICATION DETAILS

International Journals

1. **Jambeswar Sahu,** S.S. Mahapatra ; "Parametric Optimization Of Electrical Discharge Machining by Neuro-Fuzzy And Particle Swarm Optimization using Response Surface Method design", *International Journal of Advanced Manufacturing Technology*(IJAMT). (Communicated)

2. **Jambeswar Sahu**, D Puhan, S.S. Mahapatra; "Parametric Optimization of Electric Discharge Machining Process using Response Surface Methodology and Particle Swarm Optimization", *International Journal of Experimental Design and Process Optimization (IJEDPO)*. (Communicated)

3. **Jambeswar Sahu,** S.S. Mahapatra; "Multi-Response Optimization by Data Envelopment Analysis in EDM Process", *International Journal of Materials and Design.* (Communicated)

4. Debaprasanna Puhan, S.S. Mahapatra, **Jambeswar Sahu,** L.D. Das; "A hybrid approach for multi-response optimization of non-conventional machining on AlSiCp MMC", *Measurement.* (Communicated)

5. **Jambeswar Sahu**, Siba Sankar Mahapatra, Debaprasanna Puhan ,Layatitdev Das; **"**Paramertic optimazation of electric discharge machining by comparing of fuzzy logic and data envelopment analysis using anfis", *International Journal of Computer Sciences, Software Engineering and Electrical Communication Engineering* (IJCSSEECE) **ISSN:** 2229-3175. Second level of review **(R2).**

6. D K Mohanta**, J Sahu,** S Gangopadhyay, S S Mahapatra; "Prediction of surface roughness in turning of low carbon steel with coated and uncoated inserts", *International Journal of Advanced Materials Manufacturing & Characterization*, **Volume 1, issue 1, March 2012 ISSN 2277-3886, page 93-98**.

International Conference

7. **Jambeswar Sahu**, L.d. Das, D.P. Puhan, S.S. Mahapatra; "Optimization of multiple responses in electric discharge machining using data envelopment analysis", *International Conference on Advances in Modeling, Optimization and Computing*, (AMOC 2011) IIT Roorkee, India-247667, during Dec 5-7 2011.

8. L.d. Das, D.P. Puhan, **J. Sahu**, S.S. Mahapatra; "Multiple responses optimization of electric discharge machining using TOPSIS method", *International Conference on Advances in Modeling, Optimization and Computing*, (AMOC 2011) IIT Roorkee, India-247667, during Dec 5-7 2011.

9. D K Mohanta**, J Sahu,** S Gangopadhyay, S S Mahapatra; "Prediction of surface roughness in turning of low carbon steel with coated and uncoated inserts", *International conference on Materials Processing and characterization* (IPMPC 2012), Gokaraju Rangaraju Institute of Engineering & Technology, Hyderabad, Andhra Pradesh, India-500090, during Mar 8-10 2012.

10. **Jambeswar Sahu**, S S Mahapatra, R K Sahu, D Puhan, H Pradhan; "Electric Discharge Machining Process Parameter Optimization using Particle Swarm Optimization", *International Conference on Modelling, Optimisation and Computing* (ICMOC 2012), Noorul Islam University, Noorul Islam Centre for Higher Education, Kumaracoil, Thuckalay, Kanyakumari District, Tamilnadu State, India- 629 180, during April 10-11 2012.

11. D. Puhan, L.D. Das, **J. Sahu**, S.S. Mahapatra; "Multi-objective Optimization of Electric Discharge Machining Process Parameters", *International Conference on Modeling, Optimisation and Computing* (ICMOC 2012), Noorul Islam University, Noorul Islam Centre for Higher Education, Kumaracoil, Thuckalay, Kanyakumari District, Tamilnadu State, India- 629 180, during April 10-11 2012.

12. Ankita Singh, Kumar Abhishek, **Jambeswar Sahu**, Saurav Datta, and Siba Sankar Mahapatra, "DEA based Taguchi Approach for Multi-Objective Optimization: A Case Study", *International Conference on Modeling, Optimization and Computing* (ICMOC 2012), Noorul Islam University, Noorul Islam Centre for Higher Education, Kumaracoil, Thuckalay, Kanyakumari District, Tamilnadu State, India- 629 180, during April 10-11 2012.

National Conference

13. **J. Sahu**, S.S. Mahapatra , D.P. Puhan, L.d. Das; "Parametric optimization of electric discharge machining by comparing of fuzzy logic and data envelopment analysis using anfis", *National Conference on Emerging Trend & its Application in Engineering* (NCETAE 2011), Indira Gandhi Institute of Technology (IGIT), Sarang, Odisha, India-759146, p:165-169, 2011.

14. **J. Sahu**, S.S. Mahapatra, D.P. Puhan, L.d. Das; "Optimization of the electric discharge machining process of AISI D2 steel by Fuzzy Logic and Response Surface Method", *National Conference on Emerging Trend & its Application in Engineering*(NCETAE 2011), Indira Gandhi Institute of Technology (IGIT), Sarang, Odisha, India-759146, p:170-174, 2011.

15. **Jambeswar Sahu**, S.S. Mahapatra, R.K. Sahoo; "Production of biodiesel from jatropha (jatropha curcas) oil", *National Conference on Renewable and New Energy Systems*, Synergy Institute of Engineering & Technology, Dhenkanal, Odisha, India-759001, during Dec 22-23 2011.

16. **J. Sahu**, H. Pradhan, D. Puhan, S.S. Mahapatra, S. Datta; "Parametric optimization of electrical discharge machining by neuro-fuzzy and particle swarm optimization designed by response surface method", *National conference On advances in simulation & optimization Techniques in mechanical engineering* (NASOME 2012), Kalinga Institute of Indusrtial Technology, KIIT University, Bhubaneswar, Odisha, India-751024, during Feb 18-19 2012.

17. Kumar Abhishek, **Jambeswar Sahu**, Dr. Saurav Datta, Prof. Siba Sankar Mahapatra, " DEA Based Taguchi Approach For Multi-Objective Optimization In Machining Polymers: A Case Study", *National conference On advances in simulation & optimization Techniques in mechanical engineering* (NASOME 2012), Kalinga Institute of Indusrtial Technology, KIIT University, Odisha, India-751024, during Feb 18-19 2012.

18. Kumar Abhishek, **Jambeswar Sahu**, Dr. Saurav Datta, Prof. Siba Sankar Mahapatra, " DEA Based Taguchi Approach For Multi-Objective Optimization In Machining Polymers: A Case Study", *National conference On advances in simulation & optimization Techniques in mechanical engineering* (NASOME 2012), Kalinga Institute of Indusrtial Technology, KIIT University, Odisha, India-751024, during Feb 18-19 2012.

19. Rahul Ranjan, Kumar Abhishek, **Jambeswar Sahu**, Saurav Datta*, SS Mahapatra, "Multi-Response Optimization In CNC End Milling", *National conference On advances in simulation & optimization Techniques in mechanical engineering* (NASOME 2012), Kalinga Institute of Indusrtial Technology, KIIT University, Bhubaneswar, Odisha, India-751024, during Feb 18-19 2012.

20. C.P.Mohanty, A.K.Behura, **Jambeswar Sahu**, D.N.Thatoi, S.S.Mahapatra, "Optimization Of Geometrical Parameters Of Cactus Against High Wind Velocity: A Computational Investigation", *National conference On advances in simulation & optimization Techniques in mechanical engineering* (NASOME 2012), Kalinga Institute of Indusrtial Technology, KIIT University, Odisha, India-751024, during Feb 18-19 2012.

21. **Jambeswar sahu**, Siba Sankar Mahapatra, "Improvement of dimensional accuracy of fused deposition modeling (FDM) processed parts using grey Taguchi method'. Advance in Production Technology and Engineering Materials. Aryan Institute of Engineering and Technology, Bhubaneswar, Odisha, India-752050, on Feb 11th 2012